P-05-29

Forsmark site investigation

Formation factor logging in-situ by electrical methods in KFM01A and KFM02A

Measurements and evaluation of methodology

Martin Löfgren, Ivars Neretnieks
Department of Chemical Engineering and Technology
Royal Institute of Technology

April 2005

Svensk Kärnbränslehantering AB
Swedish Nuclear Fuel
and Waste Management Co
Box 5864
SE-102 40 Stockholm Sweden
Tel 08-459 84 00
+46 8 459 84 00
Fax 08-661 57 19
+46 8 661 57 19

ISSN 1651-4416
SKB P-05-29

Forsmark site investigation

Formation factor logging in-situ by electrical methods in KFM01A and KFM02A

Measurements and evaluation of methodology

Martin Löfgren, Ivars Neretnieks
Department of Chemical Engineering and Technology
Royal Institute of Technology

April 2005

Keywords: AP PF 400-04-79, In-situ, Formation factor, Surface conduction, Rock resistivity, Electrical conductivity.

Abstract

This report presents measurements and interpretations of the formation factor of the rock surrounding the boreholes KFM01A and KFM02A in Forsmark, Sweden. The formation factor was logged in-situ by electrical methods and is compared to formation factors obtained in the laboratory by electrical methods.

During the review process it was discovered that the nomenclature for fractures had been changed, and that the evaluation of the in-situ formation factor was based on "old" nomenclature. This could imply minor uncertainties in the statistics of the reported "rock matrix formation factors", since data have been excluded. However, since the data still are judged useful (e.g. as indications of spatial variability) and a re-analysis will take some time, it was decided to publish this report and then evaluate the effects as a separate activity.

The in-situ rock matrix formation factors obtained in KFM01A and KFM02A ranged from $5.4 \cdot 10^{-6}$ to $1.5 \cdot 10^{-4}$ and from $1.2 \cdot 10^{-5}$ to $2.5 \cdot 10^{-2}$, respectively. The in-situ fractured rock formation factors obtained ranged from $5.4 \cdot 10^{-6}$ to $6.1 \cdot 10^{-4}$ and from $1.2 \cdot 10^{-5}$ to $1.3 \cdot 10^{-2}$ in KFM01A and KFM02A, respectively. The laboratory (rock matrix) formation factors obtained on bore core samples from KFM01A and KFM02A ranged from $1.8 \cdot 10^{-5}$ to $2.8 \cdot 10^{-3}$ and from $7.2 \cdot 10^{-5}$ to $7.2 \cdot 10^{-4}$ respectively. The formation factors appear to be distributed according to the log-normal distribution.

The porous system of the rock surrounding KFM01A and KFM02A appears to be more compressed due to the overburden than expected. An alternative interpretation is that the rock samples brought to the laboratory are more disturbed than expected.

The rock type specific formation factor histograms presented in this report suggest that the formation factor within a rock type may range over at least two orders of magnitude.

The focused rock resistivity tool Century 9072 was calibrated up to 80,000 ohm.m by using the focused rock resistivity tool Antares Dual-Laterolog.

Sammanfattning

Denna rapport presenterar mätningar och tolkningar av bergets formationsfaktor runt borrhålen KFM01A och KFM02A i Forsmark, Sverige. Formationsfaktorn har loggats in-situ med elektriska metoder och jämförs med formationsfaktorn erhållen i laboratoriet med elektriska metoder.

Under granskningsfasen av denna rapport upptäcktes att nomenklaturen för sprickor hade ändrats och att utvärderingen av in-situ formationsfaktorn baserats på den gamla nomenklaturen. Detta kan medföra vissa mindre osäkerheter i statistiken för de rapporterade formationsfaktorerna för bergmatrisen, eftersom en del data utelämnats. Eftersom data trots detta bedömts vara användbara (t ex som indikation på rumslig variation) och att en ny analys tar tid, bestämdes det att publicera denna rapport och genomföra en analys av effekterna som en separat aktivitet.

Den erhållna in-situ formationsfaktorn för bergmatrisen för KFM01A och KFM02A varierade från $5{,}4 \cdot 10^{-6}$ till $1{,}5 \cdot 10^{-4}$ och från $1{,}2 \cdot 10^{-5}$ till $2{,}5 \cdot 10^{-2}$ för respektive borrhål, medan den erhållna in-situ formationsfaktorn för sprickigt berg för KFM01A och KFM02A varierade från $5{,}4 \cdot 10^{-6}$ till $6{,}1 \cdot 10^{-4}$ respektive från $1{,}2 \cdot 10^{-5}$ till $1{,}3 \cdot 10^{-2}$. Slutligen varierade den erhållna laborativa formationsfaktorn (för bergmatrisen) för KFM01A och KFM02A från $1{,}8 \cdot 10^{-5}$ till $2{,}8 \cdot 10^{-3}$ och från $7{,}2 \cdot 10^{-5}$ till $7{,}2 \cdot 10^{-4}$ för respektive borrhål.

Porsystemet i berget som omger KFM01A och KFM02A verkar vara mer komprimerat på grund av trycket från överliggande bergmassa än väntat. En alternativ tolkning är att bergsproven som tagits till laboratoriet är mer störda än väntat.

De bergartsspecifika formationsfaktorhistogrammen som presenteras i denna rapport tyder på att formationsfaktorn inom samma bergart kan variera över åtminstone två tiopotenser.

Den fokuserade bergresistivitetsloggen Century 9072 kalibrerades upp till 80 000 ohm.m med hjälp av den fokuserade bergresistivitetsloggen Antares Dual-Laterolog.

Contents

1 Introduction 7

2 Objective and scope 9

3 Equipment 11
3.1 Rock resistivity measurments 11
3.2 Groundwater electrical conductivity measurments 11
3.3 Difference flow loggings 12
3.4 Boremap loggings 12

4 Execution 13
4.1 Theory 13
4.1.1 The formation factor 13
4.1.2 Surface conductivity 14
4.1.3 Artefacts 14
4.1.4 Fractures in-situ 14
4.1.5 Rock matrix and fractured rock formation factor 16
4.2 Rock resistivity measurements in-situ 16
4.2.1 Rock resistivity log KFM01A 16
4.2.2 Rock matrix resistivity log KFM01A 17
4.2.3 Fractured rock resistivity log KFM01A 18
4.2.4 Rock resistivity KFM02A 19
4.2.5 Rock matrix resistivity log KFM02A 20
4.2.6 Fractured rock resistivity log KFM02A 21
4.3 Groundwater EC measurements in-situ 22
4.3.1 EC measurements in KFM01A 22
4.3.2 EC measurements in KFM02A 22
4.3.3 EC measurements in KFM01A–KFM04A 23
4.3.4 EC extrapolations in KFM01A and KFM02A 24
4.3.5 EC of the pore water 26
4.4 Calibration of the Century 9072 rock resistivity tool. 26
4.5 Formation factor measurements in the laboratory 27
4.6 Nonconformities 27

5 Results 29
5.1 General comments 29
5.2 Laboratory formation factor 29
5.3 In-situ rock matrix formation factor 31
5.4 In-situ fractured rock formation factor 32
5.5 Comparison of formation factors of KFM01A 33
5.6 Comparison of formation factors of KFM02A 34

6 Summary and discussions 35

References 37
Appendix A 39
Appendix B 41
Appendix C 61
Appendix D 73

1 Introduction

This document reports data gained from measurements of the formation factor of rock surrounding the boreholes KFM01A and KFM02A, within the Forsmark site investigation area. The formation factor was logged in-situ by electrical methods. Comparisons are made with formation factors obtained in the laboratory on samples from the bore cores of KFM01A and KFM02A.

This work has been conducted according to the activity plan AP PF 400-04-79 (SKB internal controlling document).

Other contractors performed the fieldwork and laboratory work, and that work is outside the framework of this activity. The interpretation of in-situ data and compilation of formation factor logs were performed by Chemical Engineering and Technology at the Royal Institute of Technology in Stockholm, Sweden.

Figure 1-1 shows the Forsmark site investigation area and the location of different drill sites. KFM01A and KFM02A are located at the drill sites DS1 and DS2 respectively.

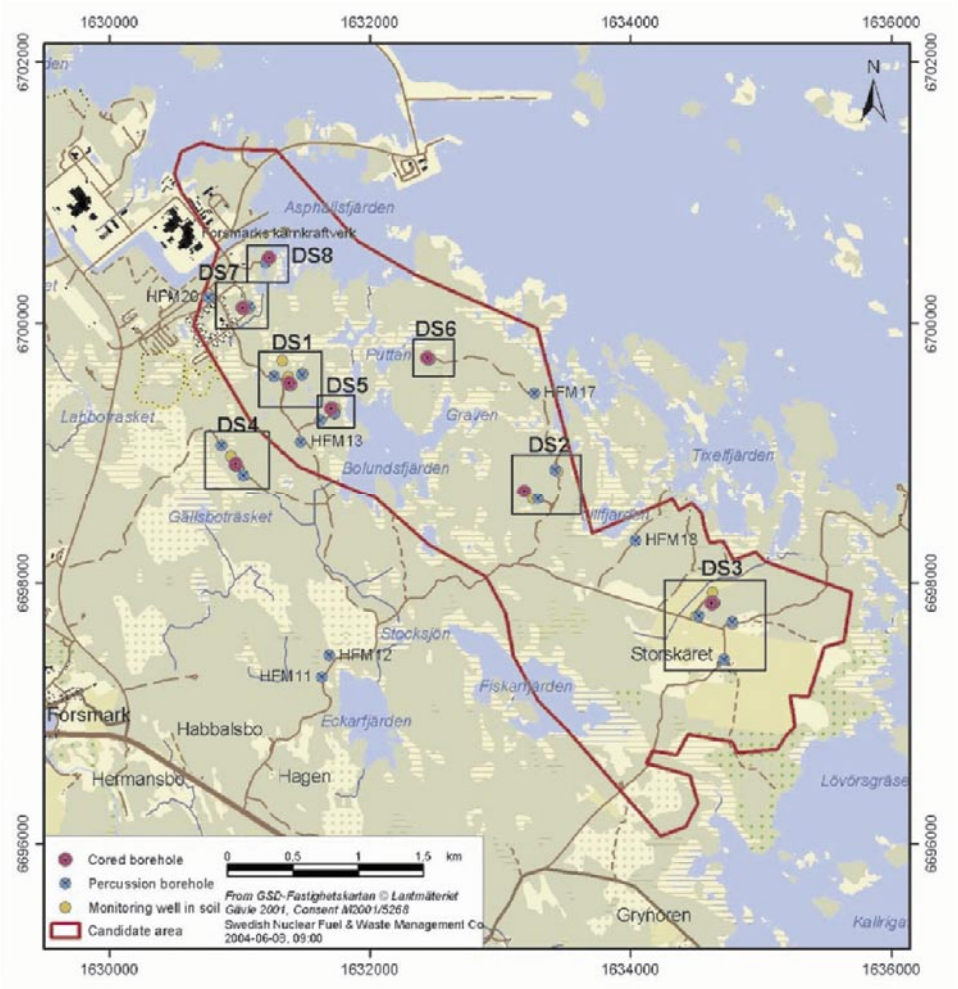

Figure 1-1. *General overview over the Forsmark site investigation area.*

2 Objective and scope

The formation factor is an important parameter that may be used directly in the safety assessment. The main objective of this work is to obtain the formation factor of the rock mass surrounding the boreholes KFM01A and KFM02A. This has been achieved by performing formation factor loggings by electrical methods both in-situ and in the laboratory. The in-situ method gives a great number of formation factors obtained under more natural conditions than in the laboratory. To obtain the in-situ formation factor, results from previous loggings were used. The laboratory formation factor was obtained by performing measurements on rock samples from the bore cores of KFM01A and KFM02A. Other contractors carried out the fieldwork and laboratory work.

3 Equipment

3.1 Rock resistivity measurments

The resistivity of the rock surrounding the boreholes KFM01A and KFM02A was logged in a campaign using the focused rock resistivity tool Antares Dual-Laterolog DLLs (shallow configuration) /1/. The tool emits an alternating current perpendicular to the borehole axis from a main current electrode. The shape of the current field is controlled by electric fields emitted by guard electrodes. By using focused tools, the disturbance from the borehole is minimized. The upper quantitative response limit of the Antares DLLs tool is 400,000 ohm.m and the vertical resolution is 10 cm according to the manufacturer. The rock resistivity of KFM01A was logged on the 7th of September 2004 whereas the rock resistivity of KFM02A was logged on the 8th of September 2004.

3.2 Groundwater electrical conductivity measurments

The EC (electrical conductivity) of the borehole fluid in KFM01A and KFM02A was logged using the POSIVA difference flow meter. The tool is shown in Figure 3-1.

When logging the EC of the borehole fluid, the lower rubber disks of the tool are not used. During the measurements, no drawdown is applied. Measurements were carried out before and after the difference flow logging in each borehole. For KFM01A the measurements were made between the 19th and 20th of November 2002 and on the 28th of November 2002. The measurements are described in /2/. For KFM02A measurements were made between the 24th and 25th of April 2003 and on the 11th of May 2003. The measurements are described in /3/.

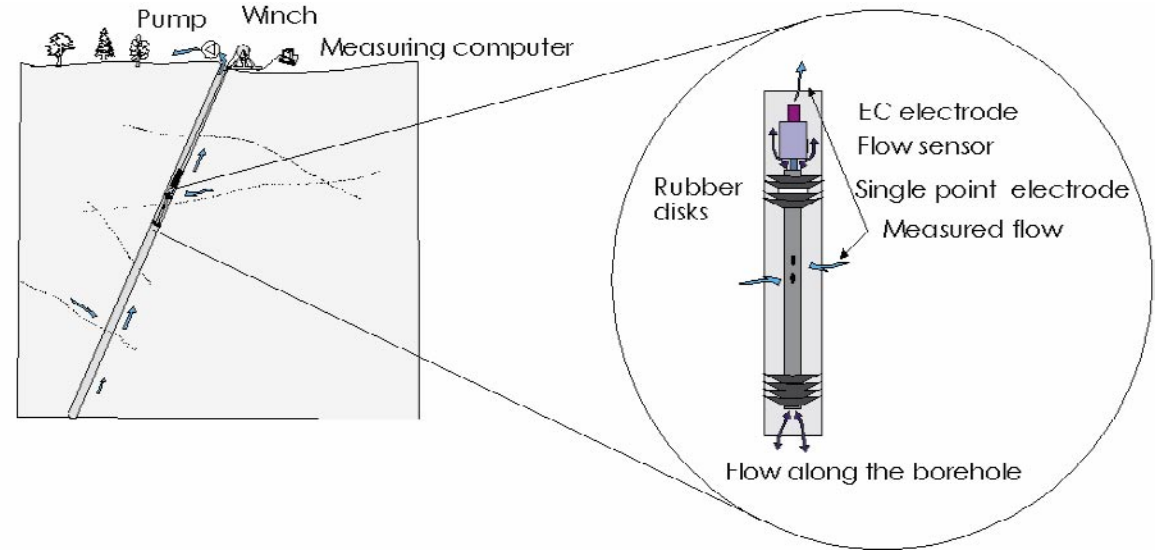

Figure 3-1. *Schematics of the POSIVA difference flow meter (image taken from /2/).*

When using both the upper and the lower rubber disks, a section around a specific fracture can be packed off. By applying a drawdown at the surface, groundwater can thus be extracted from specific fractures. By also measuring the groundwater flow out of the fracture, it is calculated how long time it will take to fill up the packed off borehole section three times. During this time the EC is measured and a transient EC curve is obtained. After this time it is assumed that the measured EC is representative for the groundwater flowing out of the fracture. The measurements may be disturbed by leakage of borehole fluid into the packed off section and development of gas from species dissolved in the groundwater. Interpretations of transient EC curves are discussed in /4/. The quantitative measuring range of the EC electrode of the POSIVA difference flow meter is 0.02–11 S/m.

In KFM02A the EC of groundwater extracted from a number of specific fractures between 110–513 m was measured. These measurements were performed between the 8th and 11th of May 2003. Further details concerning measurements with the POSIVA difference flow meter are given in /2/ and /3/.

The EC, among other entities, of the groundwater coming from fractures in larger borehole sections is measured as a part of the hydrogeochemical program. A section is packed of and by using a drawdown, groundwater is extracted from fractures within the section and brought to the surface for chemical analysis. In KFM01A the section 110.1–120.8 m was packed off and measurements were made between the 3rd and 25th of February 2003. Thereafter, the section 176.8–183.9 m was packed off and measurements were made between the 26th of February and the 1st of April 2003. The campaign is described in /5/. In KFM02A the section 509.0–516.1 m was packed off and measurements were made between the 1st of September and the 21st of October 2003. The campaign is described in /6/.

3.3 Difference flow loggings

By using the POSIVA difference flow meter, water-conducting fractures can be located. The tool, shown in Figure 3-1, has a flow sensor and the flow from fractures in packed off sections can be measured. When performing these measurements, both the upper and the lower rubber disks are used. Measurements can be carried out both with and without applying a drawdown. The quantitative measuring range of the flow sensor is 0.1–5,000 mL/min.

Difference flow loggings were performed in KFM01A between the 20th and 28th of November 2002 and are described in /2/. Difference flow loggings were performed in KFM02A between the 26th of April and the 11th of May 2003 and are described in /3/.

3.4 Boremap loggings

The bore core of KFM01A was logged between 102.08–1,000.86 m together with a simultaneous study of video images of the borehole wall, so caller boremap logging, described in /7/. The boremap logging of KFM02A was performed between 101.76–1,001.97 m and the logging is described in /8/.

In the core log, fractures parting the core are recorded. Fractures parting the core that have not been induced during the drilling or core handling are called natural fractures. Parts of the core that are crushed or lost are also recorded, as well as the spatial distribution of different rock types.

4 Execution

4.1 Theory

4.1.1 The formation factor

The theory applied for obtaining formation factors by electrical methods is described in /9/. The formation factor is the ratio between the diffusivity of the rock matrix to that of free pore water. If the species diffusing through the porous system is much smaller than the characteristic length of the pores and no interactions occur between the mineral surfaces and the species, the formation factor is only a geometrical factor that is defined by the transport porosity, the tortuosity and the constrictivity of the porous system:

$$F_f = \frac{D_e}{D_w} = \varepsilon_t \frac{\delta}{\tau^2} \qquad 4\text{-}1$$

where F_f (-) is the formation factor, D_e (m^2/s) is the effective diffusivity of the rock, D_w (m^2/s) is the diffusivity in the free pore water, ε_t (-) is the transport porosity, τ (-) is the tortuosity, and δ (-) is the constrictivity. When obtaining the formation factor with electrical methods, the Einstein relation between diffusivity and ionic mobility is used:

$$D = \frac{\mu RT}{zF} \qquad 4\text{-}2$$

where D (m^2/s) is the diffusivity, μ ($m^2/V{\cdot}s$) is the ionic mobility, z (-) the charge number and R (J/mol·K), T (K) and F (C/mol), are the gas constant, temperature, and Faraday constant respectively. From the Einstein relation it is easy to show that the formation factor also is given by the ratio of the pore water resistivity to the resistivity of the saturated rock /10/:

$$F_f = \frac{\rho_w}{\rho_r} \qquad 4\text{-}3$$

where ρ_w (ohm.m) is the pore water resistivity and ρ_r (ohm.m) is the rock resistivity. The resistivity of the saturated rock can easily be obtained by standard geophysical methods.

At present it is not feasible to extract pore water from the rock matrix. Therefore, it is assumed that the pore water is in equilibrium with the free water surrounding the rock, and measurements are performed on this free water. The validity of this assumption has to be discussed at every specific site.

The resistivity is the reciprocal to electrical conductivity. Traditionally the EC (electrical conductivity) is used when measuring on water and resistivity is used when measuring on rock.

4.1.2 Surface conductivity

In intrusive igneous rock the mineral surfaces are normally negatively charged. As the negative charge often is greater than what can be balanced by cations specifically adsorbed on the mineral surfaces, an electrical double layer with an excess of mobile cations will form at the pore wall. If a potential gradient is placed over the rock, the excess cations in the electrical double layer will move. This process is called surface conduction and this additional conduction may have to be accounted for when obtaining the formation factor of rock saturated with a pore water of low ionic strength. If the EC of the pore water is around 0.5 S/m or above, errors associated with surface conduction are deemed to be acceptable. This criterion is based on laboratory work by /11/ and /10/. The effect of the surface conduction on rock with formation factors below $1 \cdot 10^{-5}$ was not investigated in these works. In this report surface conduction has not been accounted for, as only the groundwater in the upper 100 or 200 m of the boreholes has a low ionic strength and as more knowledge is needed on surface conduction before performing corrections.

4.1.3 Artefacts

Comparative studies have been performed on a large number of 1–2 cm long samples from Äspö in Sweden /11/. Formation factors obtained with an electrical resistivity method using alternating current were compared to those obtained by a traditional through diffusion method, using uranine as the tracer. The results show that formation factors obtained by the electrical resistivity measurements are a factor of about 2 times larger that those obtained by through diffusion measurements. A similar effect was found on granitic samples up to 12 cm long, using iodide in tracer experiments /12/. The deviation of a factor 2 between the methods may be explained by anion exclusion of the anionic tracers. Previously performed work suggests that the Nernst-Einstein equation between the diffusivity and electrical conductivity is generally applicable in granitic rock and that no artefacts give rise to major errors. It is uncertain, however, to what extent anion exclusion is related to the degree of compression of the porous system in-situ due to the overburden.

4.1.4 Fractures in-situ

In-situ rock resistivity measurements are highly disturbed by free water in open fractures. The current sent out from the downhole tool in front of an open fracture will be propagated both in the porous system of the rock matrix and in the free water in open fractures. Due to the low formation factor of the rock matrix, current may be preferentially propagated in a fracture intersecting the borehole even if its aperture is only on the order of 10^{-5} m.

There could be some confusion concerning the terminology of fractures. In order to avoid confusion an organization sketch of different types of fractures is shown in Figure 4-1. The subgroups of fractures that interfere with the rock resistivity measurements are marked with grey.

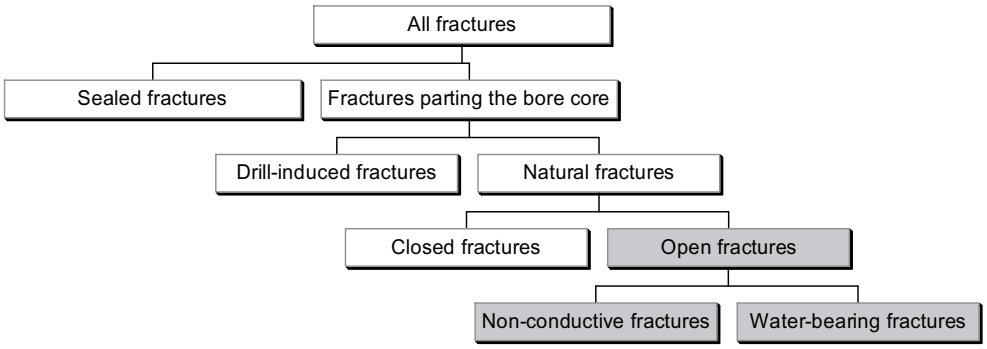

Figure 4-1. *Organization sketch of different types of fractures in-situ.*

The information of different types of fractures in-situ is obtained from the boremap logging and in the hydraulic flow logging. A fracture intersecting the borehole is most likely to part the bore core. In the core log, fractures that part the core are either natural or drill-induced fractures. Sealed fractures, which do not part the core, are also recorded in the core log. Laboratory results suggest that sealed fractures generally have no major interference on rock resistivity measurements. However, some fractures that are only partly sealed may influence the measurements.

Natural fractures are either open or closed, depending on the aperture. A fracture is closed when its aperture is so small that the amount of water it holds is comparative to that held in the adjacent porous system. In this case the "adjacent porous system" is the porous system of the rock matrix the first few centimetres from the fracture. An open fracture has a larger aperture, may be hydraulically conductive, and holds enough water to interfere with the rock resistivity measurements. Currently there is no way of obtaining the fracture aperture in the boremap log and one cannot separate open from closed fractures. Open fractures could either be hydraulically conductive or non-conductive, depending on how they are connected to the fracture network and on the hydraulic gradients of the system. Figure 4-2 shows different fractures intersecting a borehole.

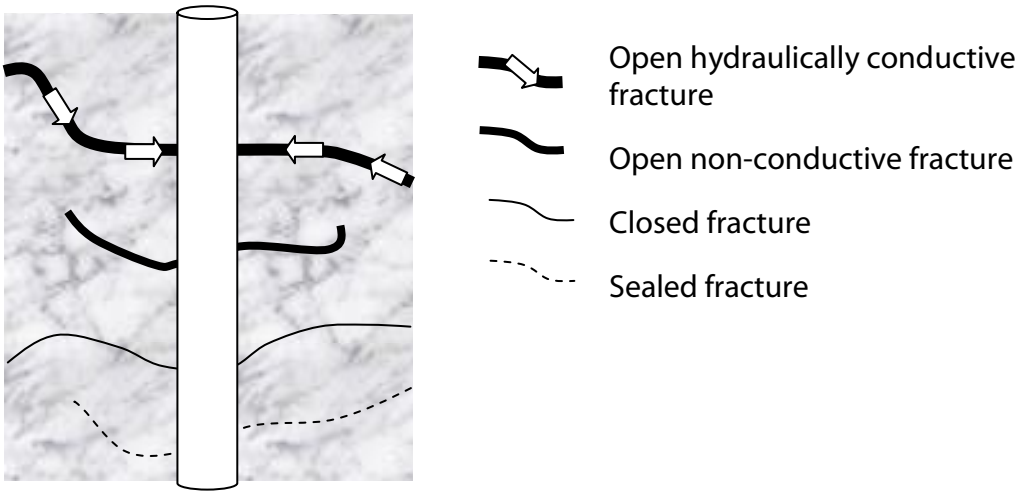

Figure 4-2. *Fractures intersecting a borehole.*

4.1.5 Rock matrix and fractured rock formation factor

In this report the rock resistivity is used to obtain formation factors of the rock surrounding the borehole. The obtained formation factors may later be used in models for radionuclide transport in fractured crystalline rock. Different conceptual approaches may be used in the models. Therefore this report aims to deliver formation factors that are defined in two different ways. The first is the "rock matrix formation factor", denoted by F_f^{rm}. This formation factor is representative for the solid rock matrix, as the traditional formation factor. The other one is the "fractured rock formation factor", denoted by F_f^{fr}, which represents the diffusive properties of a larger rock mass, where fractures and voids holding stagnant water is included in the porous system of the rock matrix. Further information on the definition of the two formation factors could be found in /4/.

The rock matrix formation factor is obtained from rock matrix resistivity data. When obtaining the rock matrix resistivity log from the in-situ measurements, all resistivity data that may have been affected by open fractures have to be sorted out. With present methods one cannot separate open from closed natural fractures in the core logging. By investigating the rock resistivity log at a fracture, one could draw conclusions weather it is open or closed. However, for formation factor logging by electrical methods this is not an independent method and cannot be used. Therefore, all natural fractures have to be considered as potentially open and all resistivities obtained close to a natural fracture detected in the core logging are sorted out. By examining the resistivity logs obtained by the Antares DLLs tool it has been found that resistivity values obtained within 0.5 m from a natural fracture generally should be sorted out. This distance includes a safety margin of 0.1–0.2 m.

The fractured rock formation factor is obtained from fractured rock resistivity data. When obtaining the fractured rock resistivity log from the in-situ measurements, all resistivity data that may have been affected by hydraulically conductive fractures detected in the in-situ flow logging have to be sorted out. By examining the resistivity logs obtained by the Antares DLLs tool it has been found that resistivity values obtained within 0.5 m from a hydraulically conductive fracture generally should be sorted out. This distance includes a safety margin of 0.1–0.2 m.

4.2 Rock resistivity measurements in-situ

4.2.1 Rock resistivity log KFM01A

The in-situ rock resistivity was obtained using the focused rock resistivity tool Antares DLLs (shallow configuration). The borehole was logged between 103–1,000 m. As most of the rock surrounding KFM01A is sparsely fractured, the borehole length of the rock resistivity log could be calibrated by matching resistivity dips with isolated fractures detected in the core logging. The natural fractures shown in Table 4-1 were used in the calibration.

Table 4-1. Natural fractures used when calibrating the borehole length.

Natural fracture at borehole length recorded in the core log (m)								
109.58	194.67	236.94	263.85	311.11	367.39	437.80	478.51	534.71
572.40	628.06	685.39	720.43	773.30	832.77	886.39	955.51	

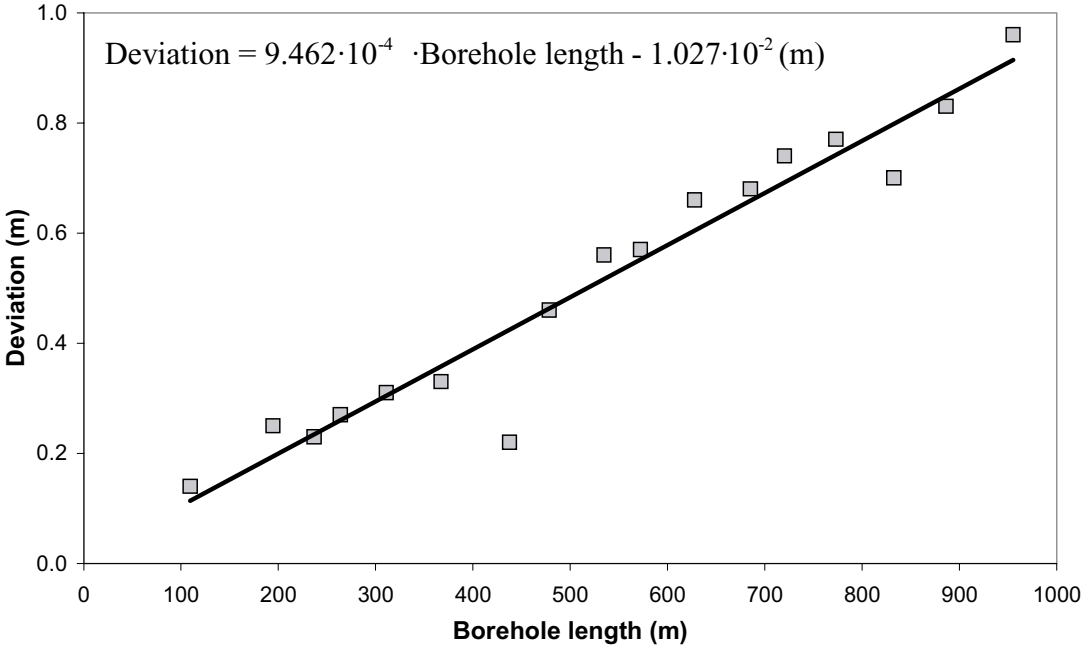

Figure 4-3. *Deviation of borehole lengths in the rock resistivity log, KFM02A.*

Figure 4-3 shows the deviation of the borehole length of the in-situ rock resistivity log and the borehole length of the natural fractures, shown in Table 4-1, obtained in the boremap logging.

As can be seen in Figure 4-3, the deviation is fairly linear with the borehole length of the boremap log. The borehole length of the rock resistivity log was corrected by subtracting the deviation obtained by the linear equation shown in Figure 4-3.

4.2.2 Rock matrix resistivity log KFM01A

After adjusting the borehole length of the in-situ rock resistivity log, all resistivity data obtained within 0.5 m from a natural fracture detected in the core log were sorted out. In the core log, a total of 818 natural fractures are recorded. No crush zones or zones where the core have been lost are recorded. The locations of natural fractures in KFM01A are shown in Appendix B1. A total of 10,845 rock matrix resistivities were obtained between 105–995 m. All values were within the quantitative measuring range of the Antares DLLs tool. The rock matrix resistivity log between 105–995 m is shown in Appendix B1.

Figure 4-4 shows the distribution of the rock matrix resistivities obtained between 105–995 m in KFM01A. The histogram ranges from 0–100,000 ohm.m and is divided into sections of 5,000 ohm.m.

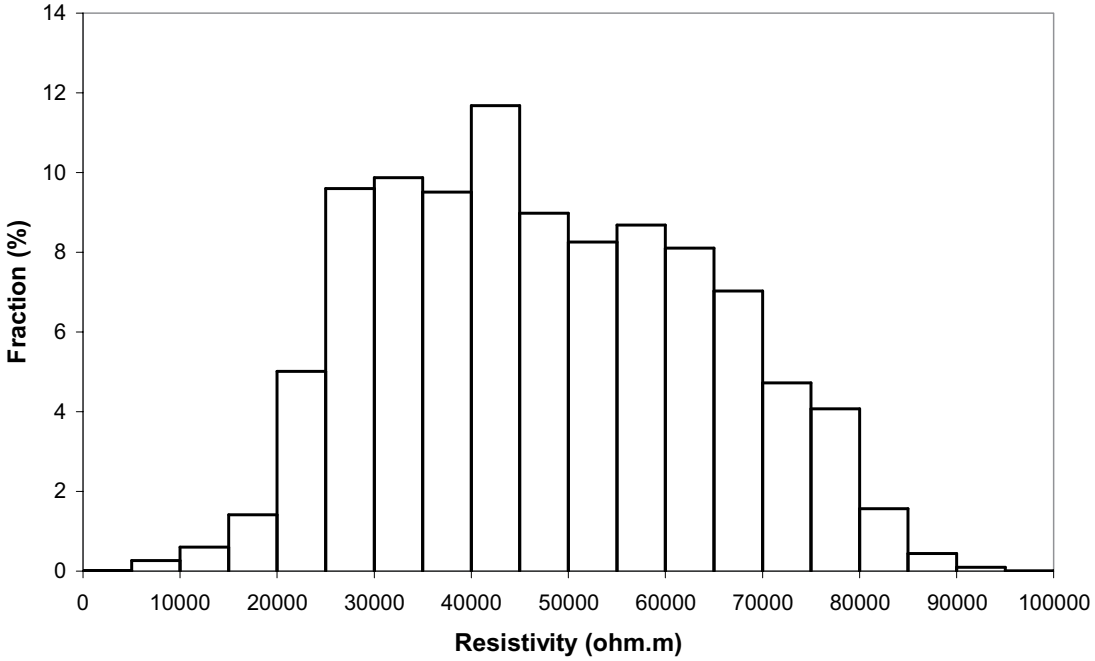

Figure 4-4. *Distribution of rock matrix resistivities in KFM01A.*

4.2.3 Fractured rock resistivity log KFM01A

After adjusting the borehole length of the in-situ rock resistivity log, all resistivity data obtained within 0.5 m from a hydraulically conductive fracture, detected in the difference flow logging /2/, were sorted out. For the difference flow log, no correction in the reported borehole length was needed. A total of 34 hydraulically conductive fractures were detected in KFM01A. The locations of hydraulically conductive fractures in KFM01A are shown in Appendix B1. A total of 17,188 fractured rock resistivities were obtained between 105–995 m. All values were within the quantitative measuring range of the Antares DLLs tool. The fractured rock resistivity log between 105–995 m is shown in Appendix B1.

Figure 4-5 shows the distribution of the fractured rock resistivities obtained between 105–995 m in KFM01A. The histogram ranges from 0–100,000 ohm.m and is divided into sections of 5,000 ohm.m.

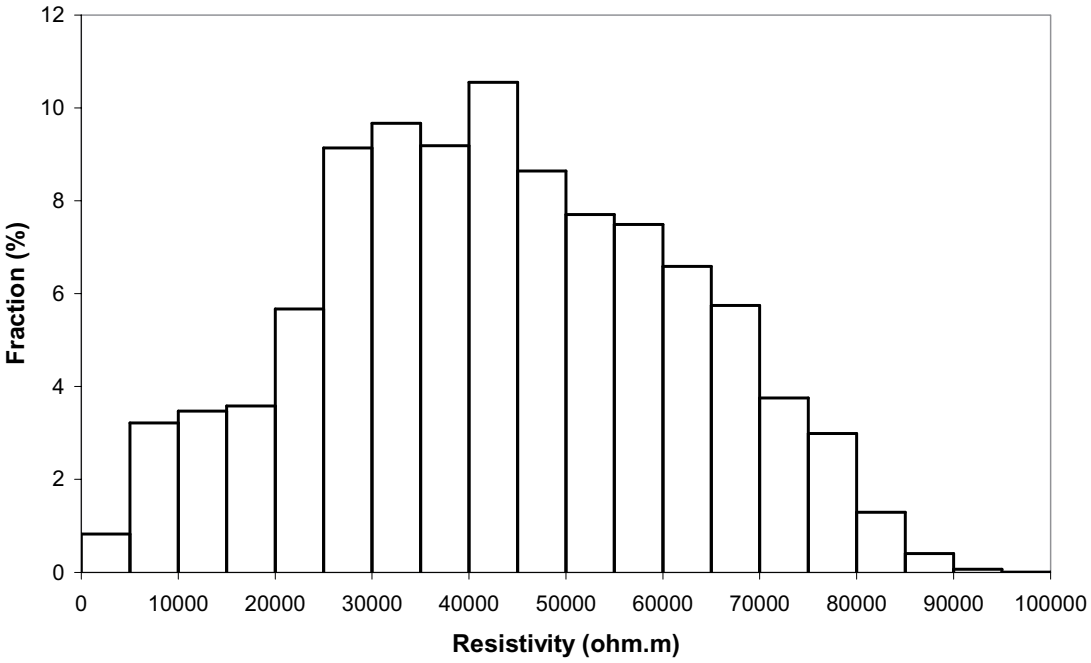

Figure 4-5. *Distribution of fractured rock resistivities in KFM01A.*

4.2.4 Rock resistivity KFM02A

The in-situ rock resistivity was obtained using the focused Antares DLLs tool. The borehole was logged between 102–1,000 m. As large parts of the rock surrounding KFM02A is sparsely fractured, the borehole length of the rock resistivity log could be calibrated by matching resistivity dips with isolated fractures detected in the boremap logging. The natural fractures shown in Table 4-2 were used in the calibration.

Table 4-2. Natural fractures used when calibrating the borehole length.

Natural fracture at borehole length recorded in the core log (m)								
139.94	229.61	345.68	431.72	539.04	571.65	621.49	678.21	709.87
575.43	859.33	932.58	967.61	990.01				

Figure 4-6 shows the deviation of the borehole length of the in-situ rock resistivity log and the borehole length of the natural fractures, shown in Table 4-2, obtained in the boremap logging.

As can be seen in Figure 4-6 the deviation is fairly linear with the borehole length of the boremap log. The borehole length of the rock resistivity log was corrected by subtracting the deviations obtained by the linear equation shown in Figure 4-6.

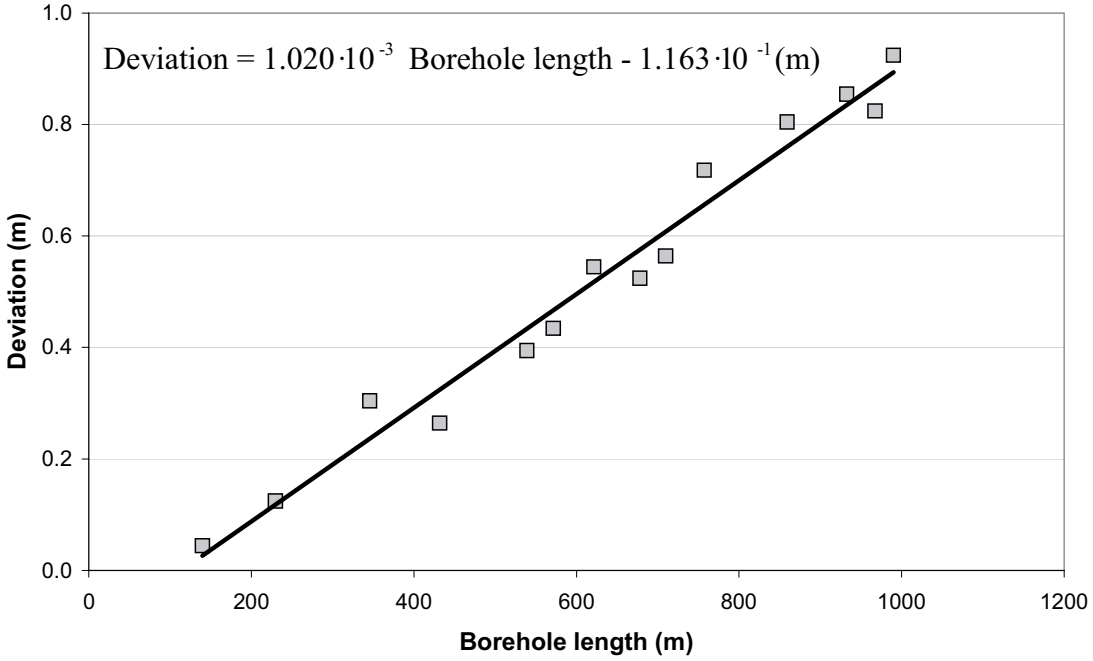

Figure 4-6. *Deviation of borehole lengths in the rock resistivity log, KFM02A.*

4.2.5 Rock matrix resistivity log KFM02A

After adjusting the borehole length of the in-situ rock resistivity log, all resistivity data obtained within 0.5 m from a natural fracture detected in the core log were sorted out. In the core log a total of 1,525 natural fractures are recorded. In addition 6 crush zones but no zones where the core is lost are recorded. A total of 1.5 m of the core is crushed. Natural fractures can potentially intersect the borehole in zones where the core is crushed or lost. Therefore, a natural fracture was assumed every decimetre in these zones. The locations of natural fractures in KFM02A are shown in Appendix B2. A total of 7,653 rock matrix resistivities were obtained between 104–1,000 m. All values were within the quantitative measuring range of the Antares DLLs tool. The rock matrix resistivity log between 104–1,000 m is shown in Appendix B2.

Figure 4-7 shows the distribution of the rock matrix resistivities obtained between 104–1,000 m in KFM02A. The histogram ranges from 0–100,000 ohm.m and is divided into sections of 5,000 ohm.m.

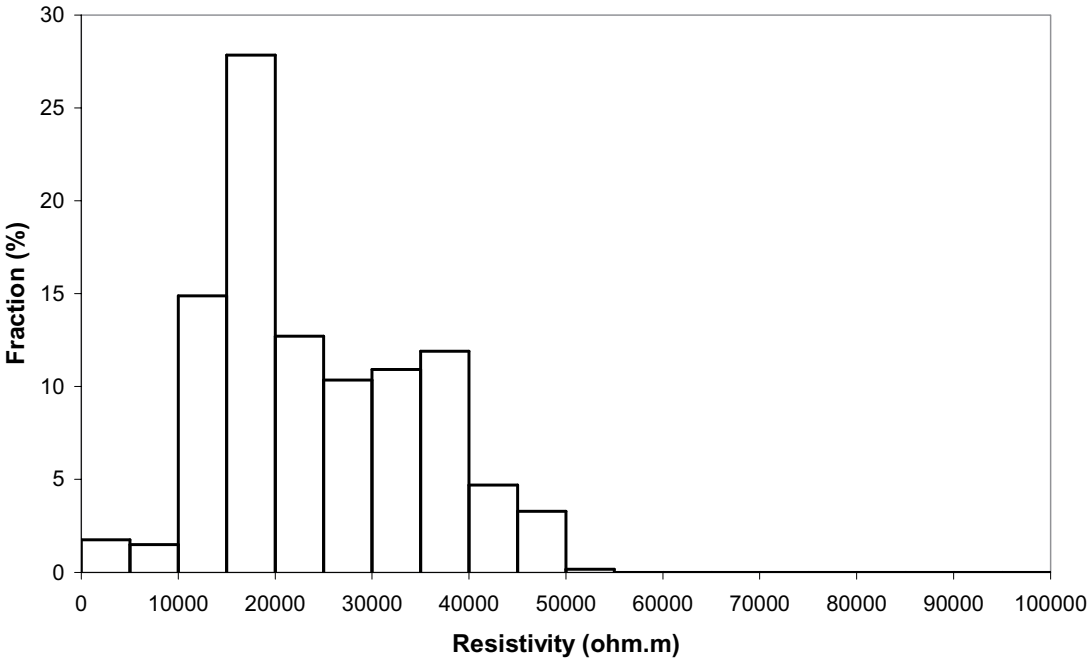

Figure 4-7. *Distribution of rock matrix resistivities in KFM02A.*

4.2.6 Fractured rock resistivity log KFM02A

After adjusting the borehole length of the in-situ rock resistivity log, all resistivity data obtained within 0.5 m from a hydraulically conductive fracture, detected in the difference flow logging, were sorted out. For the difference flow log, no correction in the reported borehole length was needed. A total of 106 hydraulically conductive fractures were detected in KFM02A. The locations of hydraulically conductive fractures in KFM02A are shown in Appendix B2. A total of 16,243 fractured rock resistivities were obtained between 104–1,000 m. All values were within the quantitative measuring range of the Antares DLLs tool. The fractured rock resistivity log between 104–1,000 m is shown in Appendix B2.

Figure 4-8 shows the distribution of the fractured rock resistivities obtained between 104–1,000 m in KFM02A. The histogram ranges from 0–100,000 ohm.m and is divided into sections of 5,000 ohm.m.

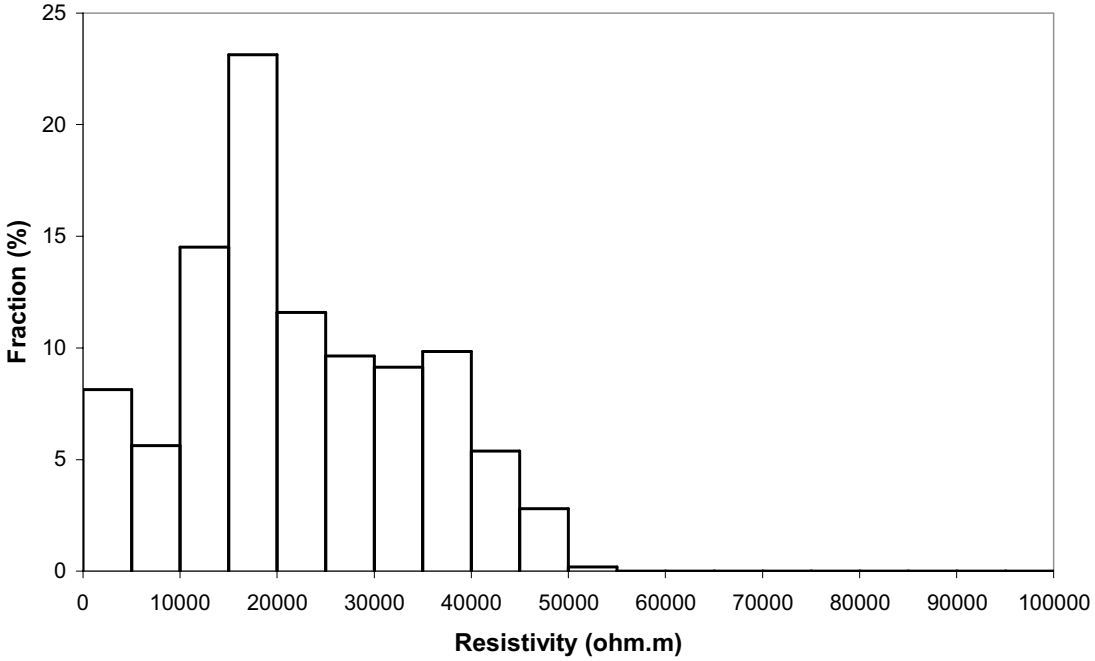

Figure 4-8. *Distribution of fractured rock resistivities in KFM02A.*

4.3 Groundwater EC measurements in-situ

4.3.1 EC measurements in KFM01A

The EC of groundwater extracted from fractures was measured in the hydrogeochemical program applied in KFM01A. The measurements are described in /5/. The borehole section 110.1–120.8 m was packed off and a groundwater EC of 1.519 ± 0.020 S/m was obtained. In this section, three hydraulically conductive fractures were identified in the in-situ flow logging at 113.8 m, 115.2 m, and 118.3 m respectively /2/. Furthermore, the borehole section 176.8–183.9 m was packed off and a groundwater EC of 1.548 ± 0.020 S/m was obtained. In this section two hydraulically conductive fractures were identified in the flow logging at 178.0 m and 178.3 m respectively.

In this work it is assumed that the groundwater ECs obtained in the hydrogeochemical program were 1.519 S/m and 1.548 S/m at the borehole lengths 116 m and 178 m, respectively.

4.3.2 EC measurements in KFM02A

A number of fracture specific groundwater ECs were obtained in KFM02A by extracting water from specific fractures using the POSIVA difference flow meter /3/. The transient EC and fracture specific EC obtained in KFM02A are shown in Figure 4-9.

Before and after the flow logging, the EC of the borehole fluid was measured. The obtained logs are shown in Figure 4-9. The EC of groundwater extracted from fractures in the borehole section 509.0–516.1 m was measured within the hydrogeochemical program. In this section, four hydraulically conductive fractures were identified in the in-situ flow logging at 512.3 m, 512.6 m, 513.1 m and 513.6 m respectively /6/. A groundwater EC of 1.613 ± 0.020 S/m was obtained. In this work it was assumed that the groundwater EC at the borehole length 513 m was 1.61 S/m.

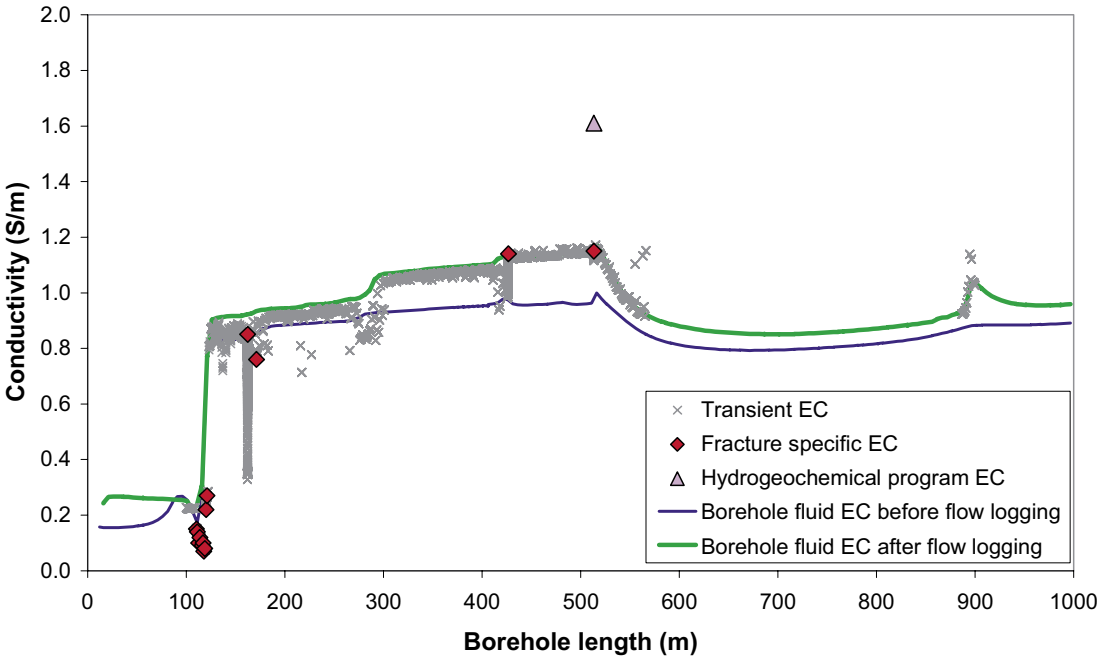

Figure 4-9. *Groundwater ECs obtained in-situ in KFM02A.*

4.3.3 EC measurements in KFM01A–KFM04A

As groundwater ECs were only obtained in the upper 178 m of KFM01A and in the upper 515 m of KFM02A, extrapolations have to be made. It is preferable to avoid such extrapolations, which may be quite uncertain, by obtaining in-situ data distributed over the entire borehole length. In this case this was not feasible. It was decided to base the extrapolations not only on the data obtained in KFM01A and KFM02A, but also on the data obtained in KFM03A and KFM04A, which are boreholes within the Forsmark site investigation area. Figure 4-10 shows the groundwater ECs obtained in the difference flow logging or in the hydrogeochemical program in these boreholes.

As the boreholes KFM01A, KFM02A, and KFM03A have an inclination of 85° while KFM04A is inclined 60°, this was corrected for and the x-axis in Figure 4-10 represents the vertical borehole depth. Different altitudes of the drilling sites were not corrected for. In the hydrogeochemical evaluation of the Forsmark site /13/ it is suggested that there is a transition from fresh-meteoric waters to brackish-marine waters in the upper 200 m of the bedrock. It is also suggested that there may be a transition towards ancient brine groundwater below 800 m. This is reflected in the data in Figure 4-10. What is interesting to note is that below 200 m, the ratio of the highest to the lowest groundwater EC shown in Figure 4-10 is only 3.4. As the groundwater EC data follow a somewhat predicted profile, where the shattering is less than the range, the errors arising from the extrapolation may be smaller than a factor of 3.4. It should be kept in mind that the variation in groundwater EC at depth is small compared to the variation found in the rock resistivity measurements.

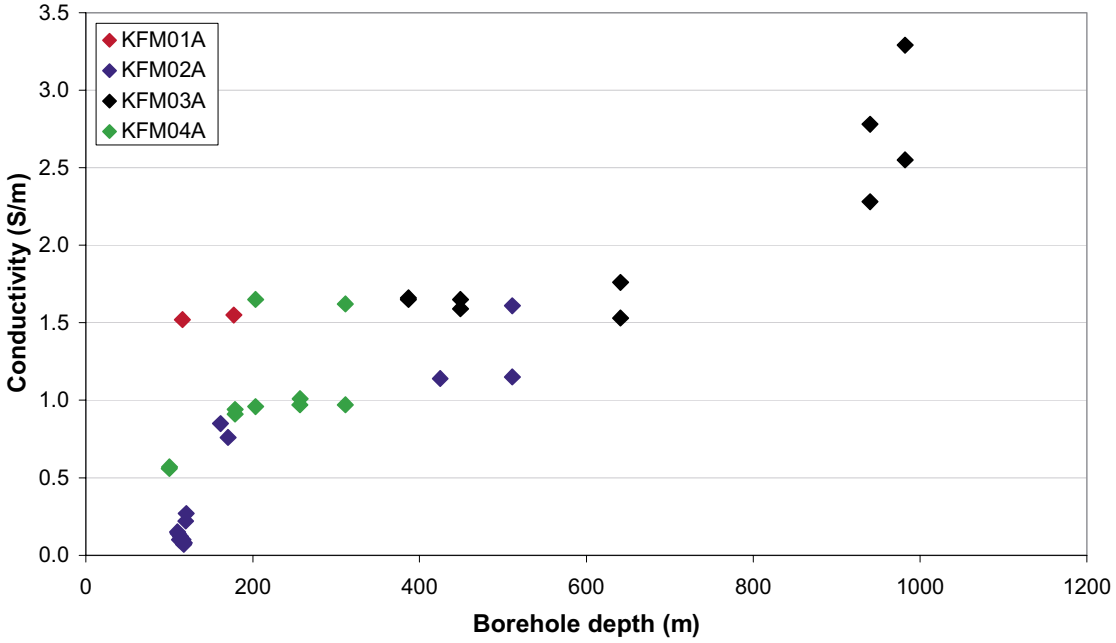

Figure 4-10. *Groundwater ECs obtained in-situ in KFM01A–KFM04A.*

Great care should be taken when making extrapolations in the zone where the transition from fresh-meteoric waters to brackish-marine waters takes place. The ratio of the highest to the lowest groundwater EC shown in Figure 4-10 that was obtained above 200 m is as much as 19. Furthermore, surface conduction greatly disturbs formation factor measurements by electrical methods in groundwater with a low salinity. Therefore, the method may not be applicable in the transition zone from fresh-meteoric waters to brackish-marine waters.

4.3.4 EC extrapolations in KFM01A and KFM02A

In KFM01A the transition from fresh-meteoric waters to brackish-marine waters appears to have taken place above the borehole length 116 m, where the first groundwater EC was obtained in the hydrogeochemical program. As it is unknown at what exact depth the transition takes place, it is recommended not to extrapolate the groundwater EC profile to shallower depths. In this work it is assumed that the EC is constant at 1.53 S/m from 116 mm down to 800 m. From 800 m to 1,000 m it is assumed that the EC increases linearly with borehole length according to:

$$\text{EC (S/m)} = 7.328 \cdot 10^{-3} \cdot \text{Borehole length (m)} - 4.293 \qquad 4\text{-}4$$

The red diamonds in Figure 4-11 marks the measured values and the red line marks the assumed groundwater EC profile in KFM01A.

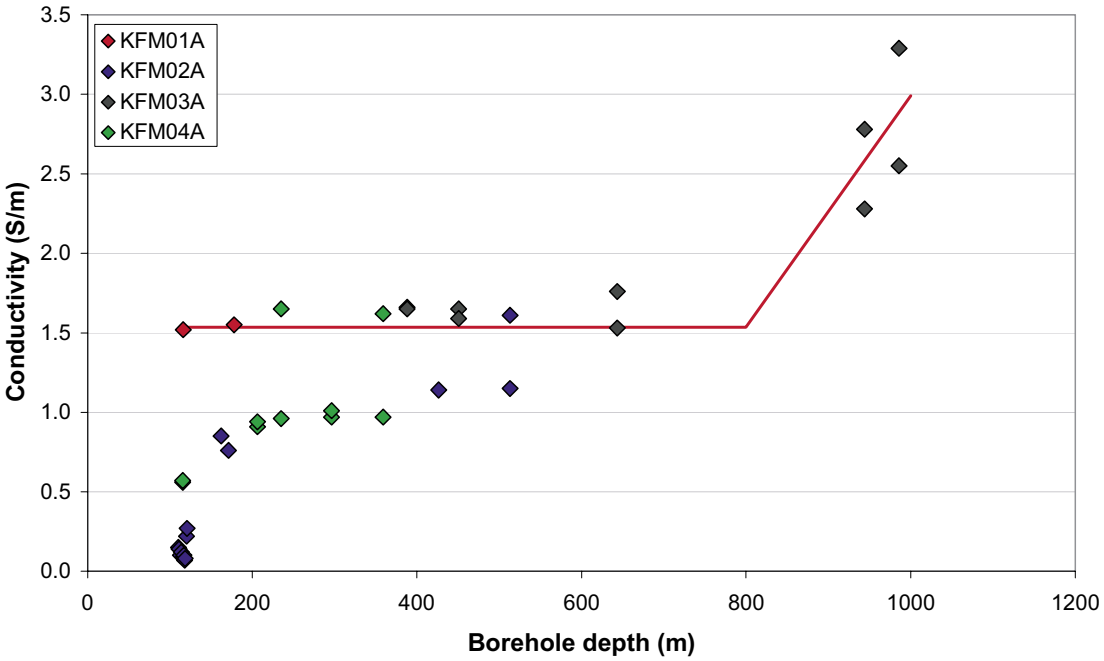

Figure 4-11. *Assumed groundwater EC profile for KFM01A.*

As no extrapolation could be made for the groundwater EC above the borehole length 116 m, no formation factors from shallower depths were obtained.

In KFM02A the transition from fresh-meteoric waters to brackish-marine waters was fairly well characterized. The assumed groundwater EC profile was obtained by using Equation 4-5, Equation 4-6, and Equation 4-7 between the borehole lengths 110 m to 200 m, 200 m to 800 m, and 800 m to 1,000 m respectively.

$$EC\ (S/m) = 1.278 \cdot 10^{-2} \cdot \text{Borehole length (m)} - 1.343 \qquad 4\text{-}5$$

$$EC\ (S/m) = 3.734 \cdot 10^{-4} \cdot \text{Borehole length (m)} - 1.138 \qquad 4\text{-}6$$

$$EC\ (S/m) = 7.776 \cdot 10^{-3} \cdot \text{Borehole length (m)} - 4.784 \qquad 4\text{-}7$$

The blue diamonds in Figure 4-12 marks the measured values and the blue line marks the assumed groundwater EC profile in KFM02A.

Due to possible interference from surface conduction that could not be corrected for, no formation factors were obtained above the borehole length 145 m, where the groundwater EC was assumed to be above 0.5 S/m.

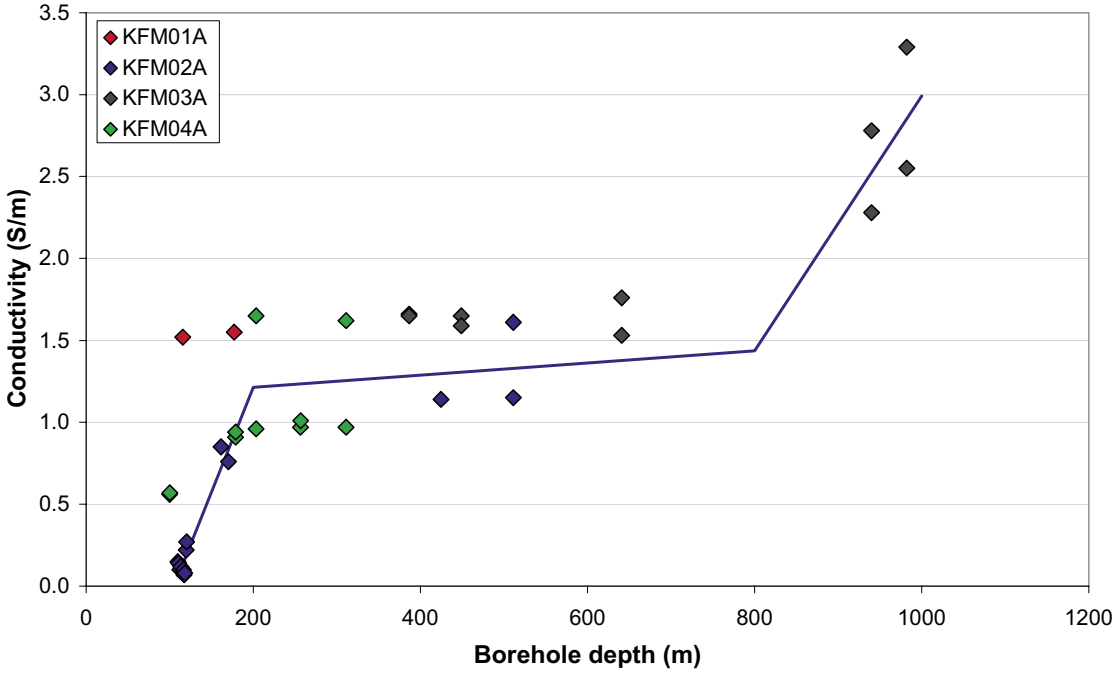

***Figure 4-12**. Assumed groundwater EC profile for KFM02A.*

4.3.5 EC of the pore water

Large parts of the rock surrounding KFM01A and KFM02A are sparsely fractured and few hydraulically conductive fractures are found. Therefore it is uncertain to what extent the pore water of the rock matrix is equilibrated with the groundwater. The rock surrounding hydraulically conductive fractures is generally more fractured and the pore water in the rock mass important for radionuclide retention is likely to be fairly well equilibrated with the groundwater. This is supported by the fact that similar groundwater ECs are found at corresponding depths in the boreholes KFM01A–KFM04A. For future work one may recommend to give formation factors obtained in more fractured rock within, say, 10 m of a hydraulically conductive fracture more weight than formation factors obtained 10th of meters away from the nearest hydraulically conductive fracture.

4.4 Calibration of the Century 9072 rock resistivity tool.

The rock resistivity was measured in-situ in KFM01A with the Century 9072 tool on the 29th of April 2003. The borehole lengths of the rock resistivity logs from the Century 9072 tool and the Antares DLLs tool were calibrated by matching resistivity dips with isolated fractures detected in the boremap logging. The natural fractures listed in Table 4-1 were used in the calibration. Rock resistivities at corresponding depths from the Century 9072 and Antares DLLs tools are plotted in Figure 4-13.

As can be seen from Figure 4-13 the Century 9072 tool delivered similar rock resistivities as the Antares DLLs tool. It appears that the Century 9072 tool can be used to measure rock resistivities up to 80,000 ohm.m with less than a 10% deviation. The shattering in Figure 4-13 is most likely due to interference from open fractures. It should be noted that the solid black line in Figure 4-13 is not a linear fitting of the data.

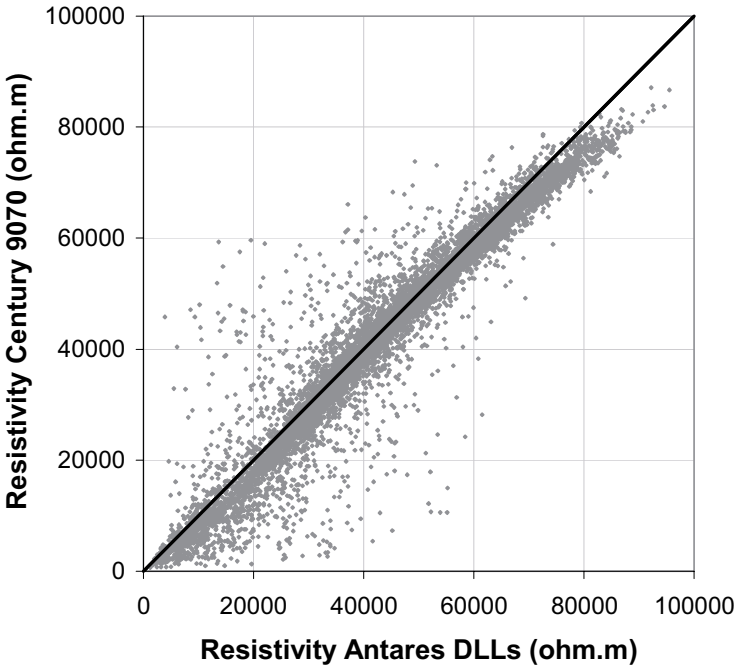

Figure 4-13. *Calibration of the Century 9072 tool in borehole KFM01A.*

4.5 Formation factor measurements in the laboratory

The laboratory work was performed by Geovista AB and is reported in /14/. The work was conducted between the 21st of May and the 13th of September 2004. Formation factors were obtained on 39 and 40 rock samples taken from the bore core of KFM01A and KFM02A respectively. The sample length was in general 3 cm. The obtained formation factors are tabulated in Appendix A1 and A2.

4.6 Nonconformities

None

5 Results

5.1 General comments

During the review process it was discovered that the nomenclature for fractures had been changed, and that the evaluation of the in-situ formation factor was based on "old" nomenclature. This could imply minor uncertainties in the statistics of the reported "rock matrix formation factors", since data have been excluded. However, since the data still are judged useful (e.g. as indications of spatial variability) and a re-analysis will take some time, it was decided to publish this report and then evaluate the effects as a separate activity.

5.2 Laboratory formation factor

The formation factors obtained in the laboratory are tabulated in Appendix A1 and A2 for KFM01A and KFM02A respectively. By using the normal-score method, as described in /15/, to determine the likelihood that a set of data is normally distributed, the mean value and standard deviation of the logarithm ($\log_{10}$) of the formation factors could be determined. Figure 5-1 shows the distributions of the laboratory formation factor obtained in KFM01A and KFM02A.

As can be seen in Figure 5-1 the obtained formation factors range over two orders of magnitude and are fairly well log-normally distributed. The mean values and standard deviations of the curves are shown in Table 5-1 and Table 5-2. The laboratory formation factor logs of KFM01A and KFM02A are shown in Appendix C1 and C2 respectively, as compared to the in-situ formation factor logs.

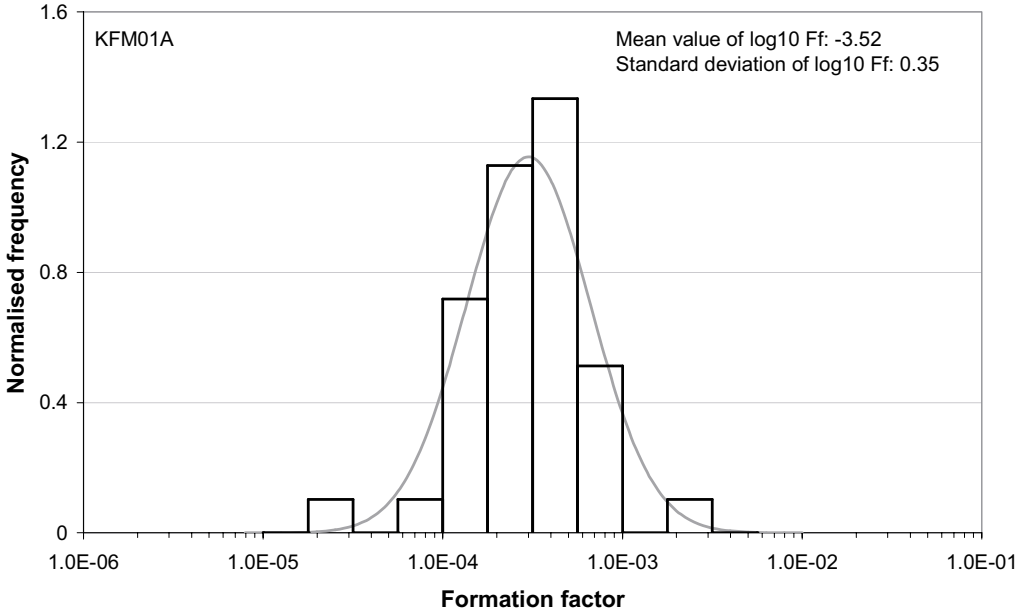

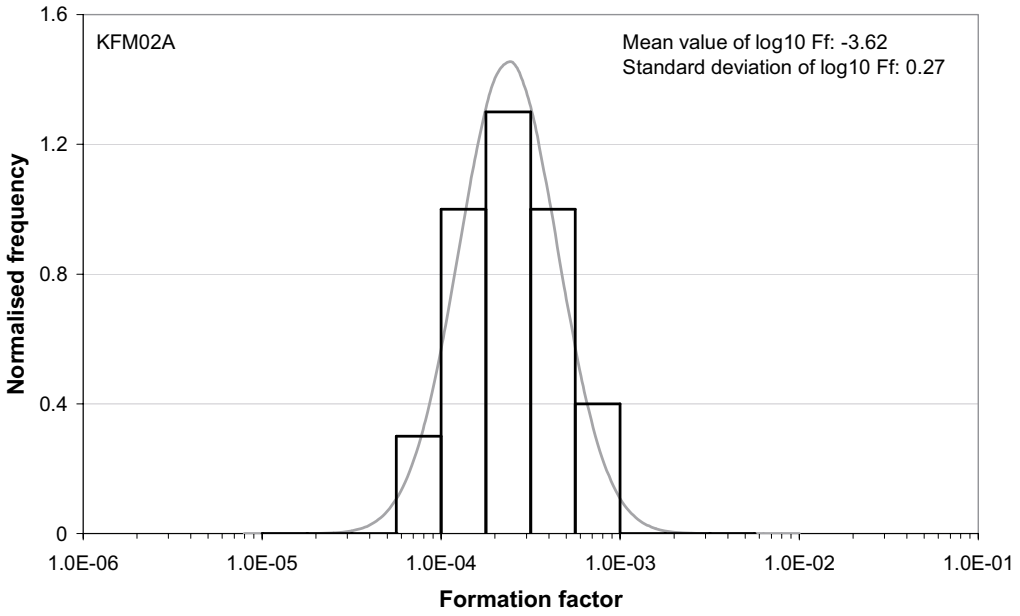

Figure 5-1. *Distribution of laboratory formation factors in KFM01A and KFM02A.*

5.3 In-situ rock matrix formation factor

Figure 5-2 shows the distributions of the rock matrix formation factors obtained in-situ in KFM01A and KFM02A.

The mean values and standard deviations of the curves are shown in Table 5-1 and Table 5-2. The in-situ rock matrix formation factor logs of KFM01A and KFM02A are shown in Appendix C1 and C2 respectively. Rock type specific histograms of the rock matrix formation factor are shown in Appendix D1 and D3 for KFM01A and KFM02A respectively.

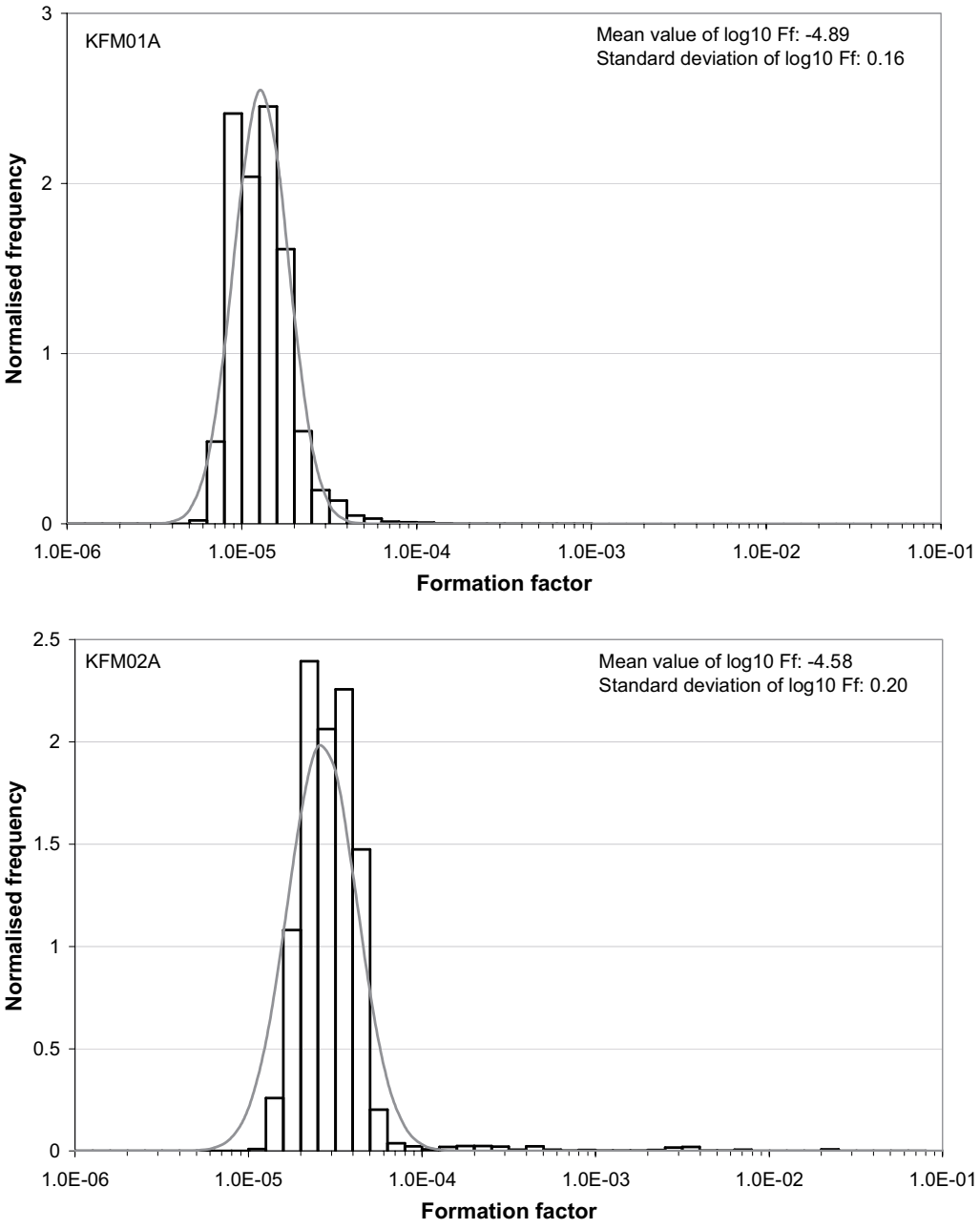

Figure 5-2. *Distribution of in-situ rock matrix formation factors in KFM01A and KFM02A.*

5.4 In-situ fractured rock formation factor

Figure 5-3 shows the distributions of the fractured rock formation factors obtained in-situ in KFM01A and KFM02A.

A deviation from the log-normal distribution was found in the upper formation factor range, where the obtained formation factors may have been affected by free water in hydraulically non-conductive fractures. In addition, a part of KFM02A is surrounded by porous episyenite /8/. The mean values and standard deviations of the curves are shown in Table 5-1 and Table 5-2. The in-situ fractured rock formation factor logs of KFM01A and KFM02A are shown in Appendix C1 and C2 respectively. Rock type specific histograms of the fractured rock formation factor are shown in Appendix D2 and D4 for KFM01A and KFM02A respectively.

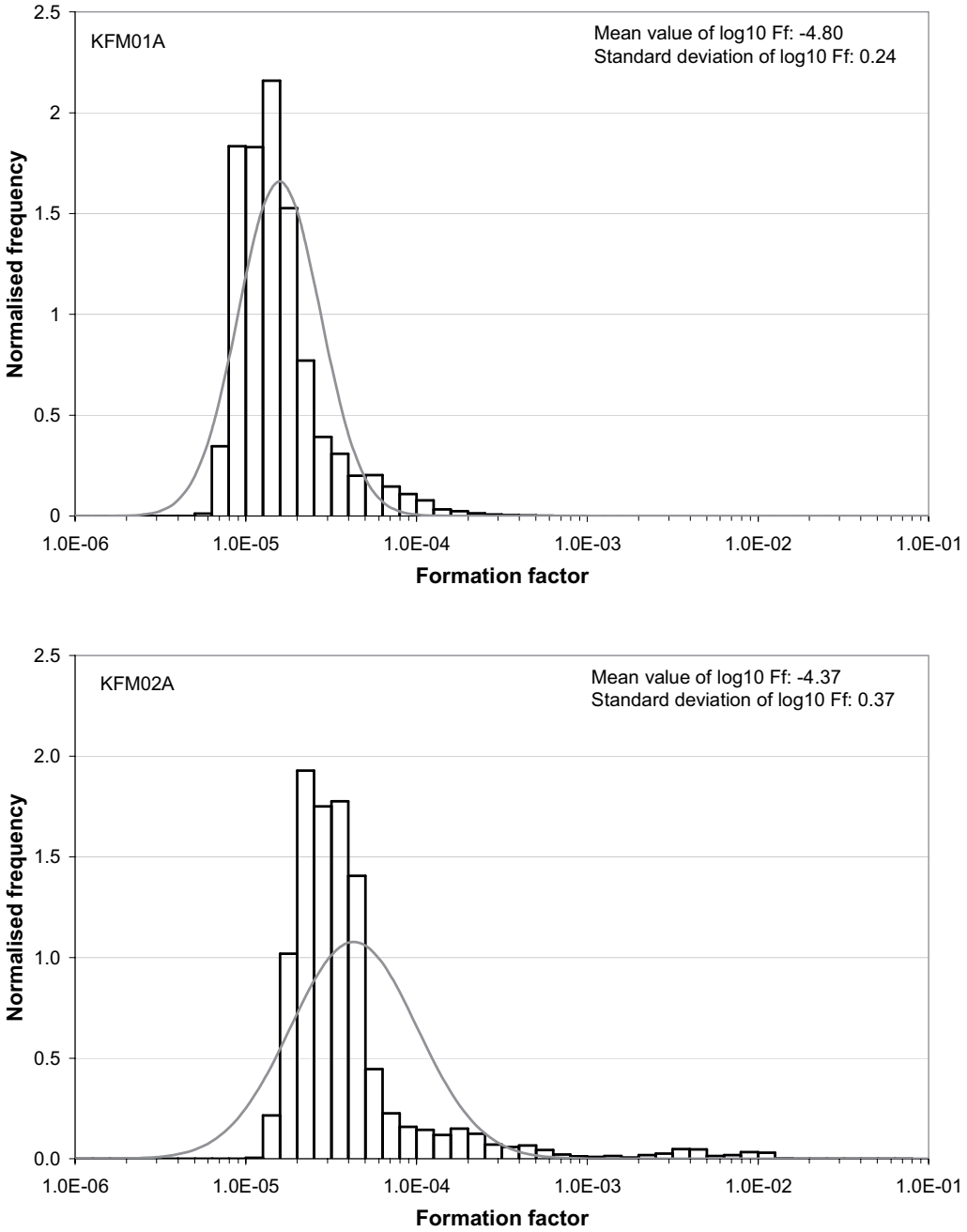

Figure 5-3. *Distribution of in-situ fractured rock formation factors in KFM01A and KFM02A.*

5.5 Comparison of formation factors of KFM01A

Figure 5-4 shows the histograms of the laboratory formation factor, in-situ rock matrix formation factor, and in-situ fractured rock formation factor obtained in KFM01A.

Table 5-1 presents mean values and the standard deviations of the log-normal distributions shown in Figures 5-1 to 5-3 for KFM01A.

Table 5-1. Data for log-normal distribution, KFM01A.

	Mean $\log_{10}$(Ff)	Standard deviation $\log_{10}$(Ff)
Laboratory Ff	–3.52	0.35
In-situ Rock matrix Ff	–4.89	0.16
In-situ Fractured rock Ff	–4.80	0.24

As indicated in Figure 5-4 and Table 5-1, the laboratory formation factors are one order of magnitude larger than those obtained in-situ. This may be due to the fact that the rock samples are de-stressed in the laboratory. The laboratory samples may also have been mechanically damaged in the drilling process and sample preparation. In both these cases, results obtained in the laboratory may be non-conservative.

An alternative comparison could be made if comparing each laboratory formation factor with the in-situ rock matrix formation factor obtained at a corresponding depth. Such a comparison is made in Appendix C3. The laboratory formation factor from a certain borehole length was compared to the mean value of the in-situ rock matrix formation factors taken within 0.5 m of that borehole length. There is a tendency that the ratio between laboratory and in-situ formation factors increases with depth. However, it should be reminded that the extrapolation of the groundwater EC is quite uncertain at depth.

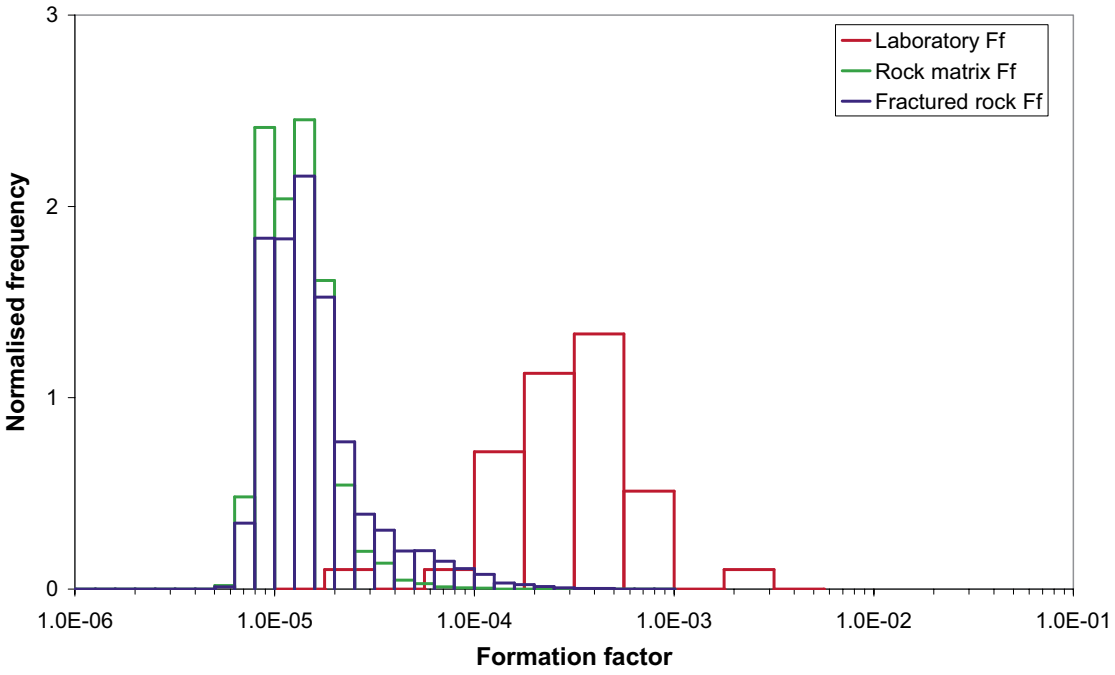

Figure 5-4. *Histograms of formation factors in KFM01A.*

5.6 Comparison of formation factors of KFM02A

Figure 5-5 shows the histograms of the laboratory formation factor, in-situ rock matrix formation factor, and in-situ fractured rock formation factor obtained in KFM02A.

Table 5-2 shows mean values and the standard deviations of the log-normal distributions shown in Figures 5-1 to 5-3 for KFM02A.

Table 5-2. Data for log-normal distribution, KFM02A.

	Mean $\log_{10}$(Ff)	Standard deviation $\log_{10}$(Ff)
Laboratory Ff	–3.62	0.27
In-situ Rock matrix Ff	–4.58	0.20
In-situ Fractured rock Ff	–4.37	0.37

As indicated in Figure 5-5 and Table 5-2, the laboratory formation factors are one order of magnitude larger than those obtained in-situ. This may be due to the fact that the rock samples are de-stressed in the laboratory. The laboratory samples may also have been mechanically damaged in the drilling process and sample preparation. In both these cases, results obtained in the laboratory may be non-conservative.

An alternative comparison could be made if comparing each laboratory formation factor with the in-situ rock matrix formation factor obtained at a corresponding depth. Such a comparison is made in Appendix C4. The laboratory formation factor from a certain borehole length was compared to the mean value of the in-situ rock matrix formation factors taken within 0.5 m of that borehole length. As for KFM01A, there is a tendency that the ratio between laboratory and in-situ formation factors increases with depth. Again, it should be reminded that the extrapolation of the groundwater EC is quite uncertain at depth.

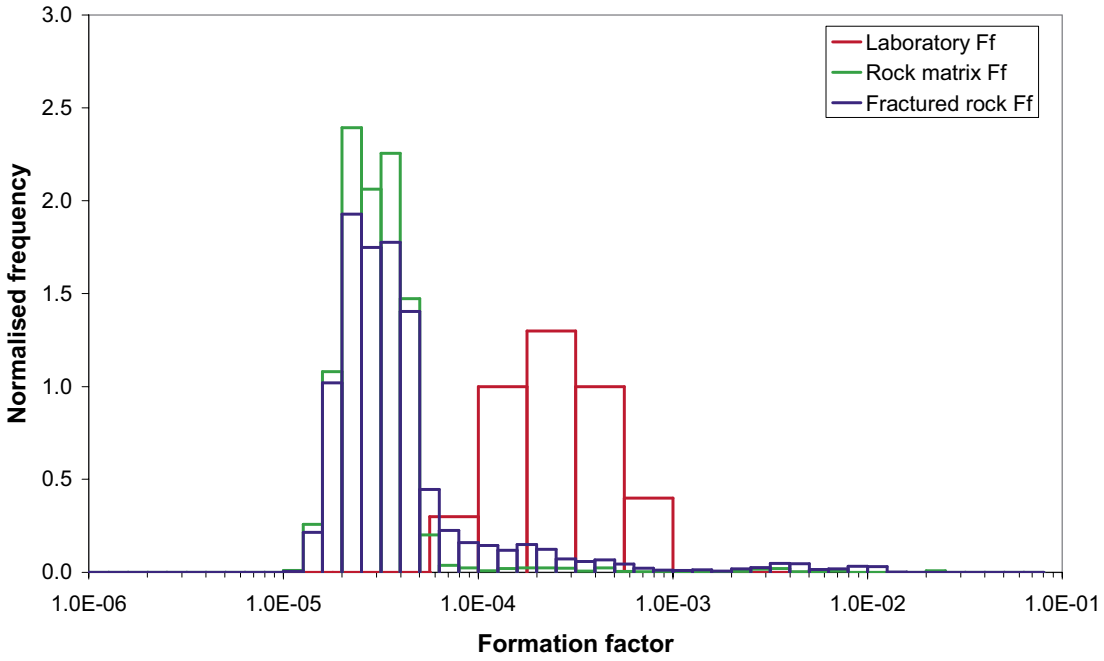

Figure 5-5. *Histograms of formation factors in KFM02A.*

6 Summary and discussions

The formation factors obtained in KFM01A and KFM02A range from $5.4 \cdot 10^{-6}$ to $2.5 \cdot 10^{-2}$. The formation factors appear to be distributed according to the log-normal distribution.

The rock within the Forsmark site investigation area is less fractured than within the Oskarshamn site investigation area, where in-situ formation factor logs previously have been obtained by electrical methods. Therefore, the rock resistivity logs obtained in Forsmark are less influenced by free water in open fractures and a more reliable comparison of laboratory and in-situ formation factors could be made. This enables a better understanding of the compression factor. The compression factor describes how many times less the formation factor is in-situ compared to that of de-stressed rock in the laboratory. It appears that the compression factor is at least one order of magnitude, which is larger than previously expected from e.g. /16/, and is slightly increasing with depth in Forsmark.

The fact that the compression factor is so large has two major implications. Firstly, effective and apparent diffusivities obtained in the laboratory may have to be corrected as they are overestimated. Secondly, one may not be able to directly say that the porous system is open for migration of anions in-situ, even if this has been shown in the laboratory on samples from bore cores. If the compression factor is large enough, the porous system may be so compressed that the positively charged diffuse double layers overlap in a significant part of the constricted pores. This may effectively hinder anion migration. Very little is known about the relation between the compression factor and anion exclusion and further investigations are recommended.

Even if one could argue that some parts of the porous system may be inaccessible for anion migration in-situ, it is likely that diffusion will occur into open fractures with stagnant water intersecting hydraulically conductive fractures. This potential source of radionuclide retention may have to be more relied upon when it comes to anions than it is at present.

Another explanation for the discrepancy, in obtained laboratory and in-situ formation factors, is that the samples brought to the laboratory have been subjected to mechanical damage in the drilling process and sample preparation. At present it has not been established if the discrepancy is mainly due to the stress release of the laboratory samples or due to the induced mechanical damage. Further investigations are recommended.

References

/1/ **Probst H, Schröter H, Kraft E, Andersson P, 2004.** Focused resistivity logging in boreholes KFM01A and KFM02A. Site investigation report. SKB P-XX-XX, in progress. Svensk Kärnbränslehantering AB.

/2/ **Rouhiainen P, Pöllänen J, 2003.** Difference flow logging of borehole KFM01A. Site investigation report. SKB P-03-28, Svensk Kärnbränslehantering AB.

/3/ **Rouhiainen P, Pöllänen J, 2004.** Difference flow logging in borehole KFM02A. Site investigation report. SKB P-04-188, Svensk Kärnbränslehantering AB.

/4/ **Löfgren M, Neretnieks I, in prep.** Formation factor logging in-situ and in the laboratory by electrical methods in KSH01A and KSH02: Measurements and evaluation of methodology. Site investigation report SKB P-05-27, Svensk Kärnbränslehantering AB.

/5/ **Wacker P, Bergelin A, Nilsson A-C, 2003.** Complete hydrochemical characterisation in KFM01A: Results from two investigated sections, 110.1–120.8 and 176.8–183.9 metres. Site investigation report SKB P-03-94, Svensk Kärnbränslehantering AB.

/6/ **Wacker P, Bergelin A, Nilsson A-C, 2004.** Hydrochemical characterisation in KFM02A: Results from three investigated borehole sections, 106.5-126.5, 413.5-433.5 and 509.0–516.1 m. Site investigation report SKB P-04-70, Svensk Kärnbränslehantering AB.

/7/ **Petersson J, Wängnerud A, 2003**. Boremap mapping of telescopic drilled borehole KFM01A. Site investigation report SKB P-03-23, Svensk Kärnbränslehantering AB.

/8/ **Petersson J, Wängnerud A, Stråhle A, 2003.** Boremap mapping of telescopic drilled borehole KFM02A. Site investigation report SKB P-03-98, Svensk Kärnbränslehantering AB.

/9/ **Löfgren M, Neretnieks I, 2002.** Formation factor logging in-situ by electrical methods. Background and methodology. SKB TR-02-27, Svensk Kärnbränslehantering AB.

/10/ **Löfgren M, 2001.** Formation factor logging in igneous rock by electrical methods. Licentiate thesis at the Royal Institute of Technology, Stockholm, Sweden. ISBN 91-7283-207-x.

/11/ **Ohlsson Y, 2000.** Studies of Ionic Diffusion in Crystalline Rock. Doctoral thesis at the Royal Institute of Technology, Stockholm, Sweden. ISBN 91-7283-025-5.

/12/ **Löfgren M, 2004.** Diffusive properties of granitic rock as measured by in-situ electrical methods. Doctoral thesis at the Royal Institute of Technology, Stockholm, Sweden. ISBN 91-7283-935-x.

/13/ **Laaksoharju M, Gimeno M, Auqué L, Gómez J, Smellie J, Tullborg E-L, Gurban I, 2004.** Hydrogeochemical evaluation of the Forsmark site, model version 1.1. SKB R-04-05, Svensk Kärnbränslehantering AB.

/14/ **Thunehed H, 2005.** Forsmark site investigation. Resistivity measurements on samples from KFM01A and KFM02A. Site investigation report. SKB P-05-26, Svensk Kärnbränslehantering AB.

/15/ **Johnson RA, 1994.** Miller and Freund's probability & statistics for engineers, 5ed Prentice-Hall Inc, ISBN 0-13-721408-1.

/16/ **Skagius K, 1986.** Diffusion of dissolved species in the matrix of some Swedish crystalline rocks. Doctoral thesis at the Royal Institute of Technology, Stockholm, Sweden.

Appendix A

Appendix A1: Laboratory formation factor for rock samples from KFM01A

Secup (m)	Formation factor	Secup (m)	Formation factor
101.48	1.54E–04	600.00	3.65E–04
119.98	2.04E–04	620.00	4.03E–04
140.00	2.75E–03	640.05	3.08E–04
159.80	1.19E–04	659.85	3.55E–04
199.95	1.85E–05	680.00	3.95E–04
240.00	3.09E–04	699.95	3.75E–04
259.90	3.66E–04	719.95	3.06E–04
300.00	1.74E–04	760.00	4.57E–04
320.00	1.52E–04	780.00	3.80E–04
340.00	1.75E–04	800.00	6.57E–04
360.00	2.34E–04	820.00	7.76E–04
380.00	1.08E–04	840.16	9.28E–05
420.00	2.04E–04	860.00	2.78E–04
440.00	2.57E–04	880.00	4.64E–04
460.00	3.48E–04	900.00	2.50E–04
480.00	1.66E–04	920.00	8.53E–04
501.72	3.68E–04	940.05	7.86E–04
520.00	2.77E–04	960.00	5.84E–04
560.00	2.86E–04	980.00	5.11E–04
580.00	4.64E–04		

Secup = upper position in borehole for sample.

Appendix A2: Laboratory formation factor for rock samples from KFM02A

Secup (m)	Formation factor	Secup (m)	Formation factor
100.00	9.33E–05	620.95	1.89E–04
121.00	1.47E–04	641.00	2.09E–04
141.00	1.21E–04	661.00	2.05E–04
161.00	1.60E–04	681.00	2.01E–04
201.00	7.19E–05	701.00	2.91E–04
221.00	2.40E–04	721.00	3.48E–04
241.00	1.28E–04	741.00	2.90E–04
261.00	7.17E–04	761.00	2.63E–04
321.00	1.97E–04	781.00	3.64E–04
361.00	1.59E–04	801.00	3.63E–04
401.00	3.06E–04	821.00	3.77E–04
420.92	2.59E–04	841.00	3.70E–04
440.95	1.00E–04	861.00	6.74E–04
460.95	3.46E–04	881.00	4.66E–04
500.67	5.65E–04	901.00	3.30E–04
521.00	2.45E–04	921.00	1.44E–04
541.00	1.52E–04	941.00	4.84E–04
561.00	1.34E–04	961.00	6.05E–04
580.88	8.04E–05	981.03	2.09E–04
601.00	1.44E–04	1,001.00	3.76E–04

Secup = upper position in borehole.

Appendix B

Appendix B1: In-situ rock resistivities and fractures KFM01A

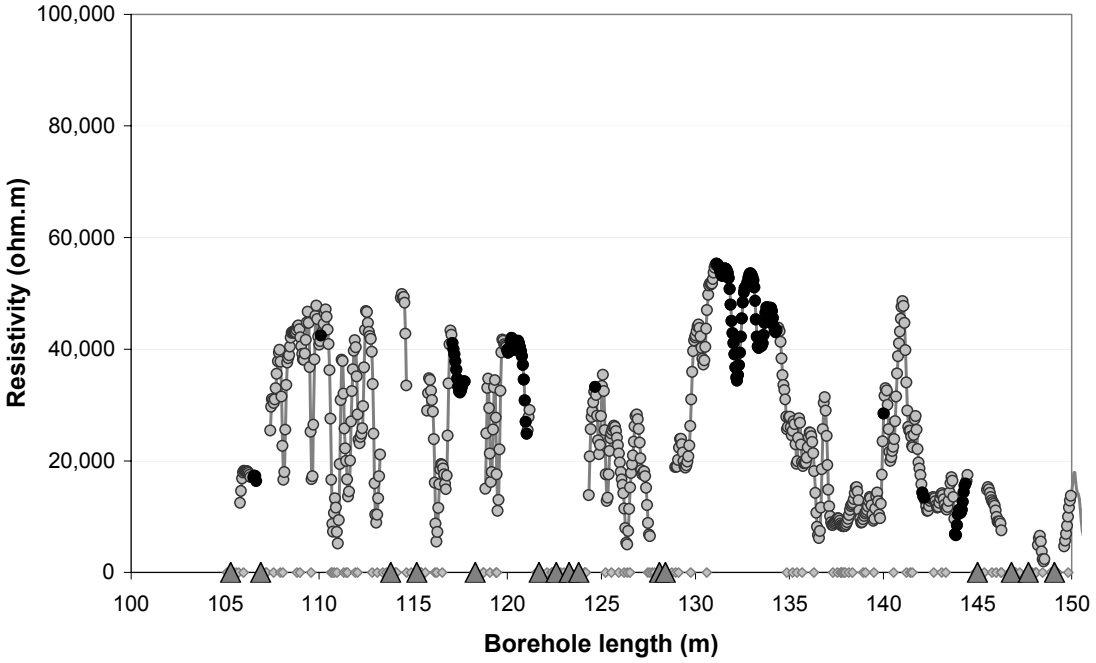

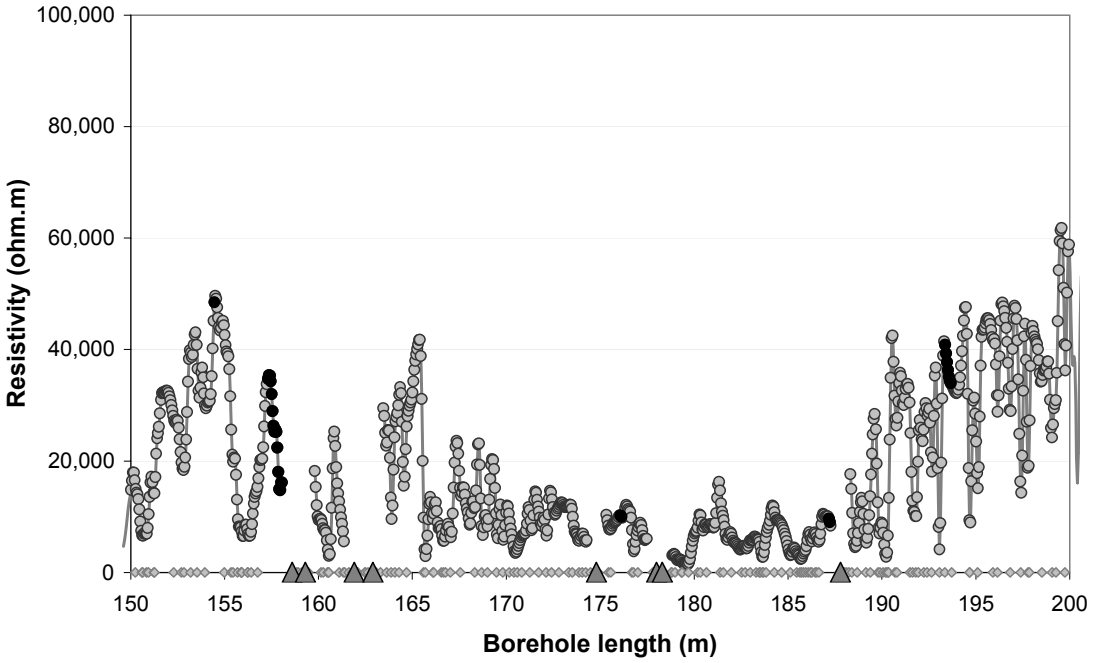

Fractured rock resistivity
Rock matrix resistivity
Location of natural fracture parting the bore core
Location of hydraulically conductive fracture detected in the difference flow logging

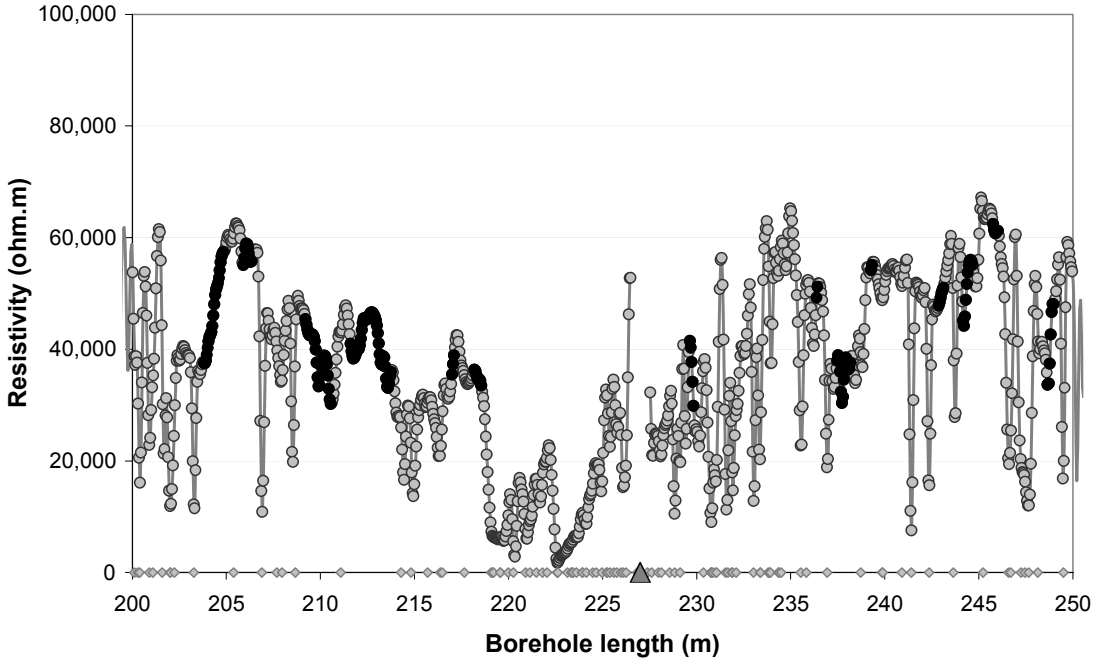

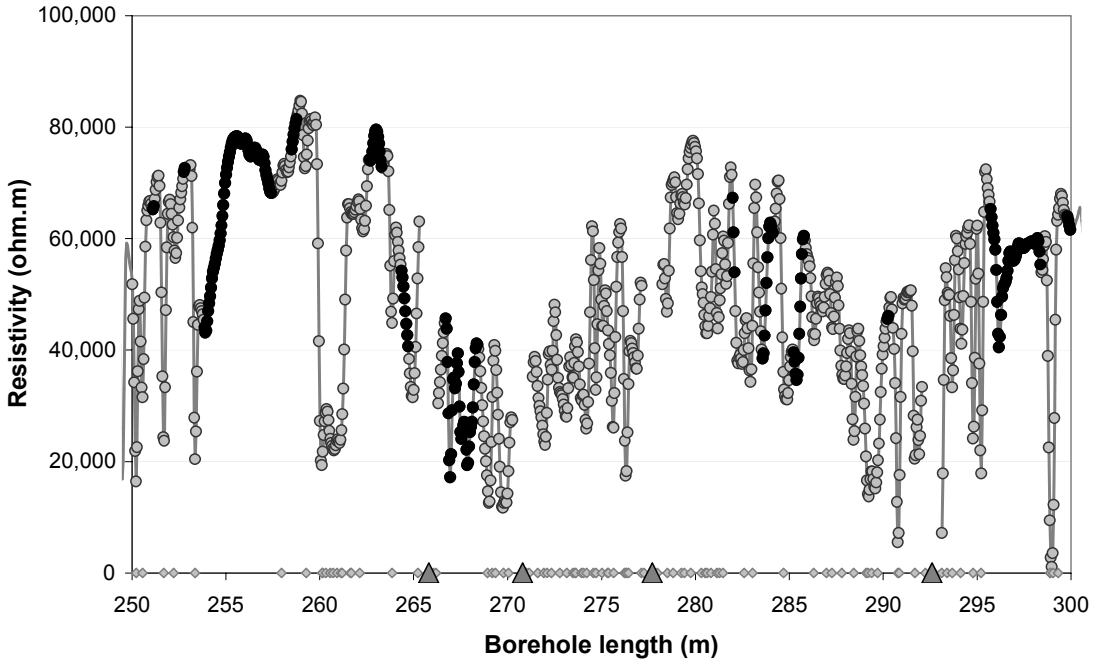

Fractured rock resistivity
Rock matrix resistivity
Location of natural fracture parting the bore core
Location of hydraulically conductive fracture detected in the difference flow logging

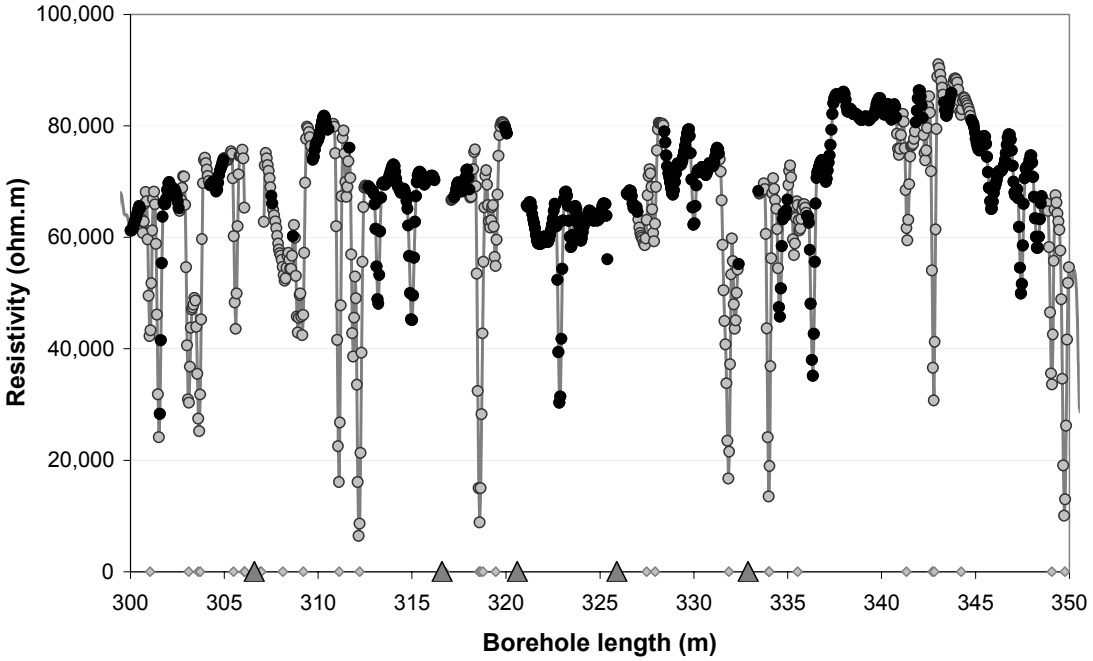

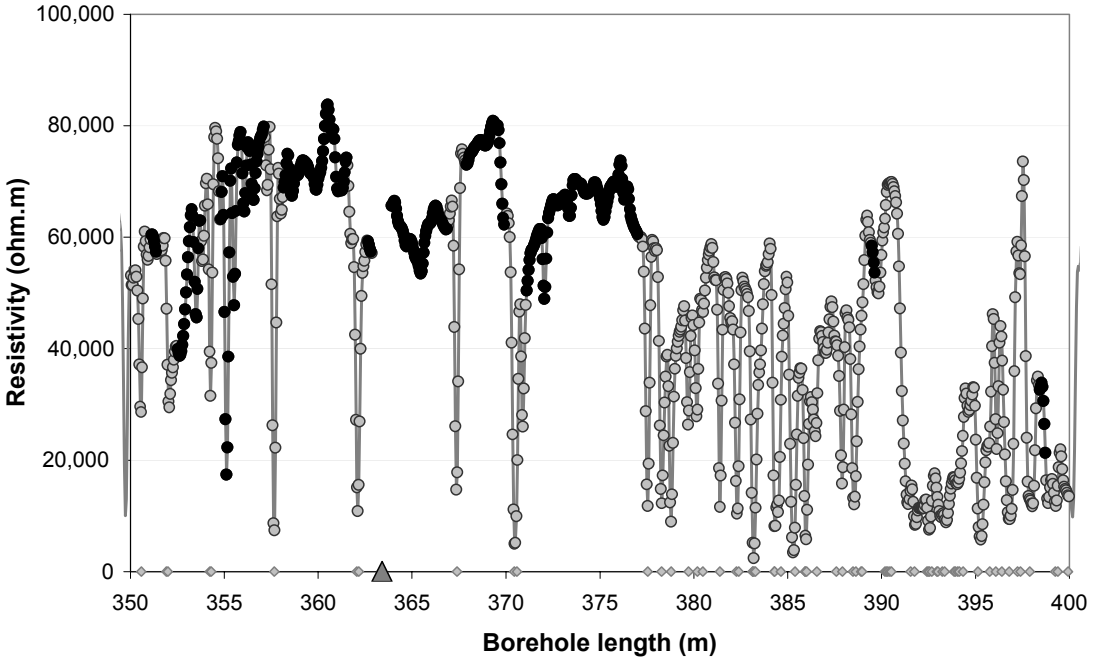

Fractured rock resistivity
Rock matrix resistivity
Location of natural fracture parting the bore core
Location of hydraulically conductive fracture detected in the difference flow logging

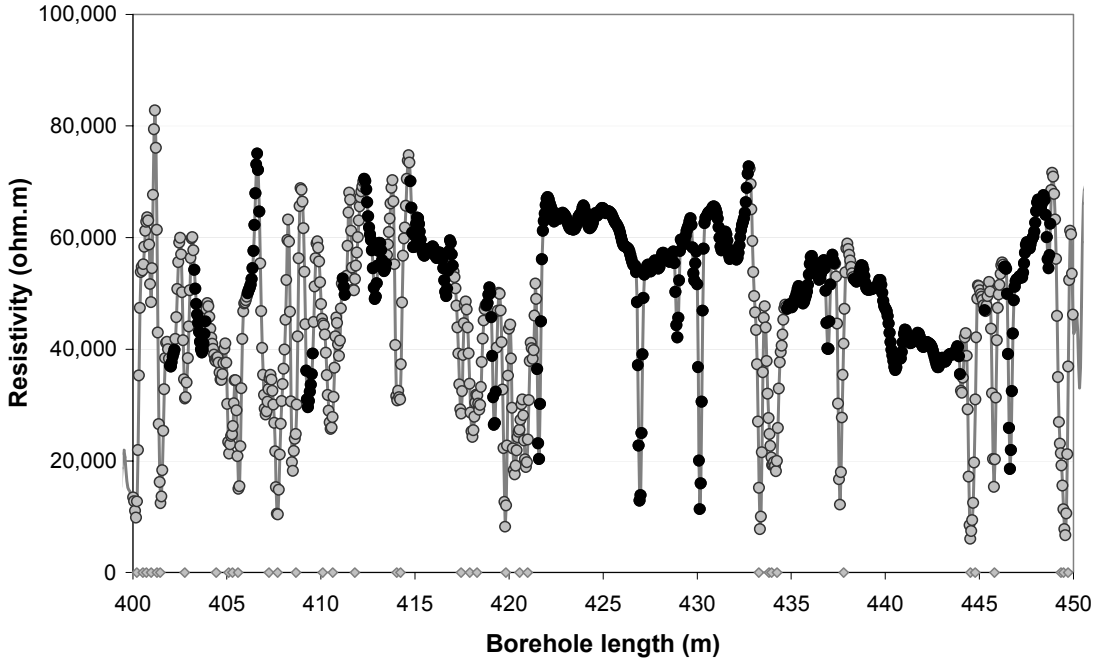

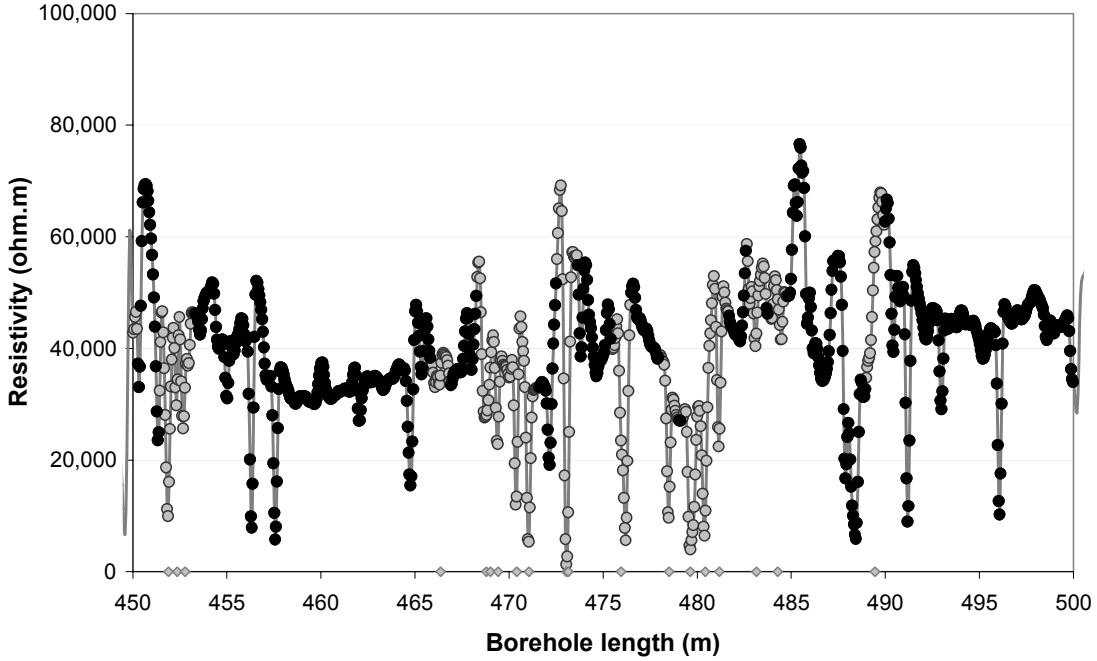

Fractured rock resistivity
Rock matrix resistivity
Location of natural fracture parting the bore core
Location of hydraulically conductive fracture detected in the difference flow logging

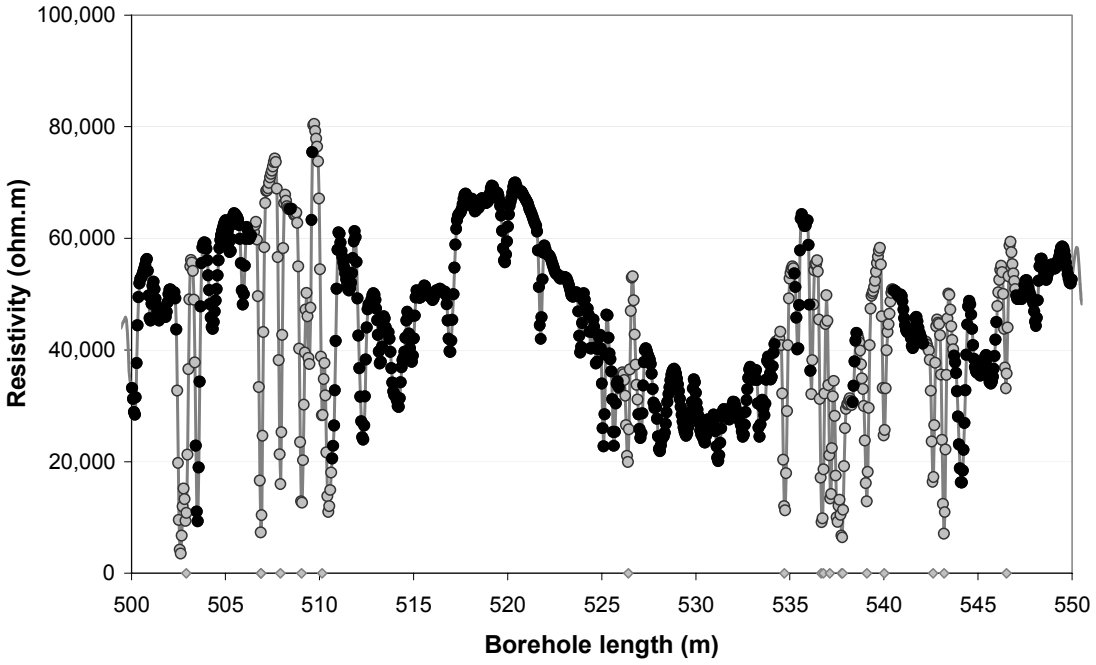

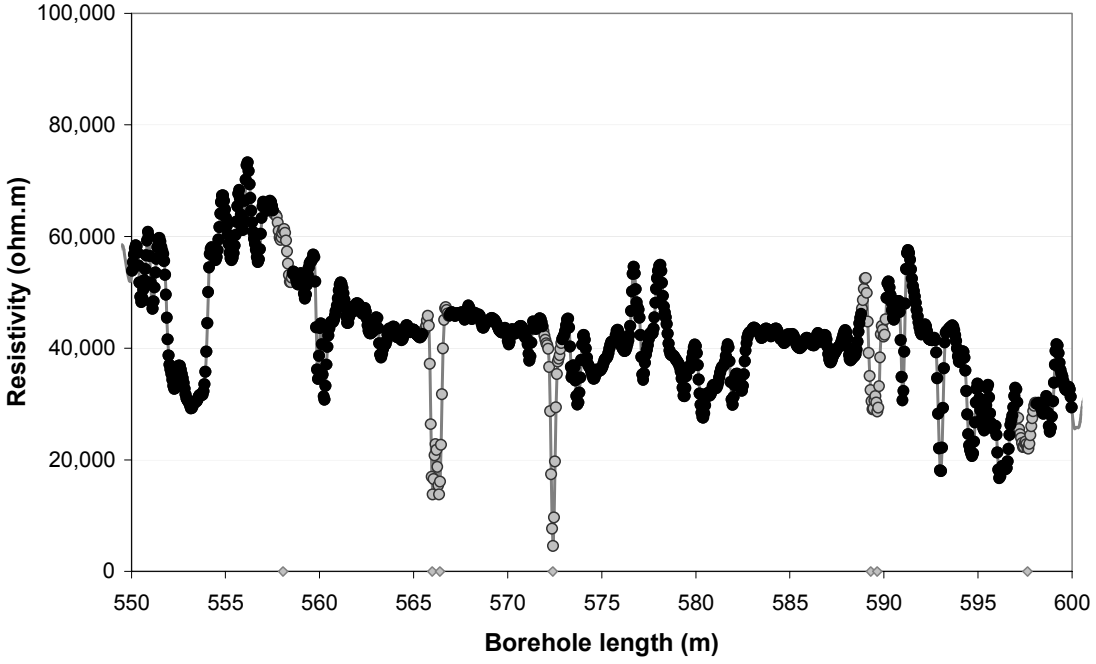

Fractured rock resistivity
Rock matrix resistivity
Location of natural fracture parting the bore core
Location of hydraulically conductive fracture detected in the difference flow logging

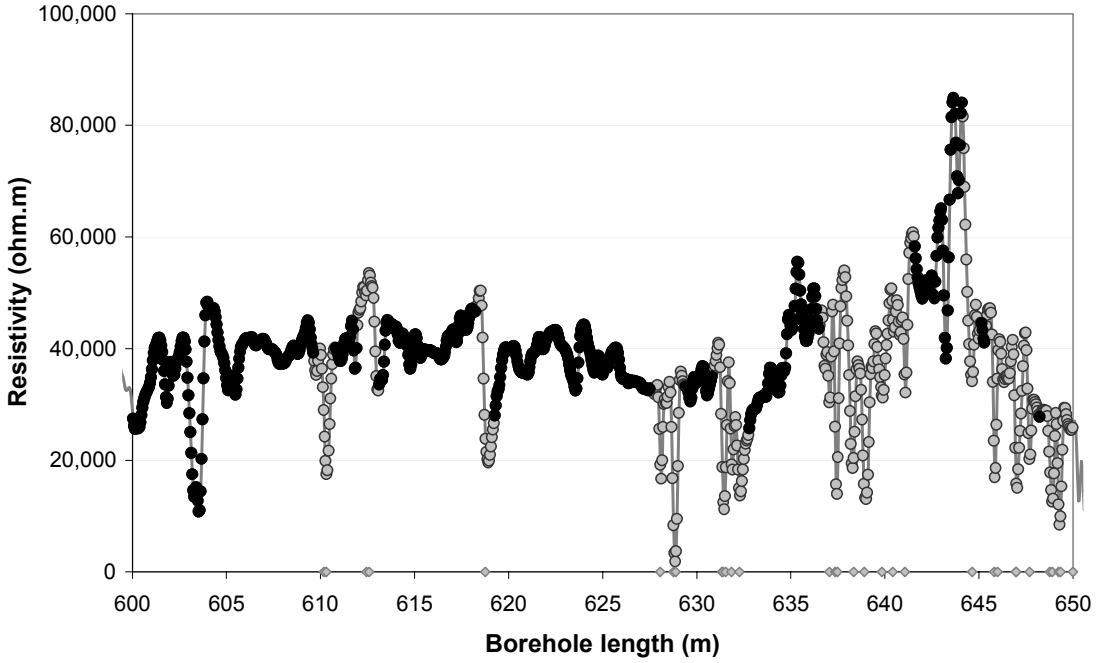

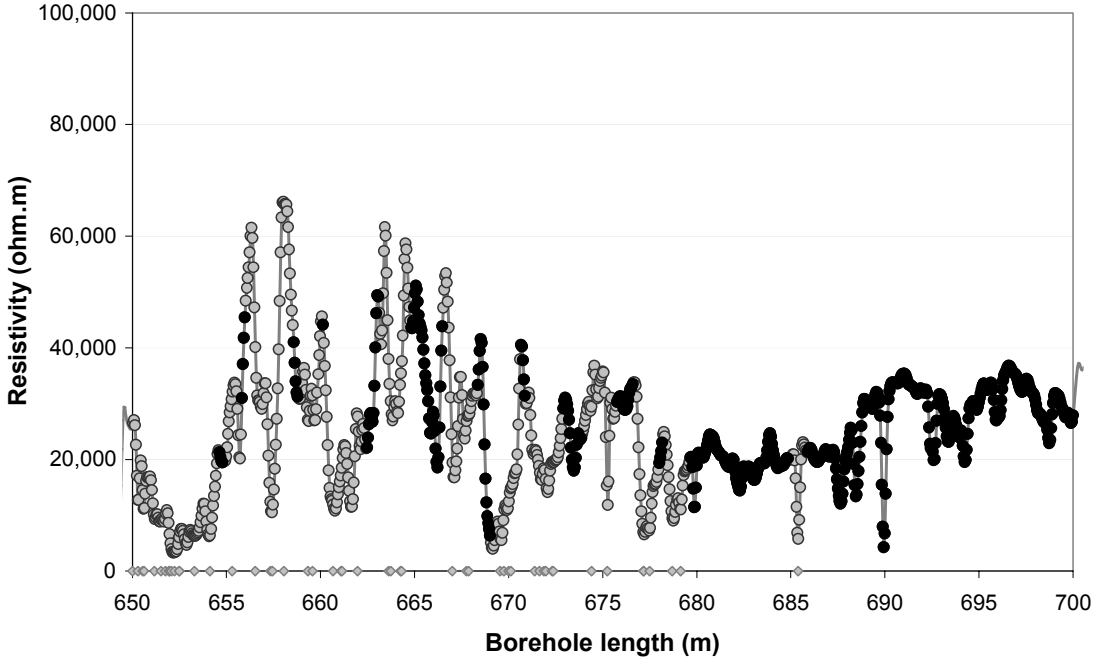

Fractured rock resistivity
Rock matrix resistivity
Location of natural fracture parting the bore core
Location of hydraulically conductive fracture detected in the difference flow logging

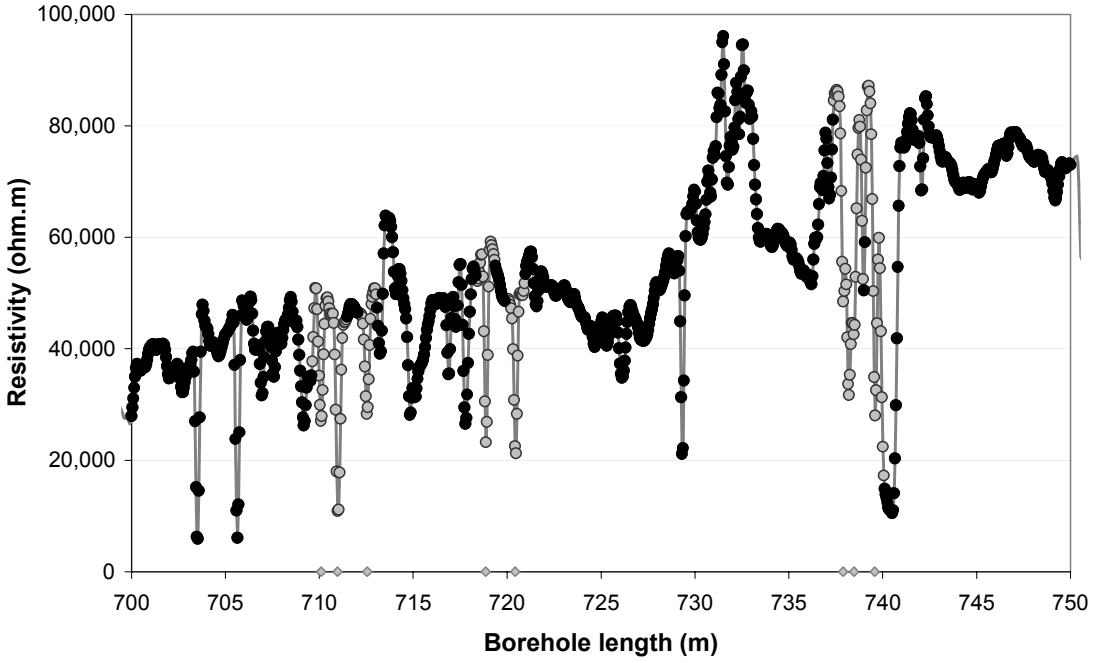

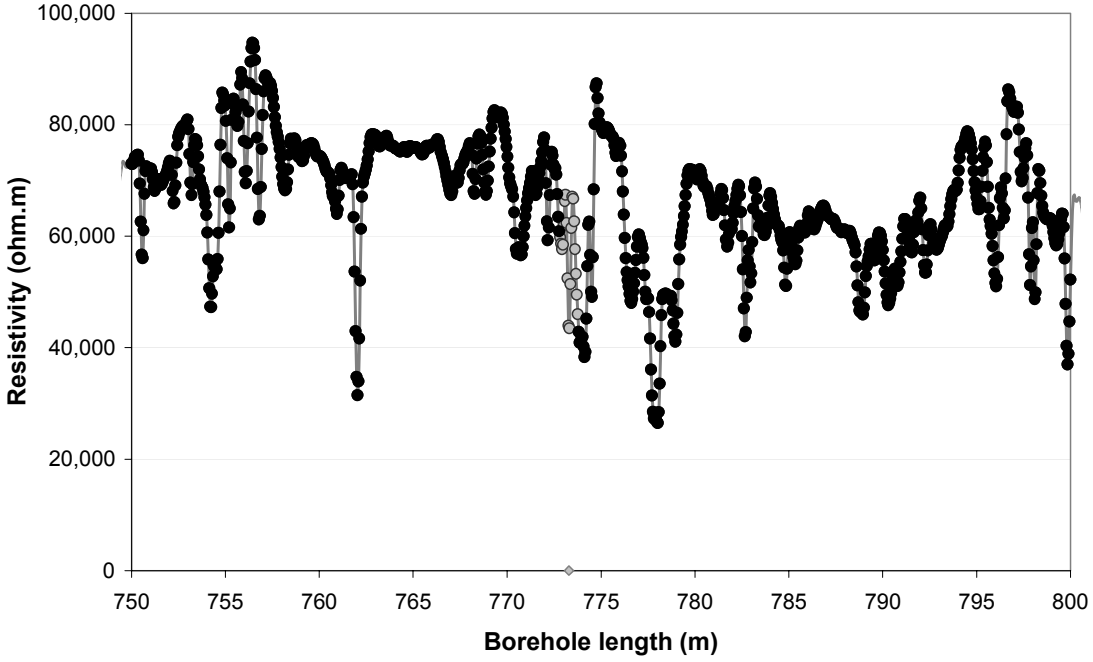

Fractured rock resistivity
Rock matrix resistivity
Location of natural fracture parting the bore core
Location of hydraulically conductive fracture detected in the difference flow logging

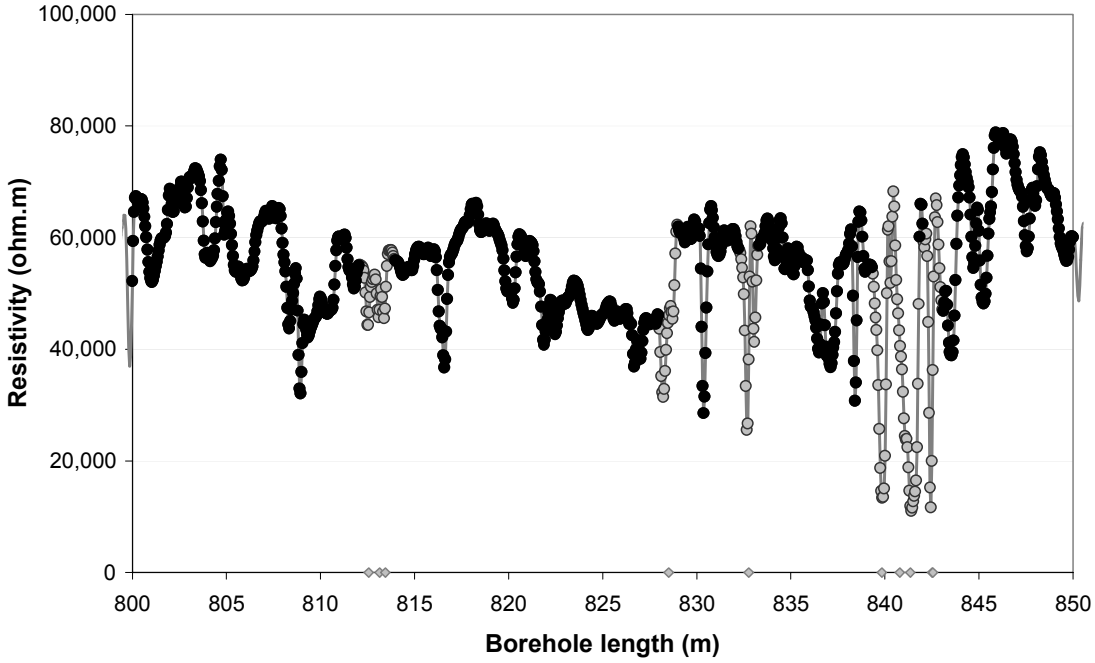

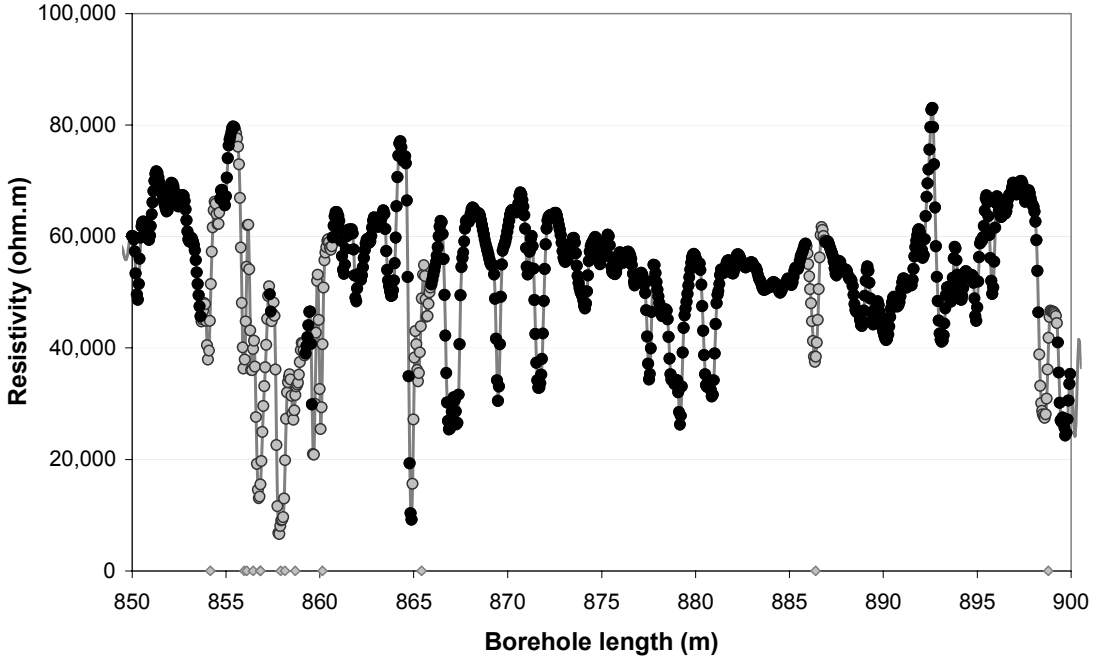

Fractured rock resistivity
Rock matrix resistivity
Location of natural fracture parting the bore core
Location of hydraulically conductive fracture detected in the difference flow logging

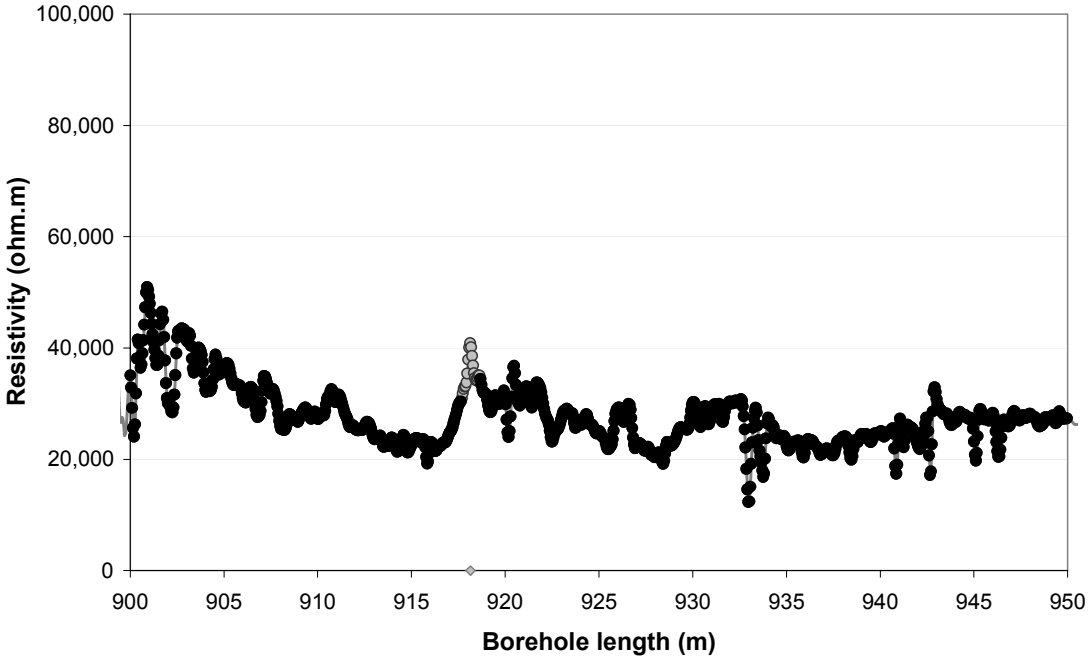

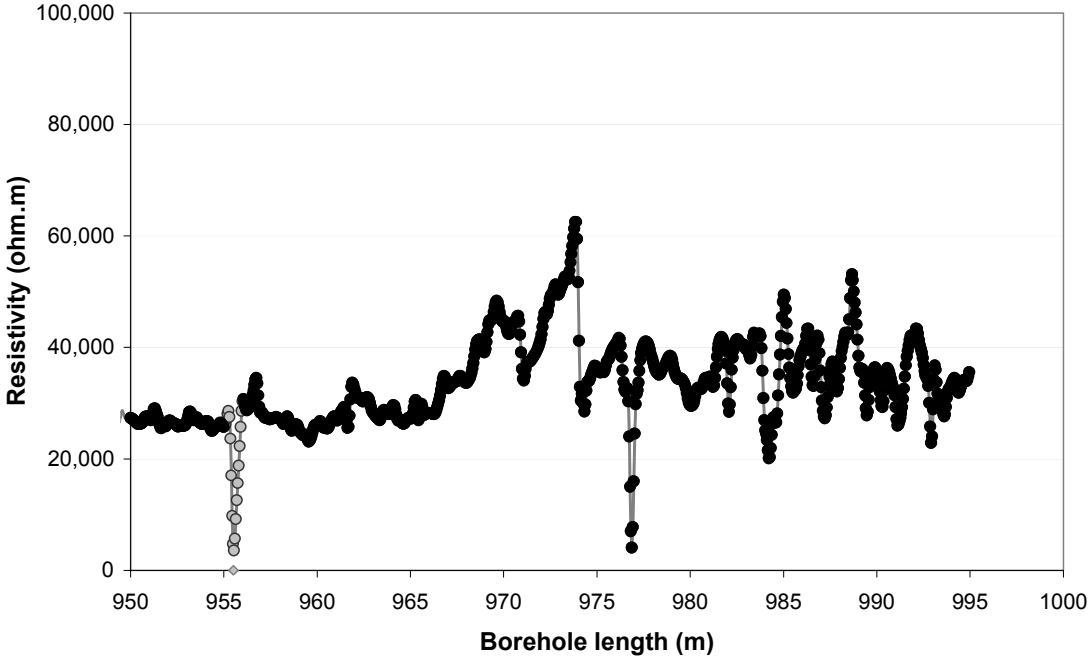

Fractured rock resistivity
Rock matrix resistivity
Location of natural fracture parting the bore core
Location of hydraulically conductive fracture detected in the difference flow logging

Appendix B2: In-situ rock resistivities and fractures KFM02A

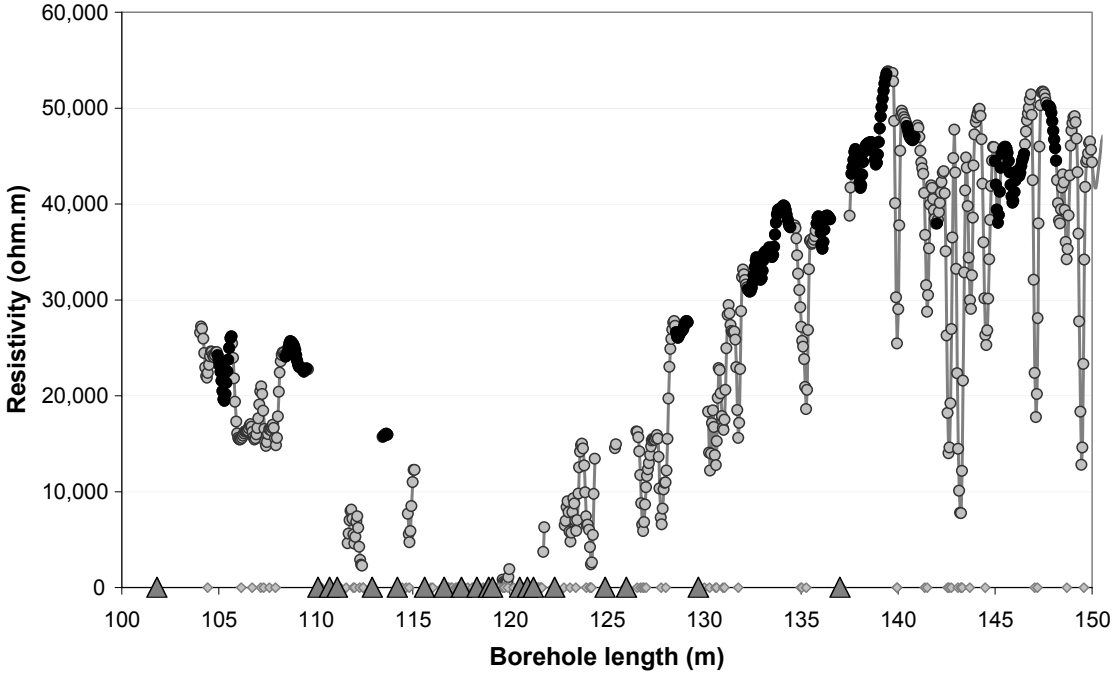

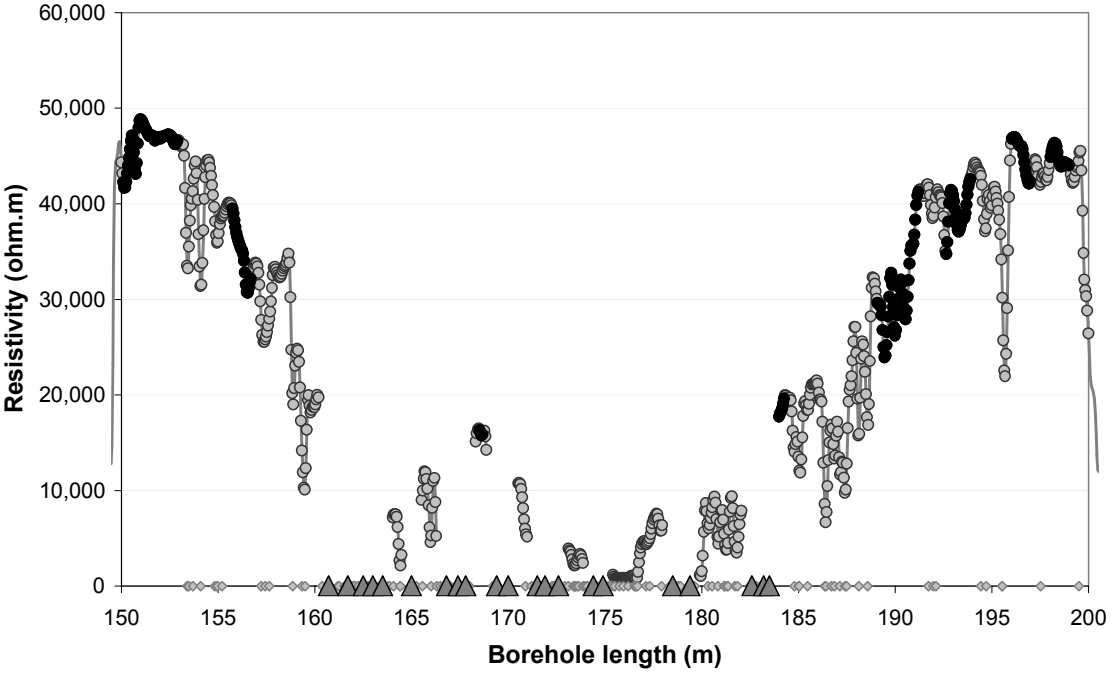

Fractured rock resistivity
Rock matrix resistivity
Location of natural fracture parting the bore core
Location of hydraulically conductive fracture detected in the difference flow logging

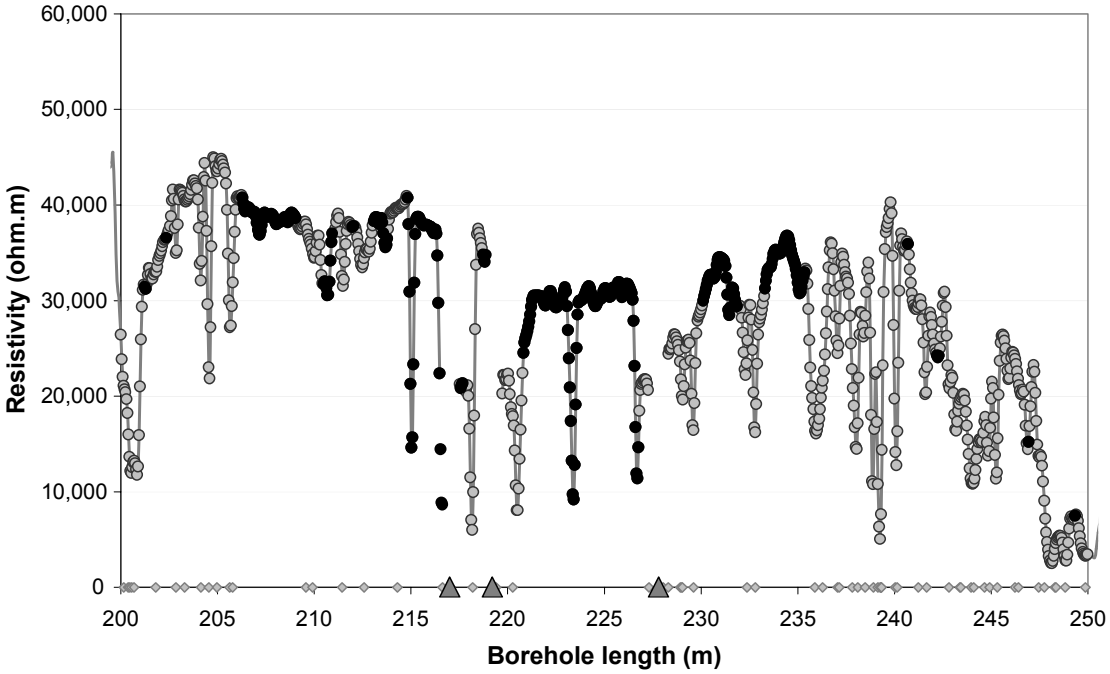

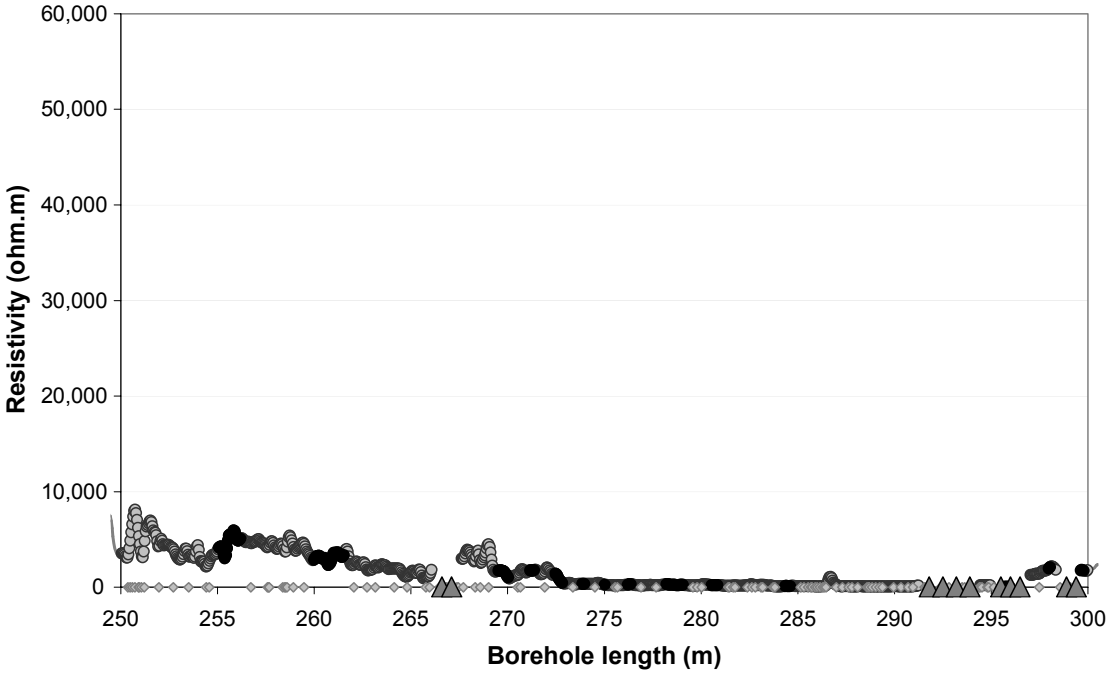

Fractured rock resistivity
Rock matrix resistivity
Location of natural fracture parting the bore core
Location of hydraulically conductive fracture detected in the difference flow logging

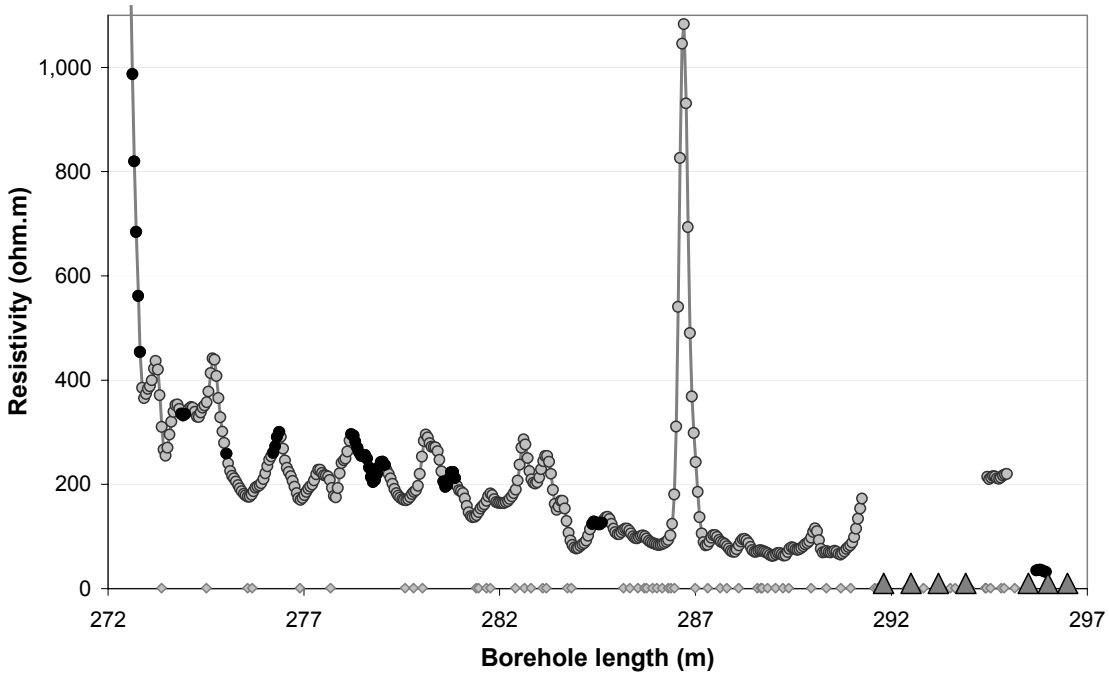

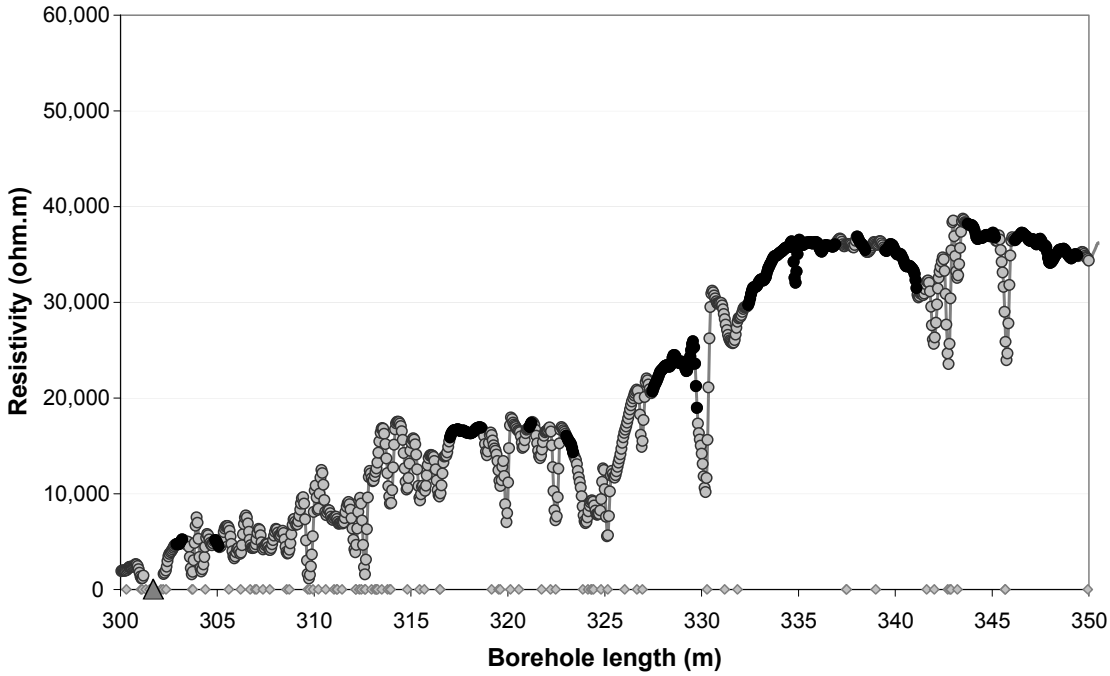

Fractured rock resistivity
Rock matrix resistivity
Location of natural fracture parting the bore core
Location of hydraulically conductive fracture detected in the difference flow logging

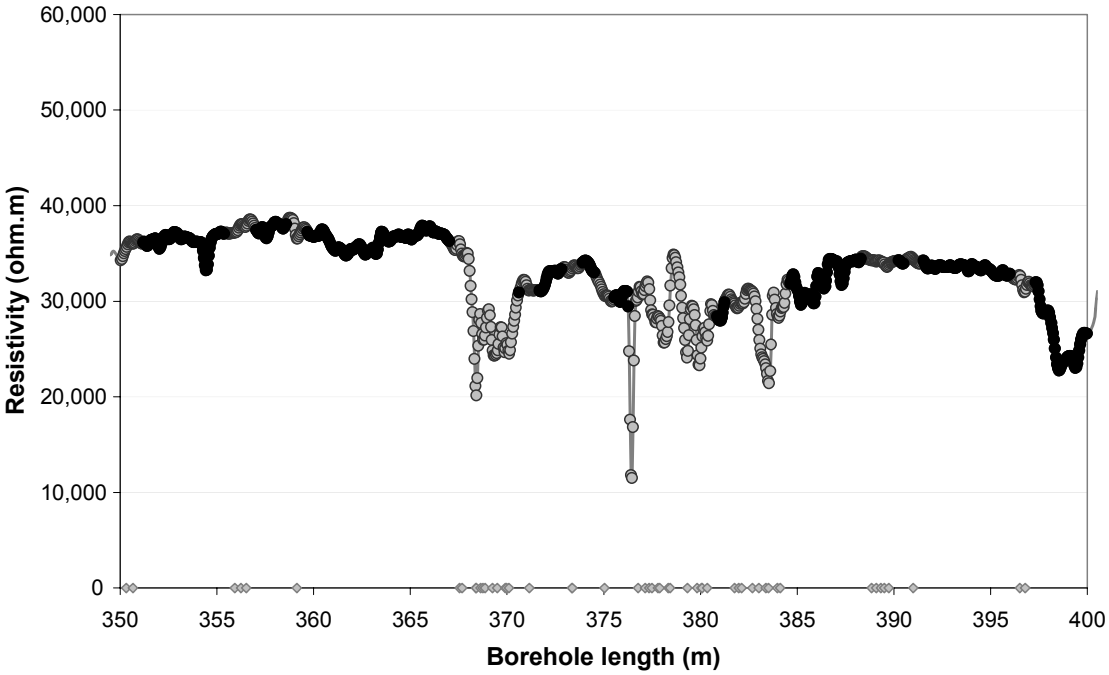

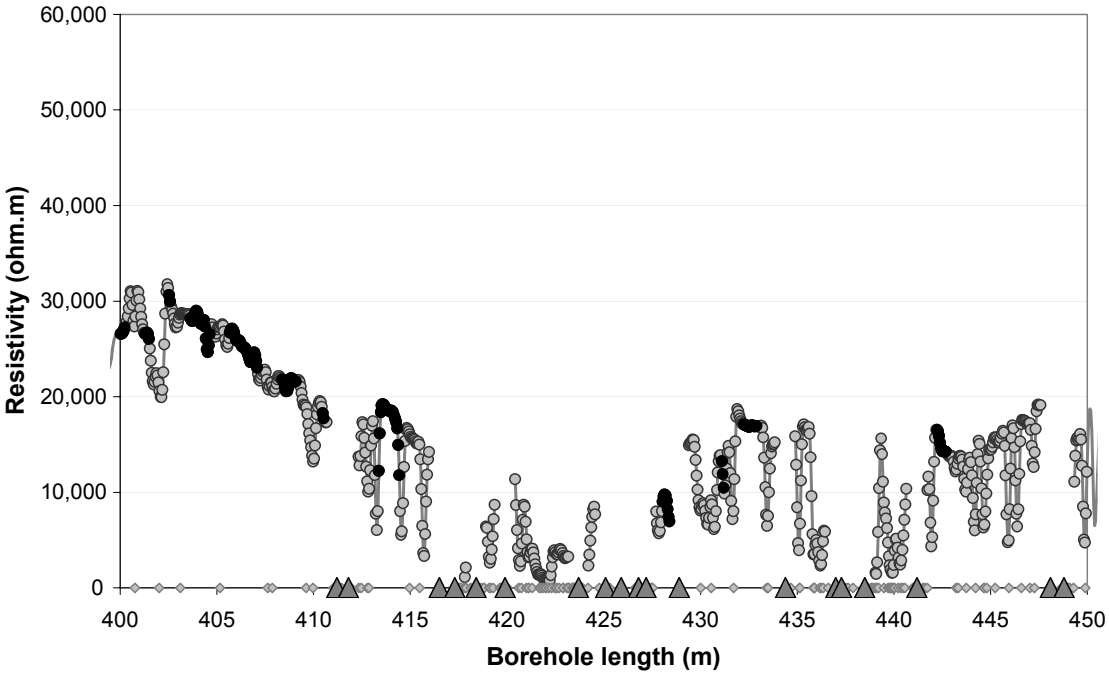

Fractured rock resistivity
Rock matrix resistivity
Location of natural fracture parting the bore core
Location of hydraulically conductive fracture detected in the difference flow logging

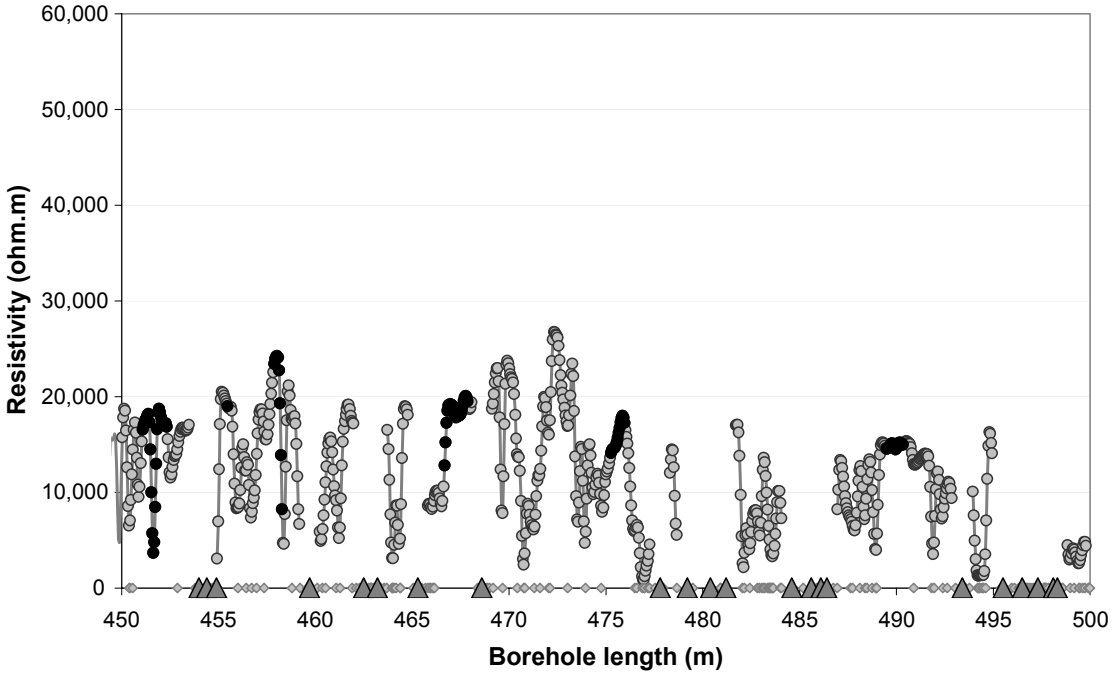

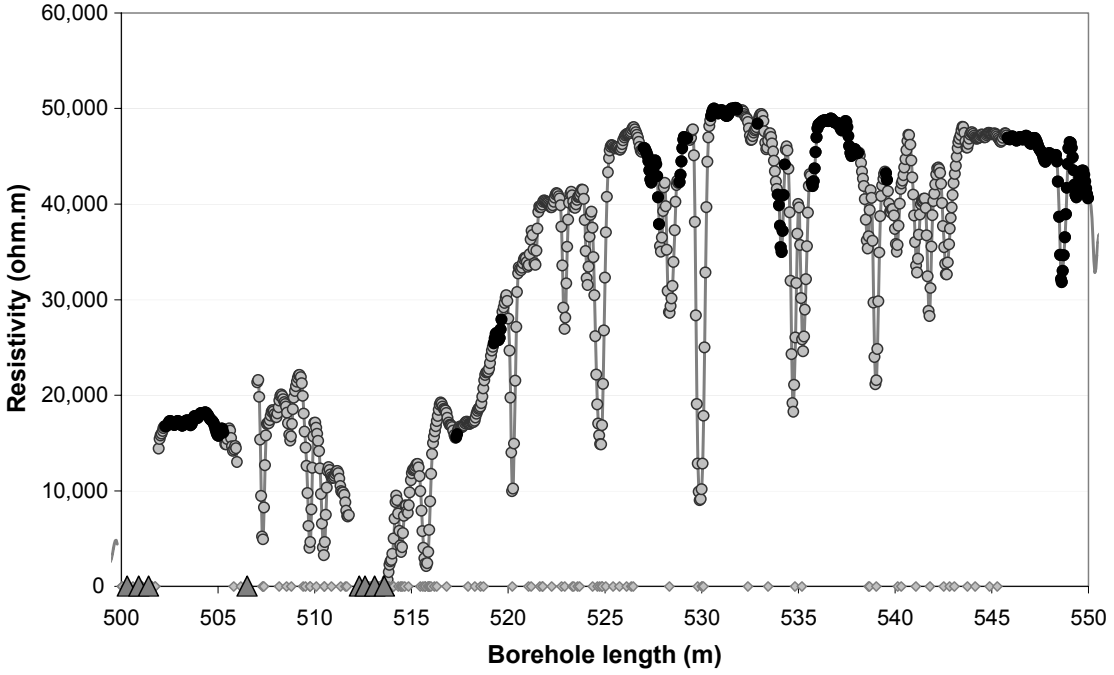

Fractured rock resistivity
Rock matrix resistivity
Location of natural fracture parting the bore core
Location of hydraulically conductive fracture detected in the difference flow logging

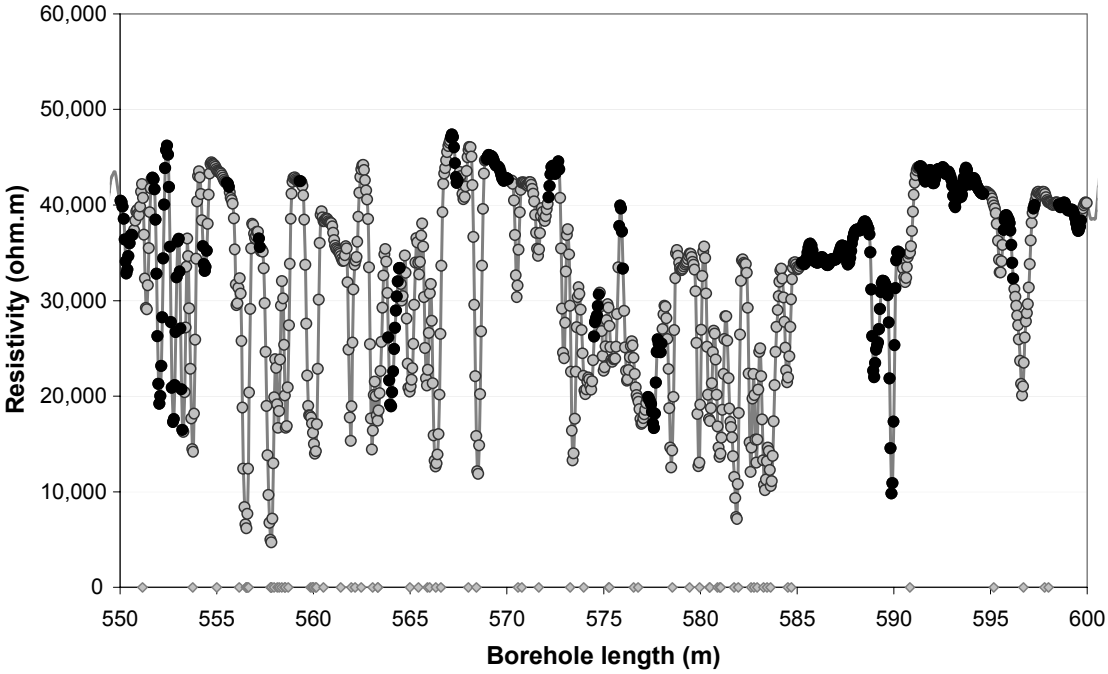

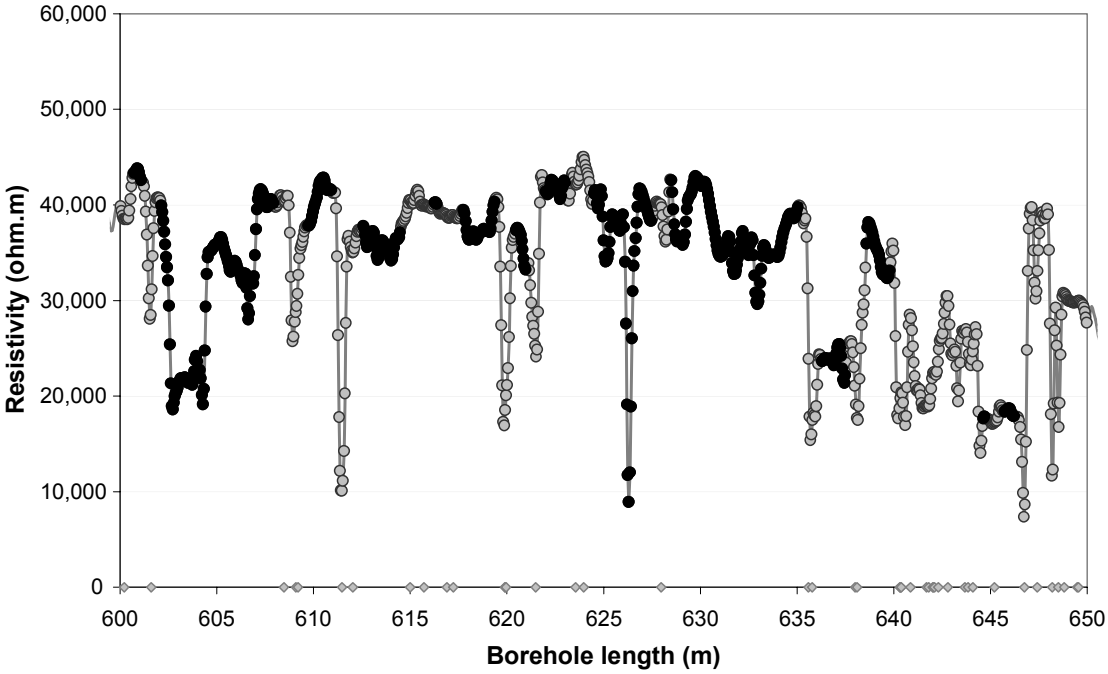

Fractured rock resistivity
Rock matrix resistivity
Location of natural fracture parting the bore core
Location of hydraulically conductive fracture detected in the difference flow logging

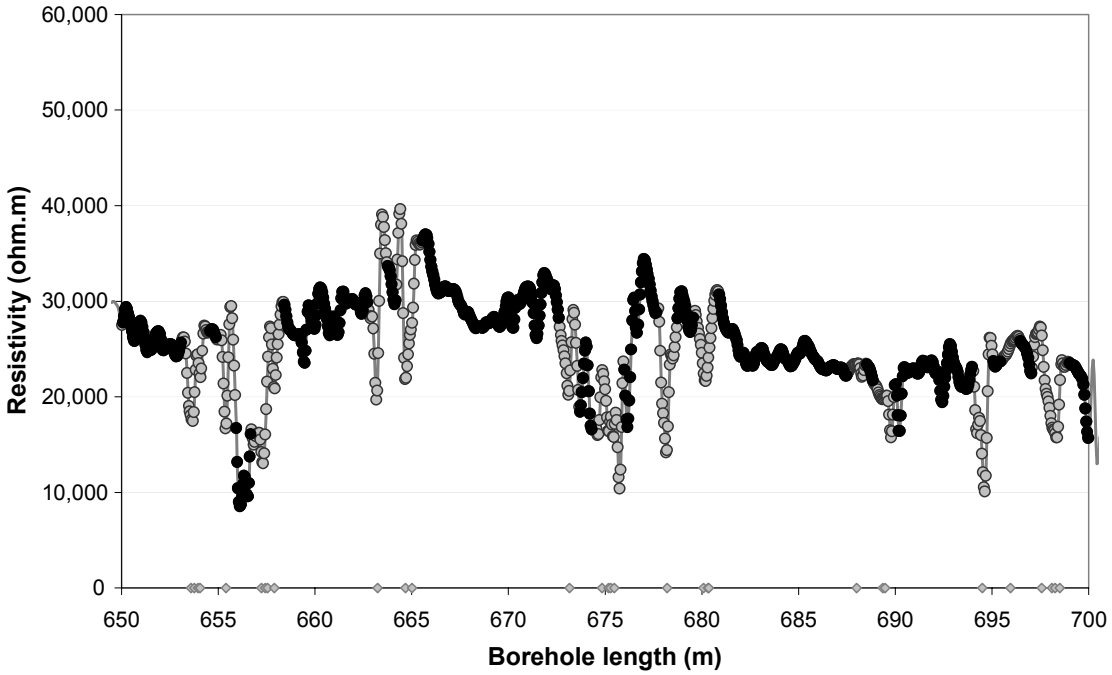

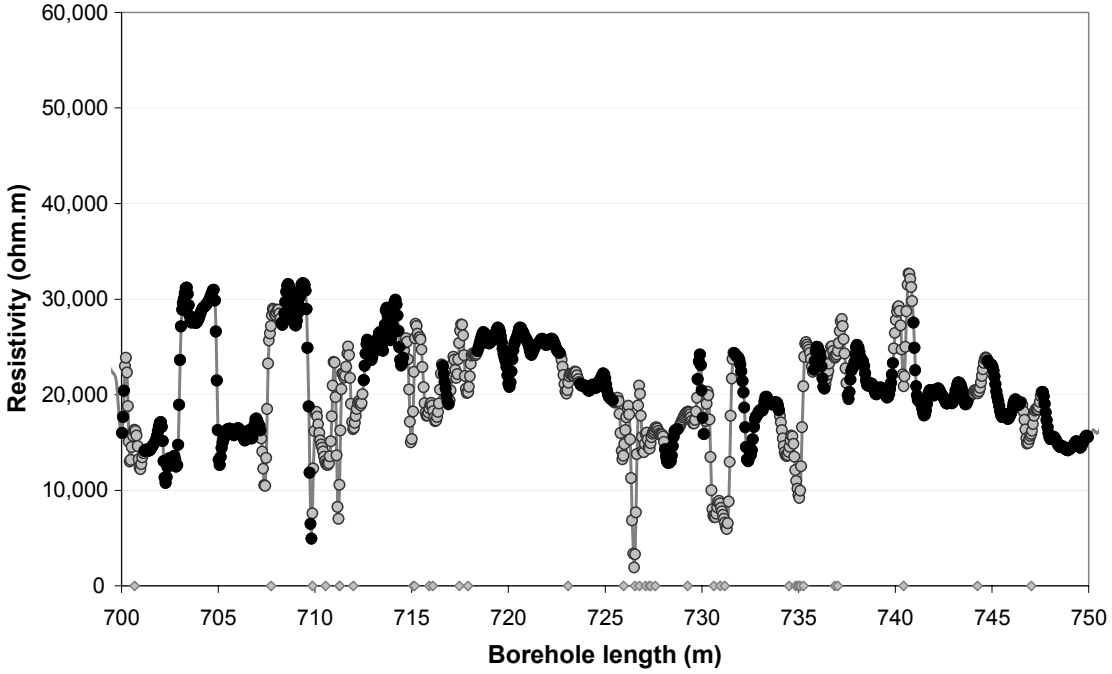

Fractured rock resistivity
Rock matrix resistivity
Location of natural fracture parting the bore core
Location of hydraulically conductive fracture detected in the difference flow logging

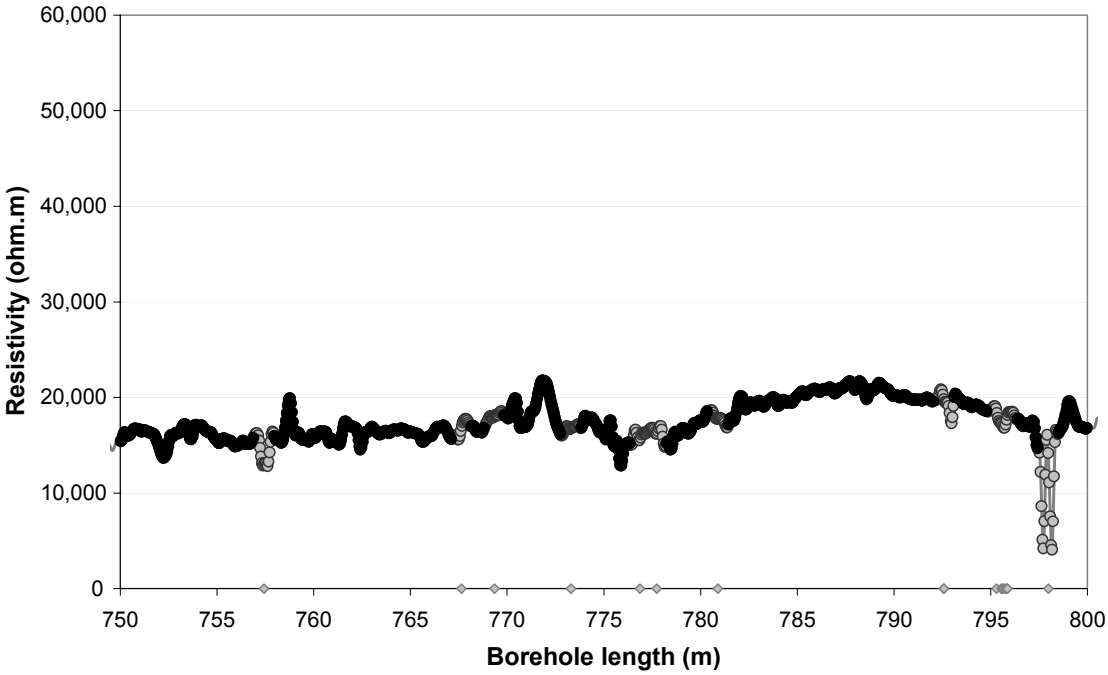

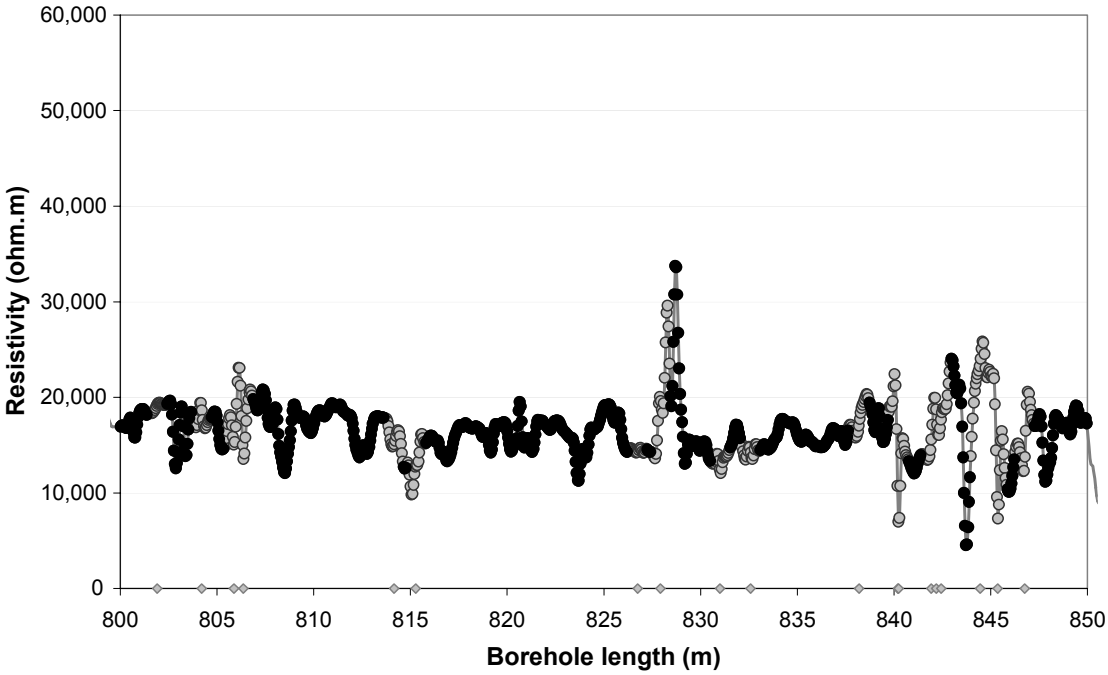

Fractured rock resistivity
Rock matrix resistivity
Location of natural fracture parting the bore core
Location of hydraulically conductive fracture detected in the difference flow logging

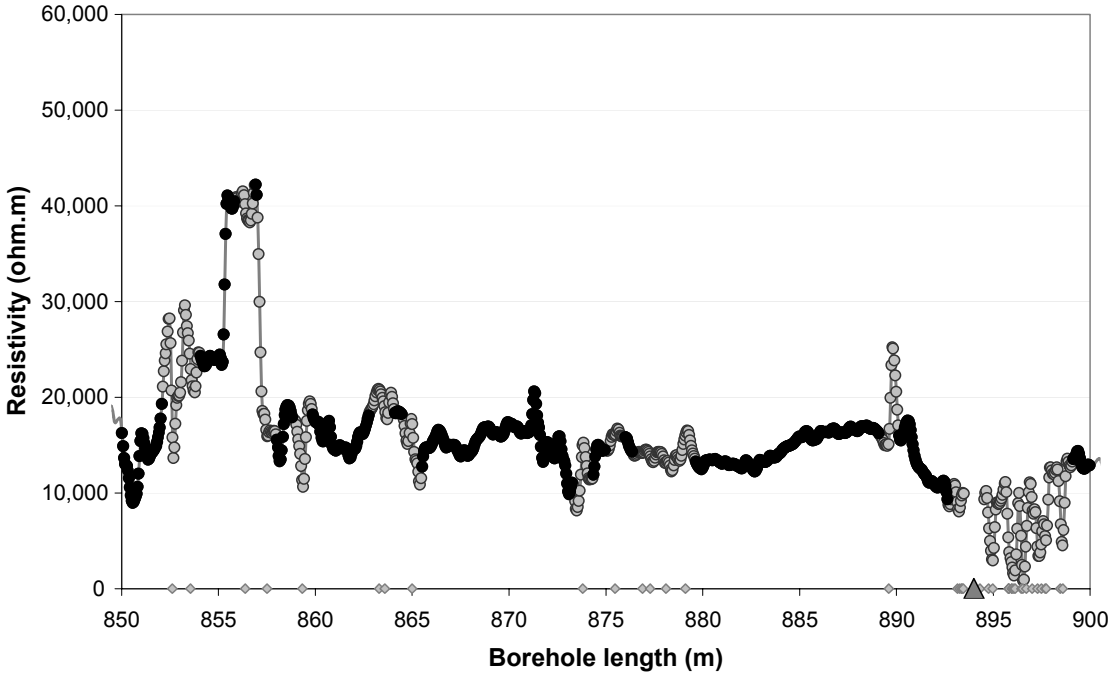

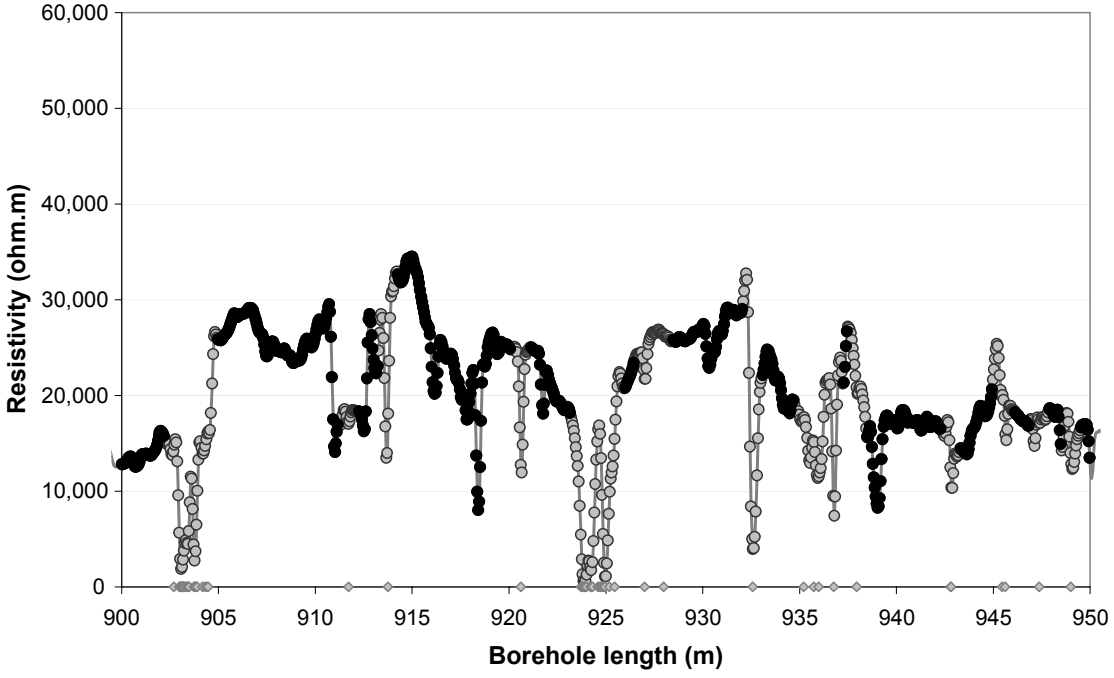

Fractured rock resistivity
Rock matrix resistivity
Location of natural fracture parting the bore core
Location of hydraulically conductive fracture detected in the difference flow logging

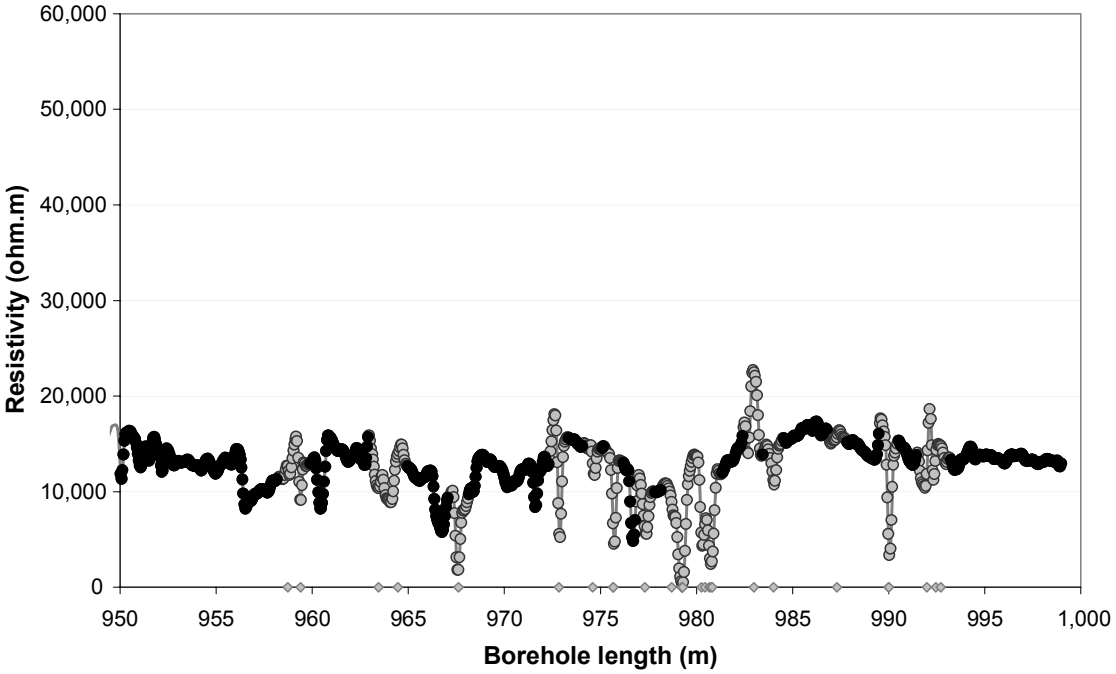

Fractured rock resistivity
Rock matrix resistivity
Location of natural fracture parting the bore core
Location of hydraulically conductive fracture detected in the difference flow logging

Appendix C

Appendix C1: In-situ and laboratory formation factors KFM01A

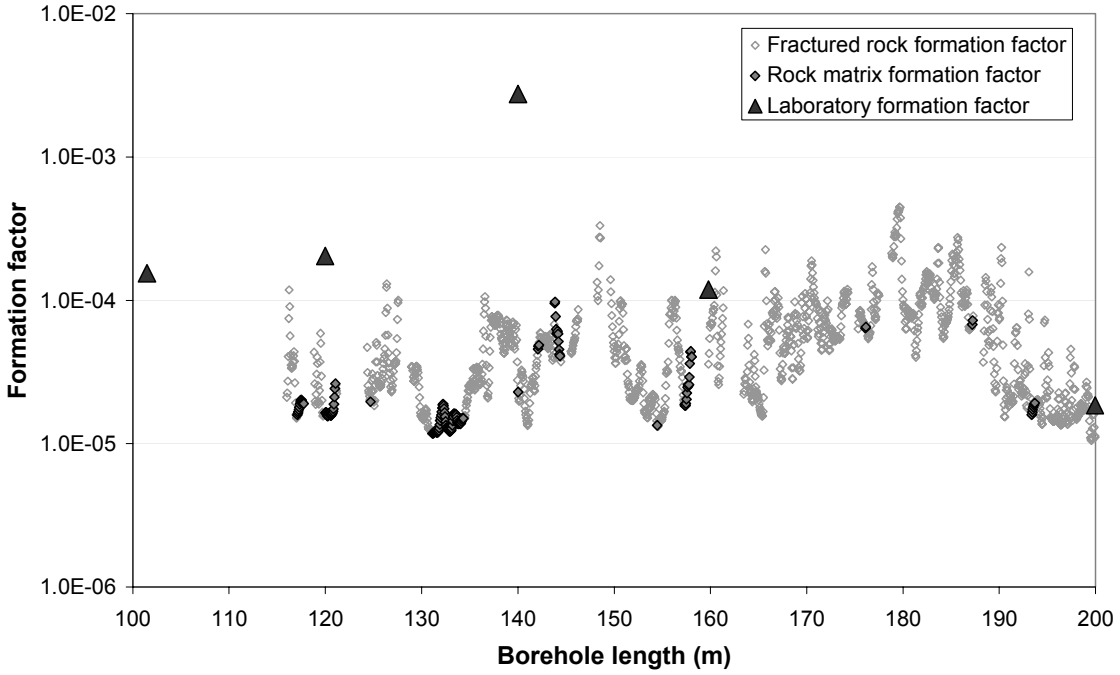

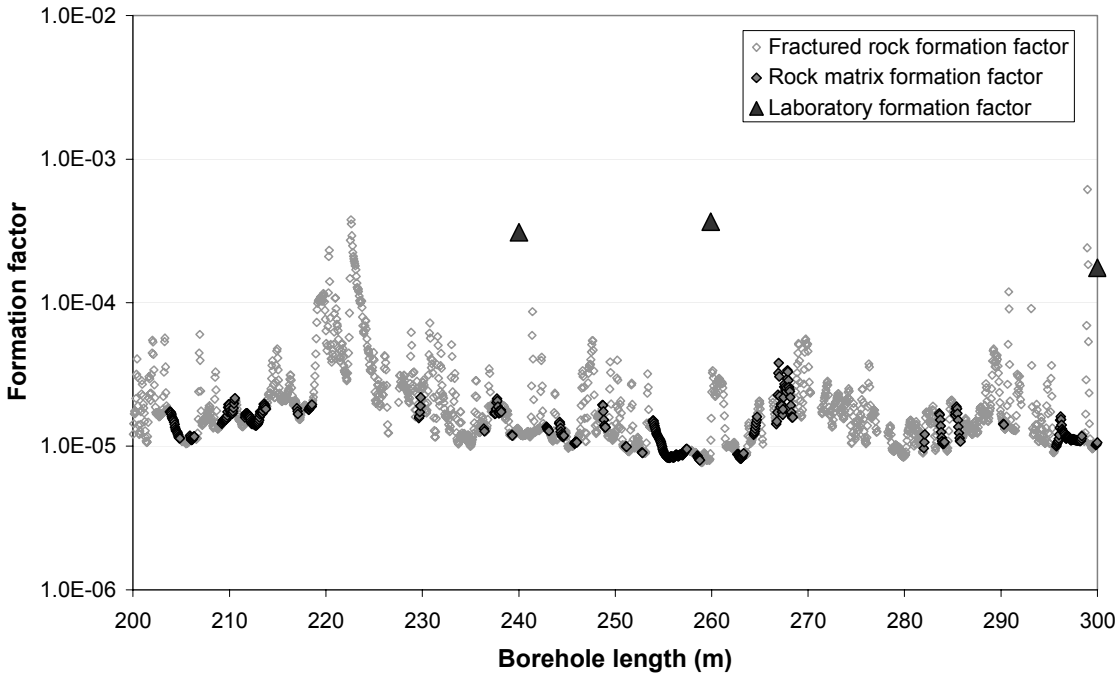

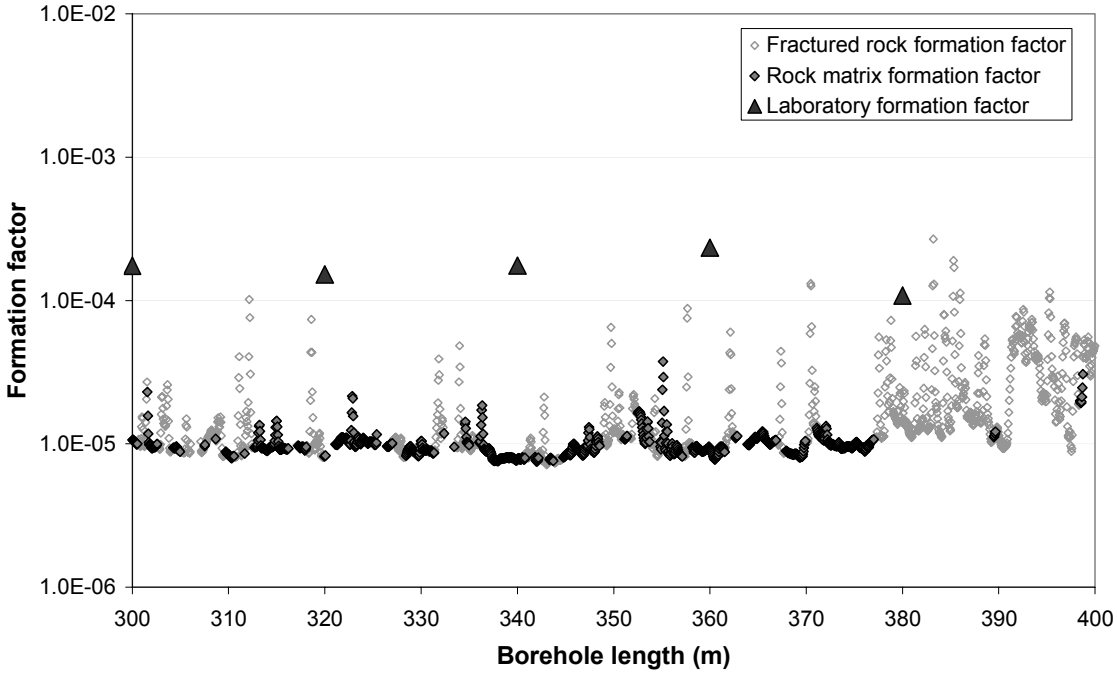
Fractured rock formation factor
Rock matrix formation factor
Laboratory formation factor
Formation factor
1.0E-02
1.0E-03
1.0E-04
1.0E-05
1.0E-06
300
310
320
330
340
350
360
370
380
390
400
Borehole length (m)

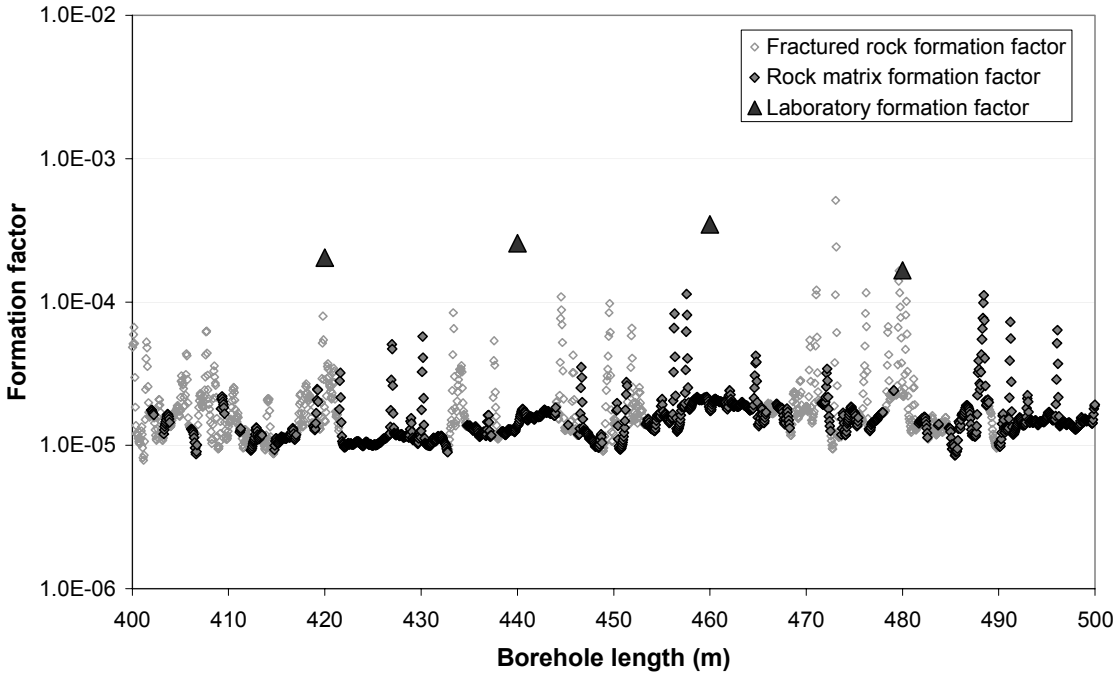
Fractured rock formation factor
Rock matrix formation factor
Laboratory formation factor
Formation factor
1.0E-02
1.0E-03
1.0E-04
1.0E-05
1.0E-06
400
410
420
430
440
450
460
470
480
490
500
Borehole length (m)

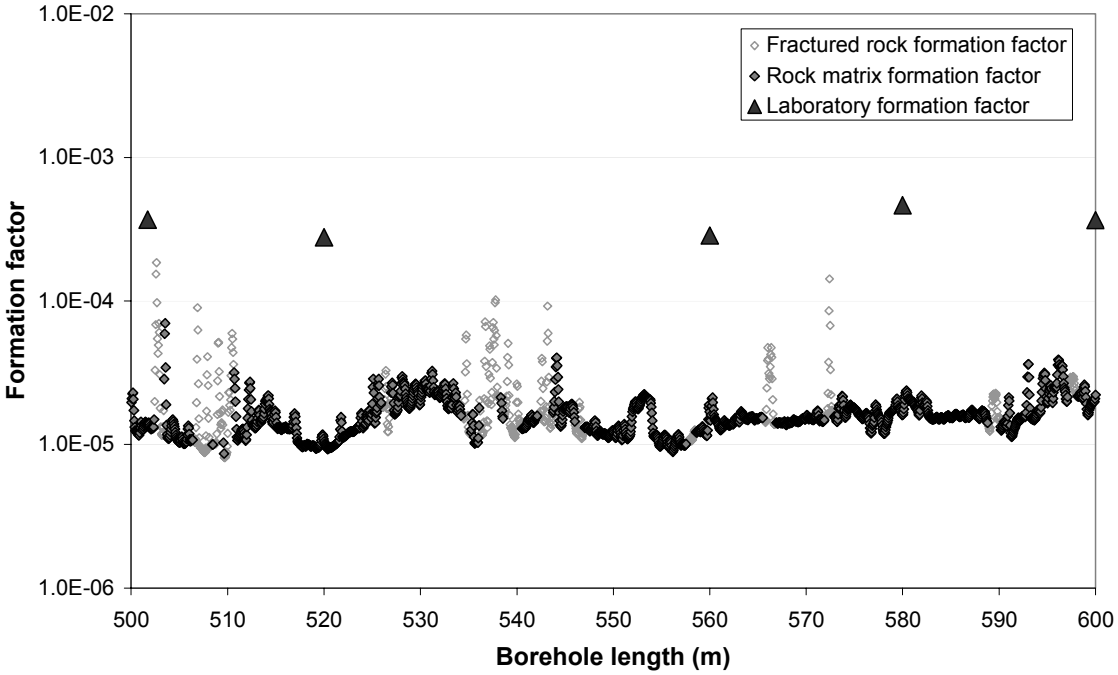
Fractured rock formation factor
Rock matrix formation factor
Laboratory formation factor
Formation factor
1.0E-02
1.0E-03
1.0E-04
1.0E-05
1.0E-06
500
510
520
530
540
550
560
570
580
590
600
Borehole length (m)

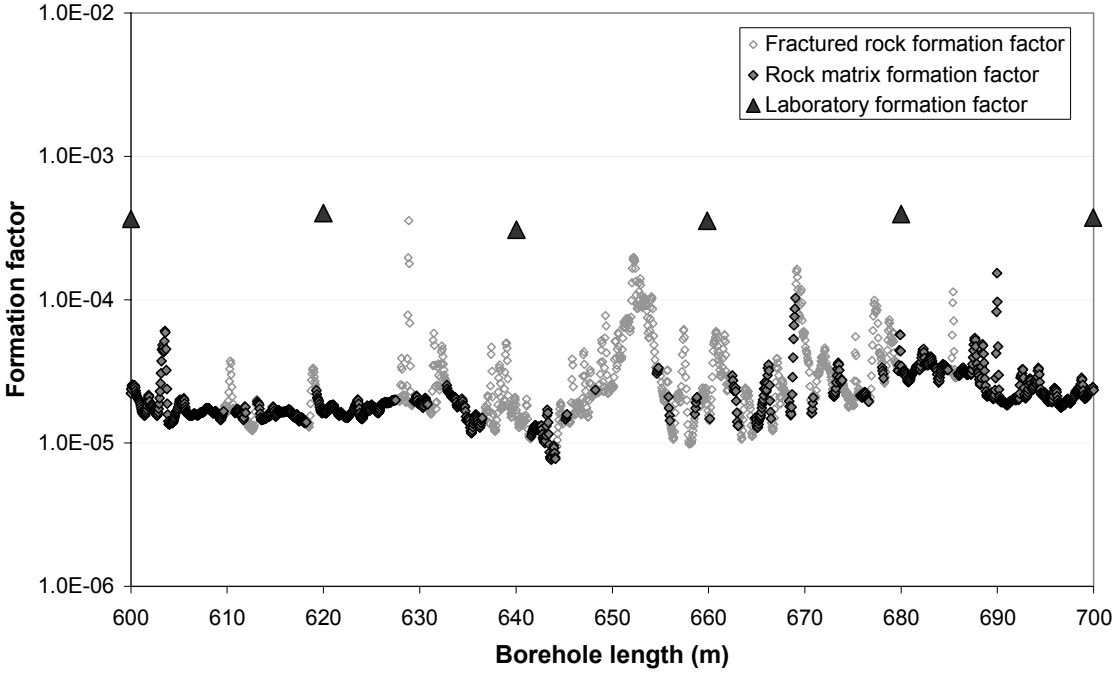
Fractured rock formation factor
Rock matrix formation factor
Laboratory formation factor
Formation factor
1.0E-02
1.0E-03
1.0E-04
1.0E-05
1.0E-06
600
610
620
630
640
650
660
670
680
690
700
Borehole length (m)

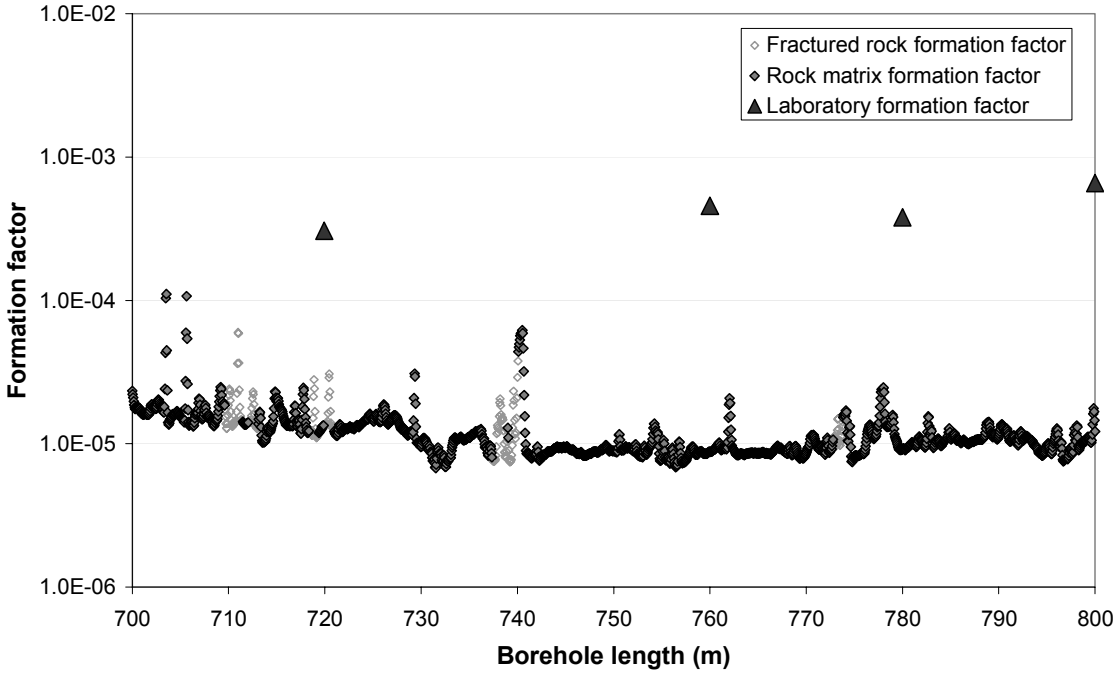
Fractured rock formation factor
Rock matrix formation factor
Laboratory formation factor
Formation factor
1.0E-02
1.0E-03
1.0E-04
1.0E-05
1.0E-06
700
710
720
730
740
750
760
770
780
790
800
Borehole length (m)

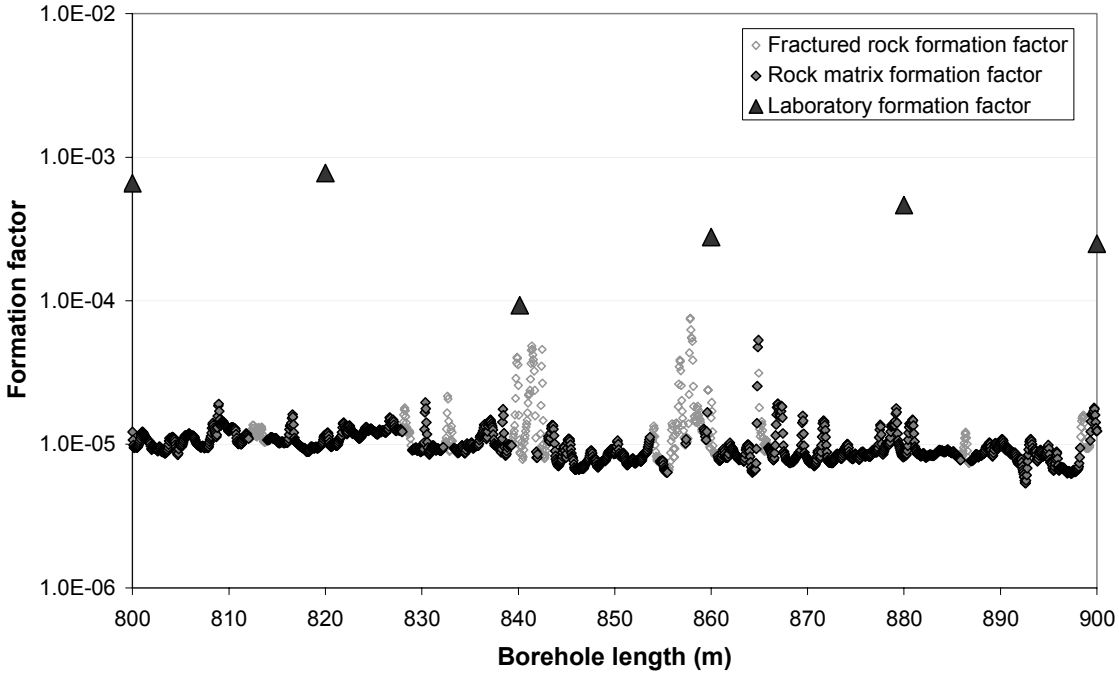
Fractured rock formation factor
Rock matrix formation factor
Laboratory formation factor
Formation factor
1.0E-02
1.0E-03
1.0E-04
1.0E-05
1.0E-06
800
810
820
830
840
850
860
870
880
890
900
Borehole length (m)

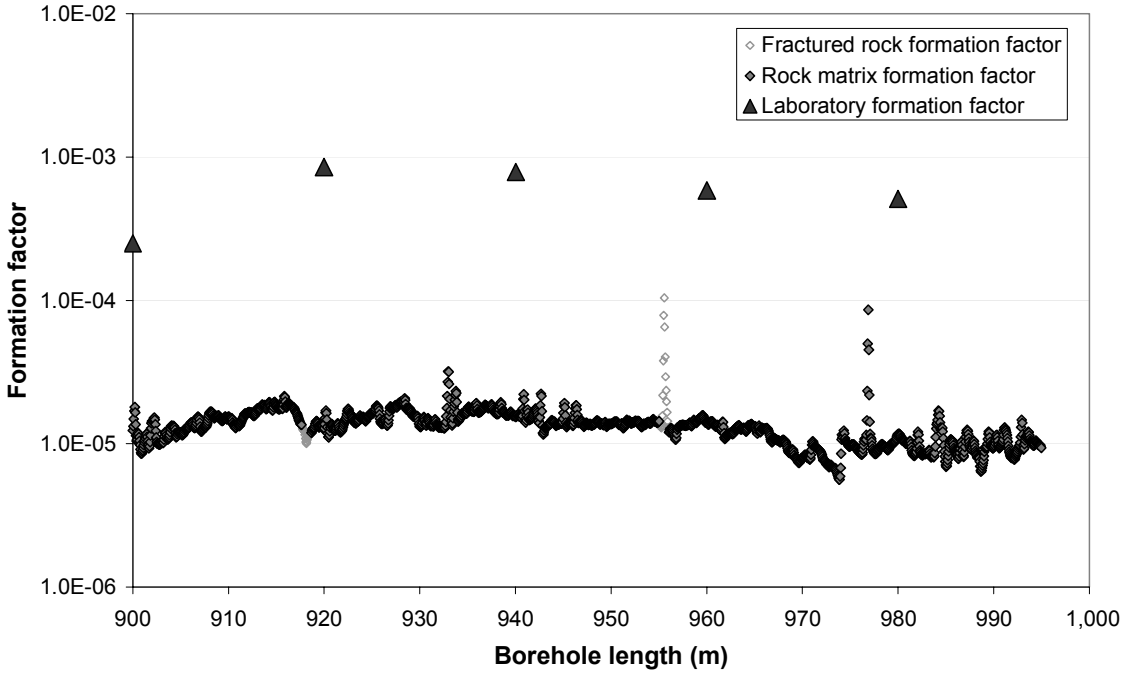
1.0E-02
1.0E-03
1.0E-04
1.0E-05
1.0E-06
Formation factor
900
910
920
930
940
950
960
970
980
990
1,000
Borehole length (m)
Fractured rock formation factor
Rock matrix formation factor
Laboratory formation factor

Appendix C2: In-situ and laboratory formation factors KFM02A

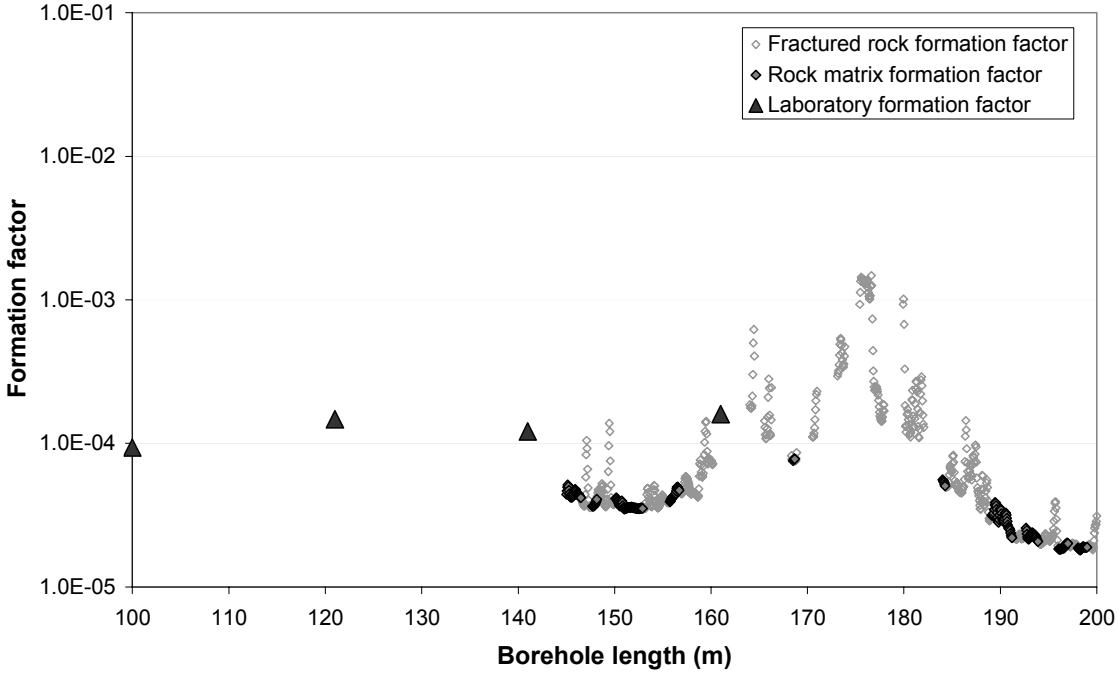

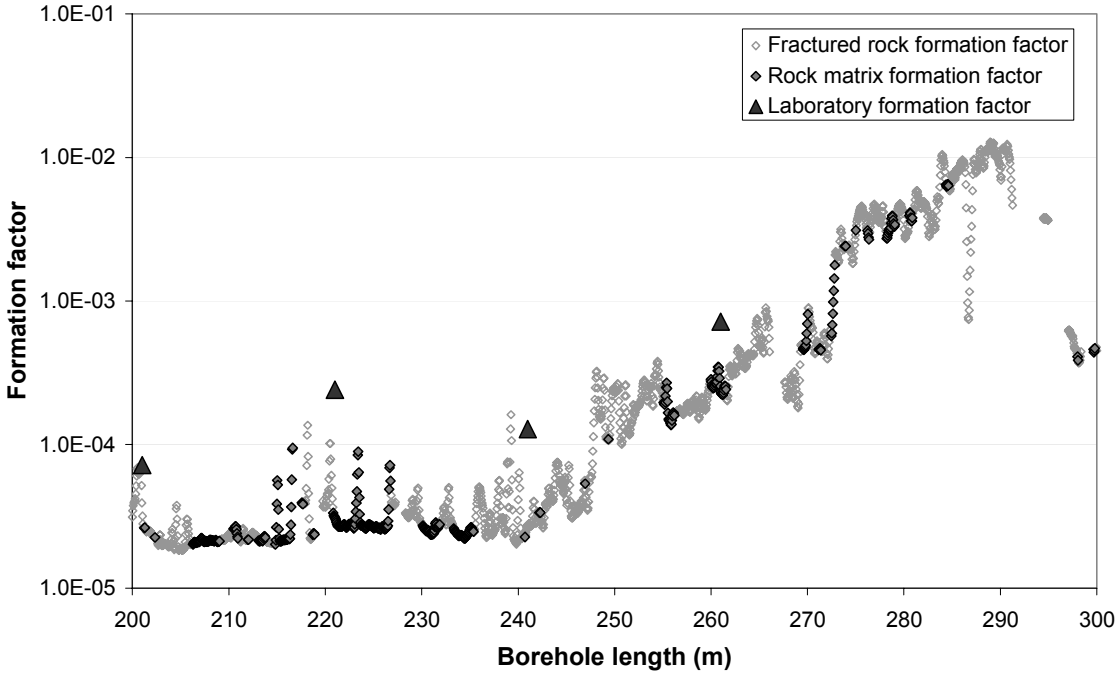

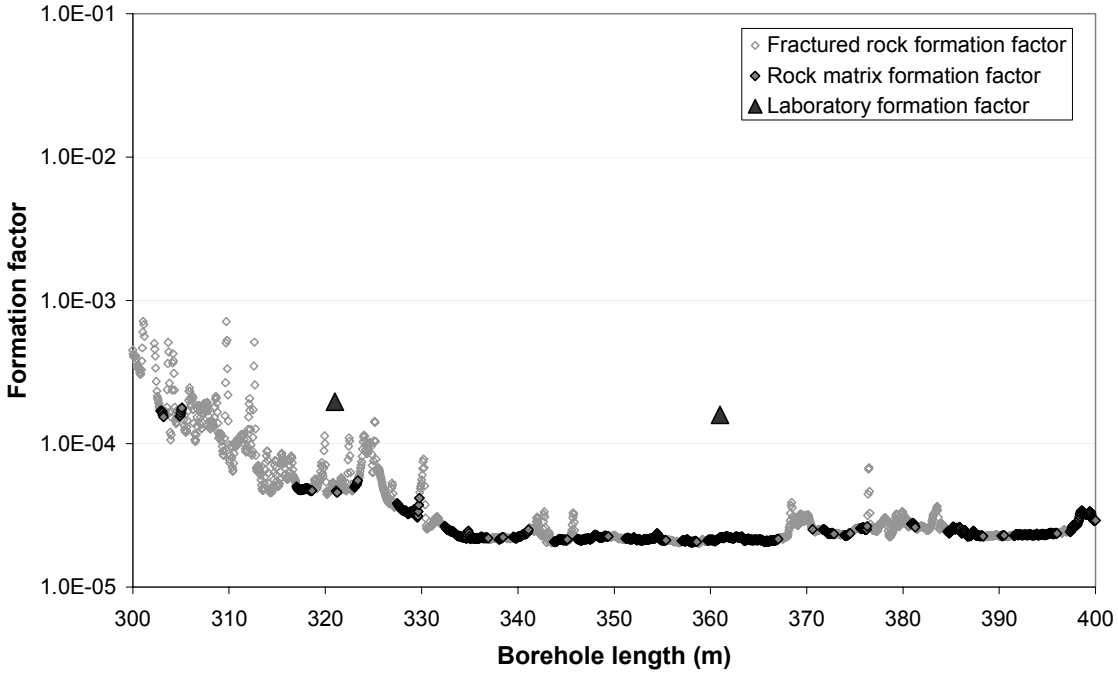
Fractured rock formation factor
Rock matrix formation factor
Laboratory formation factor
Formation factor
1.0E-01
1.0E-02
1.0E-03
1.0E-04
1.0E-05
300
310
320
330
340
350
360
370
380
390
400
Borehole length (m)

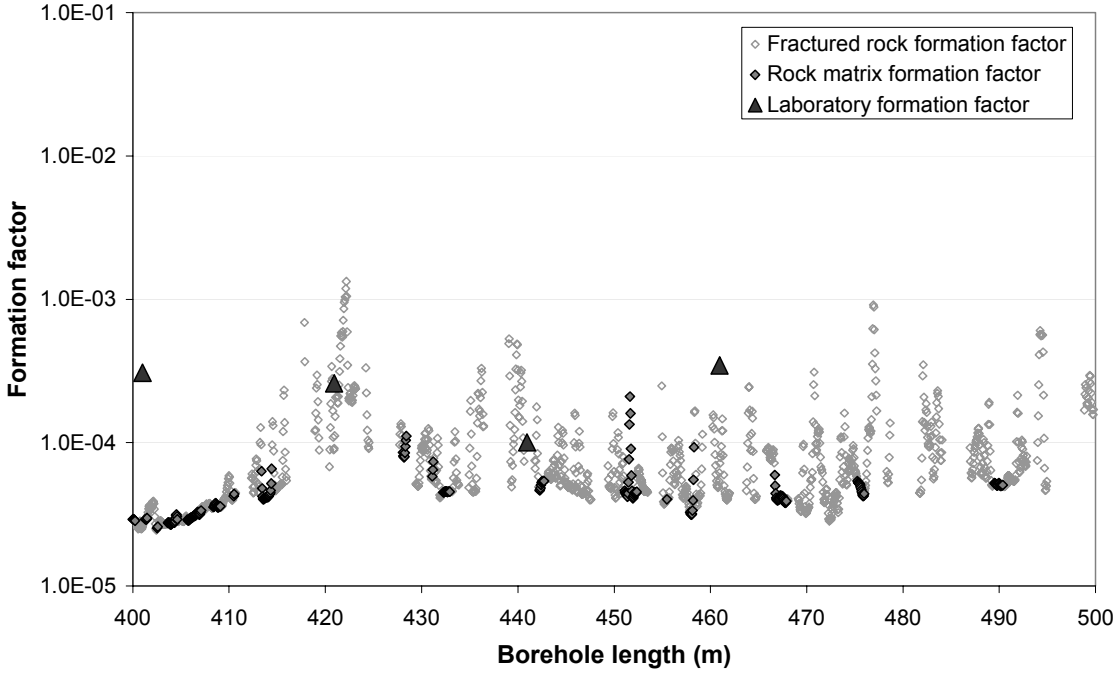
Fractured rock formation factor
Rock matrix formation factor
Laboratory formation factor
Formation factor
1.0E-01
1.0E-02
1.0E-03
1.0E-04
1.0E-05
400
410
420
430
440
450
460
470
480
490
500
Borehole length (m)

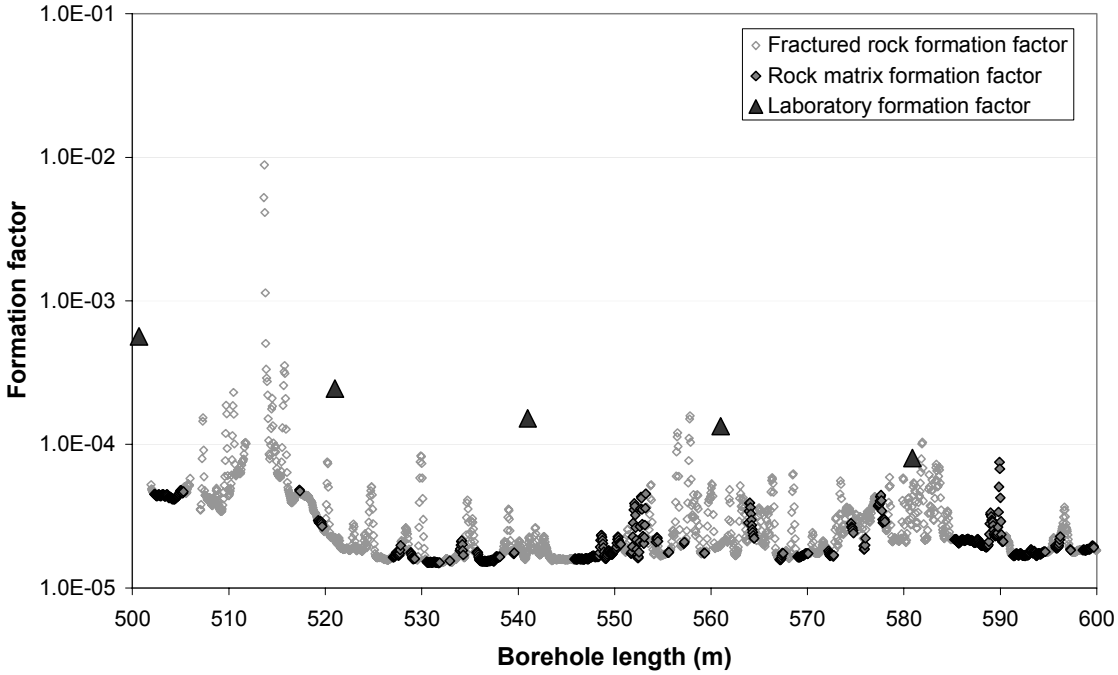
Fractured rock formation factor
Rock matrix formation factor
Laboratory formation factor
Formation factor
1.0E-01
1.0E-02
1.0E-03
1.0E-04
1.0E-05
500
510
520
530
540
550
560
570
580
590
600
Borehole length (m)

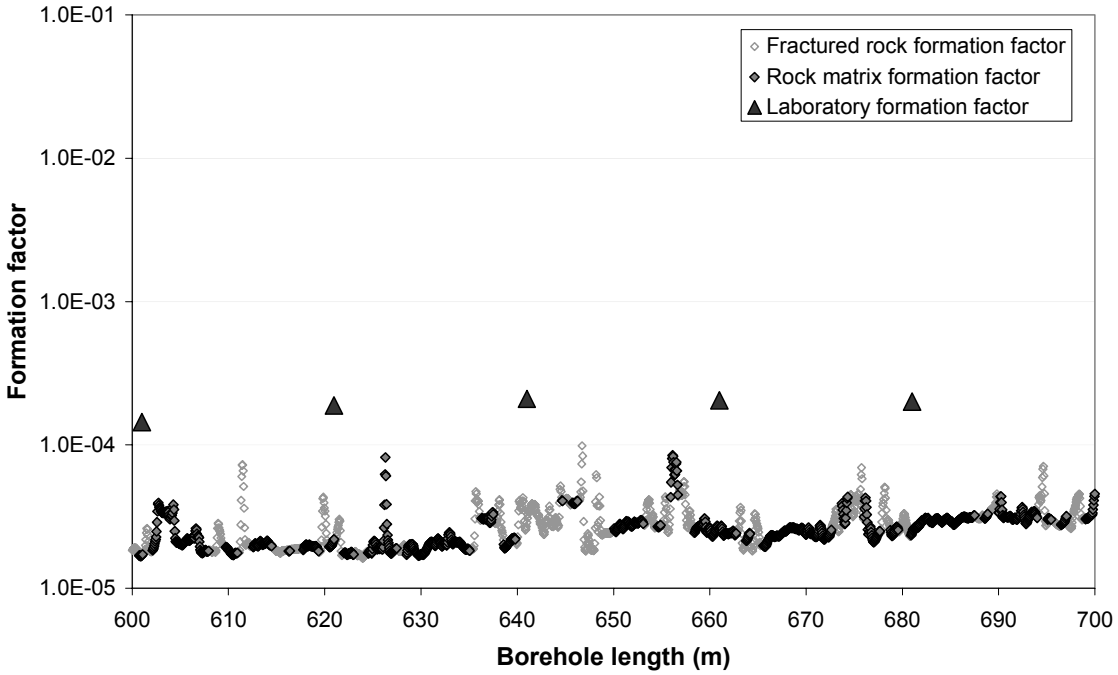
Fractured rock formation factor
Rock matrix formation factor
Laboratory formation factor
Formation factor
1.0E-01
1.0E-02
1.0E-03
1.0E-04
1.0E-05
600
610
620
630
640
650
660
670
680
690
700
Borehole length (m)

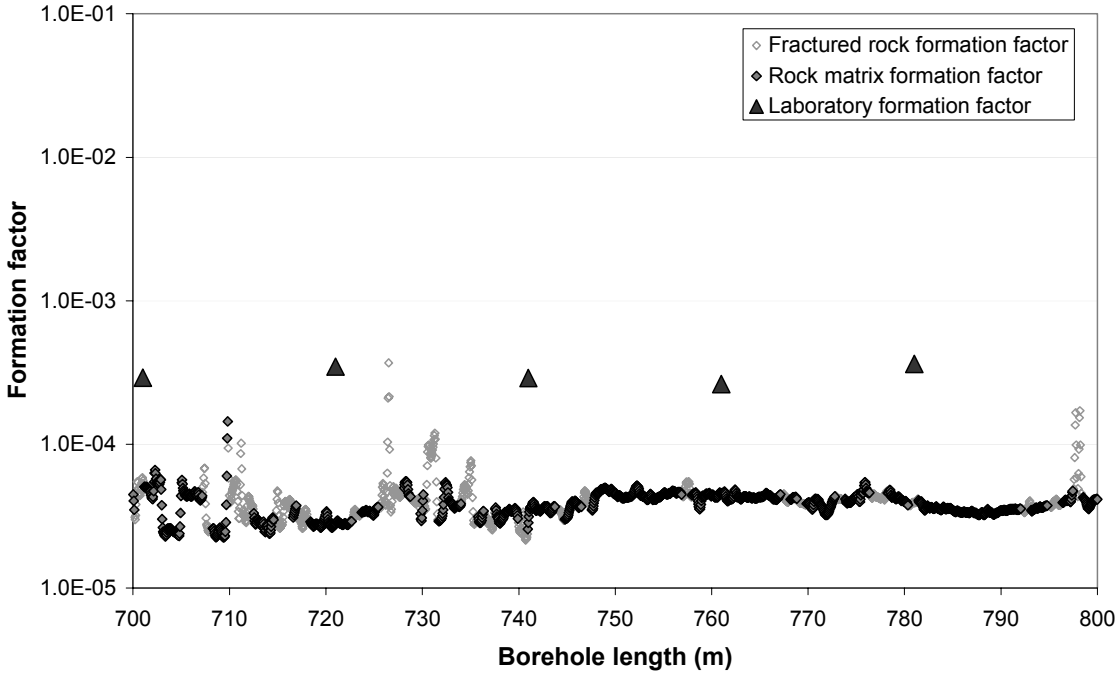
Fractured rock formation factor
Rock matrix formation factor
Laboratory formation factor
Formation factor
1.0E-01
1.0E-02
1.0E-03
1.0E-04
1.0E-05
700
710
720
730
740
750
760
770
780
790
800
Borehole length (m)

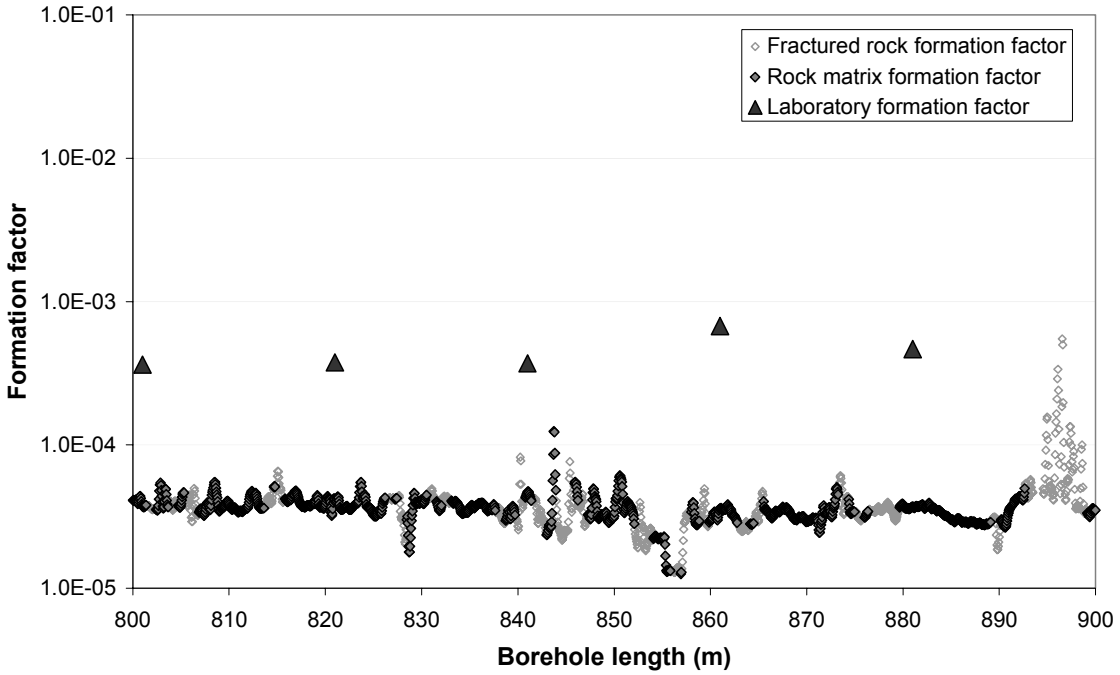
Fractured rock formation factor
Rock matrix formation factor
Laboratory formation factor
Formation factor
1.0E-01
1.0E-02
1.0E-03
1.0E-04
1.0E-05
800
810
820
830
840
850
860
870
880
890
900
Borehole length (m)

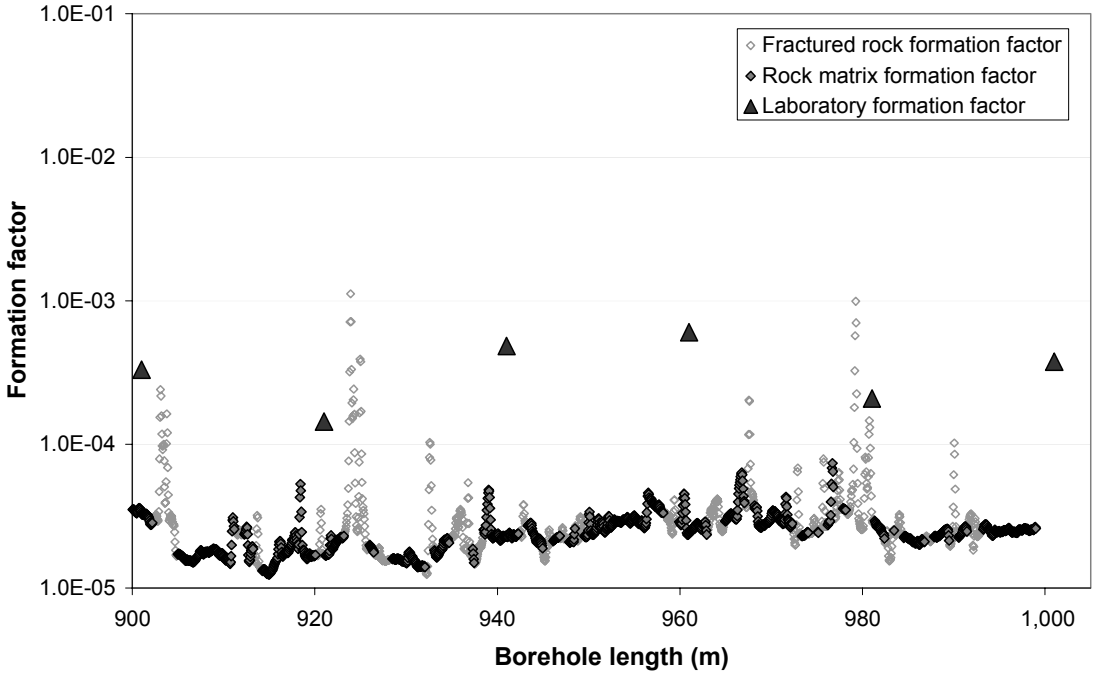
1.0E-01
1.0E-02
1.0E-03
1.0E-04
1.0E-05
Formation factor
900
920
940
960
980
1,000
Borehole length (m)
Fractured rock formation factor
Rock matrix formation factor
Laboratory formation factor

Appendix C3: Comparison of laboratory and in-situ formation factors KFM01A

Borehole length (m)	Laboratory Ff	Rock matrix Ff	Borehole length (m)	Laboratory Ff	Rock matrix Ff
101.48	1.54E–04	–	600.00	3.65E–04	2.25E–05
119.98	2.04E–04	1.61E–05	620.00	4.03E–04	1.68E–05
140.00	2.75E–03	2.29E–05	640.05	3.08E–04	–
159.80	1.19E–04	–	659.85	3.55E–04	1.48E–05
199.95	1.85E–05	–	680.00	3.95E–04	3.64E–05
240.00	3.09E–04	–	699.95	3.75E–04	2.15E–05
259.90	3.66E–04	–	719.95	3.06E–04	1.28E–05
300.00	1.74E–04	1.04E–05	760.00	4.57E–04	8.79E–06
320.00	1.52E–04	9.58E–06	780.00	3.80E–04	9.20E–06
340.00	1.75E–04	7.83E–06	800.00	6.57E–04	1.15E–05
360.00	2.34E–04	8.94E–06	820.00	7.76E–04	1.10E–05
380.00	1.08E–04	–	840.16	9.28E–05	–
420.00	2.04E–04	–	860.00	2.78E–04	1.45E–05
440.00	2.57E–04	1.42E–05	880.00	4.64E–04	8.93E–06
460.00	3.48E–04	1.99E–05	900.00	2.50E–04	1.47E–05
480.00	1.66E–04	–	920.00	8.53E–04	1.36E–05
501.72	3.68E–04	1.36E–05	940.05	7.86E–04	1.57E–05
520.00	2.77E–04	1.02E–05	960.00	5.84E–04	1.44E–05
560.00	2.86E–04	1.57E–05	980.00	5.11E–04	1.09E–05
580.00	4.64E–04	1.89E–05			

Laboratory Ff = Formation factor obtained in the laboratory.
Rock matrix Ff = Mean value of in-situ rock matrix formation factors from within 0.5 m of the borehole length.

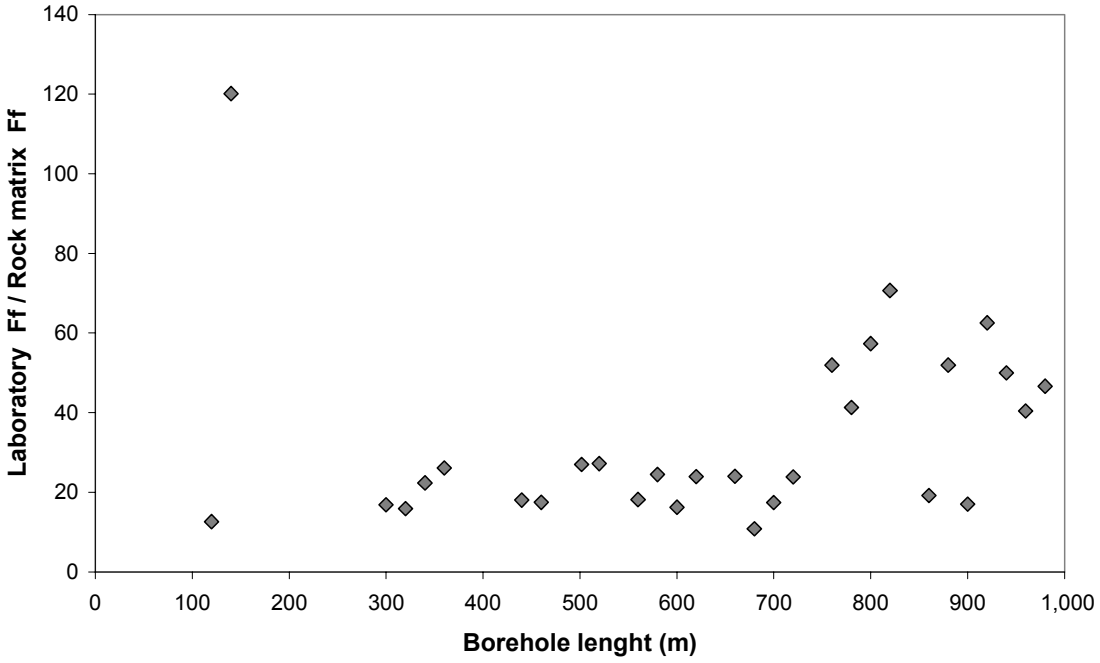

The ratio of the laboratory formation factor and the rock matrix formation factor obtained in-situ at a corresponding depth vs. borehole length in KFM01A.

Appendix C4: Comparison of laboratory and in-situ formation factors KFM02A

Borehole length (m)	Laboratory Ff	Rock matrix Ff	Borehole length (m)	Laboratory Ff	Rock matrix Ff
100.00	9.33E–05	–	620.95	1.89E–04	2.03E–05
121.00	1.47E–04	–	641.00	2.09E–04	–
141.00	1.21E–04	–	661.00	2.05E–04	2.57E–05
161.00	1.60E–04	–	681.00	2.01E–04	2.57E–05
201.00	7.19E–05	2.63E–05	701.00	2.91E–04	5.04E–05
221.00	2.40E–04	2.93E–05	721.00	3.48E–04	2.78E–05
241.00	1.28E–04	2.27E–05	741.00	2.90E–04	3.49E–05
261.00	7.17E–04	2.66E–04	761.00	2.63E–04	4.50E–05
321.00	1.97E–04	4.63E–05	781.00	3.64E–04	4.04E–05
361.00	1.59E–04	2.19E–05	801.00	3.63E–04	3.93E–05
401.00	3.06E–04	2.93E–05	821.00	3.77E–04	3.94E–05
420.92	2.59E–04	–	841.00	3.70E–04	4.45E–05
440.95	1.00E–04	4.90E–05	861.00	6.74E–04	3.42E–05
460.95	3.46E–04	–	881.00	4.66E–04	3.66E–05
500.67	5.65E–04	–	901.00	3.30E–04	3.37E–05
521.00	2.45E–04	–	921.00	1.44E–04	1.70E–05
541.00	1.52E–04	–	941.00	4.84E–04	2.31E–05
561.00	1.34E–04	–	961.00	6.05E–04	2.71E–05
580.88	8.04E–05	–	981.03	2.09E–04	2.85E–05
601.00	1.44E–04	1.69E–05	1,001.00	3.76E–04	–

Laboratory Ff = Formation factor obtained in the laboratory.
Rock matrix Ff = Mean value of in-situ rock matrix formation factors from within 0.5 m of the borehole length.

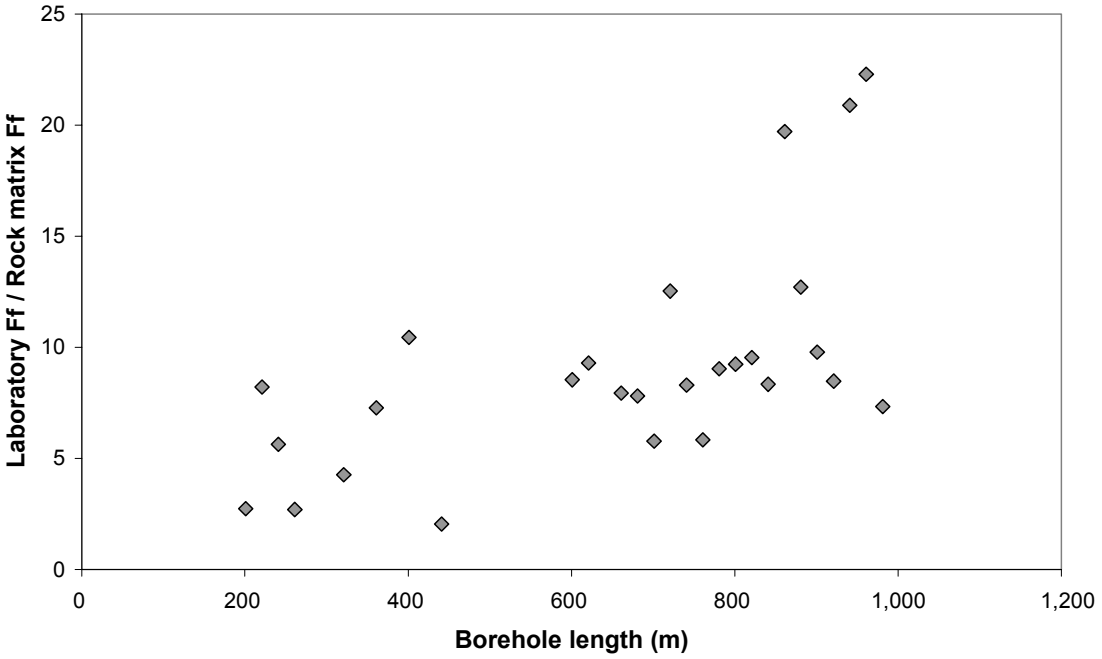

The ratio of the laboratory formation factor and the rock matrix formation factor obtained in-situ at a corresponding depth vs. borehole length in KFM02A.

Appendix D

Appendix D1: Histograms of rock matrix formation factor KFM01A

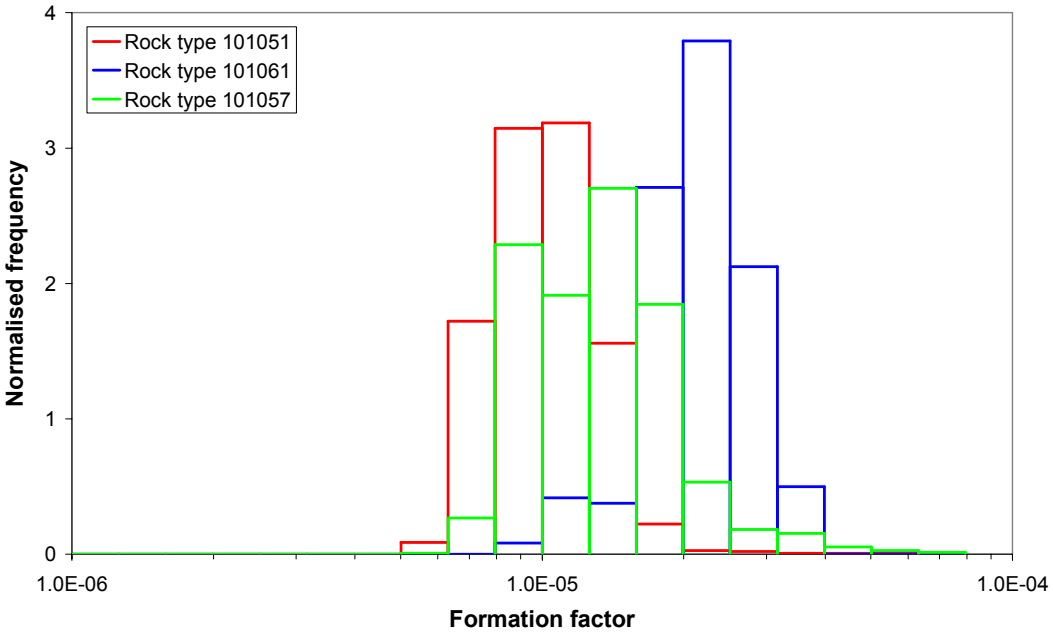

Number of data points: 101051: **1482**, 101061: **240**, 101057: **8759**

Rock types:
101051 = Granite, granodiorite and tonalite, metamorphic, fine- to medium-grained
101061 = Pegmatite, pegmatitic granite
101057 = Granite to granodiorite, metamorphic, medium-grained

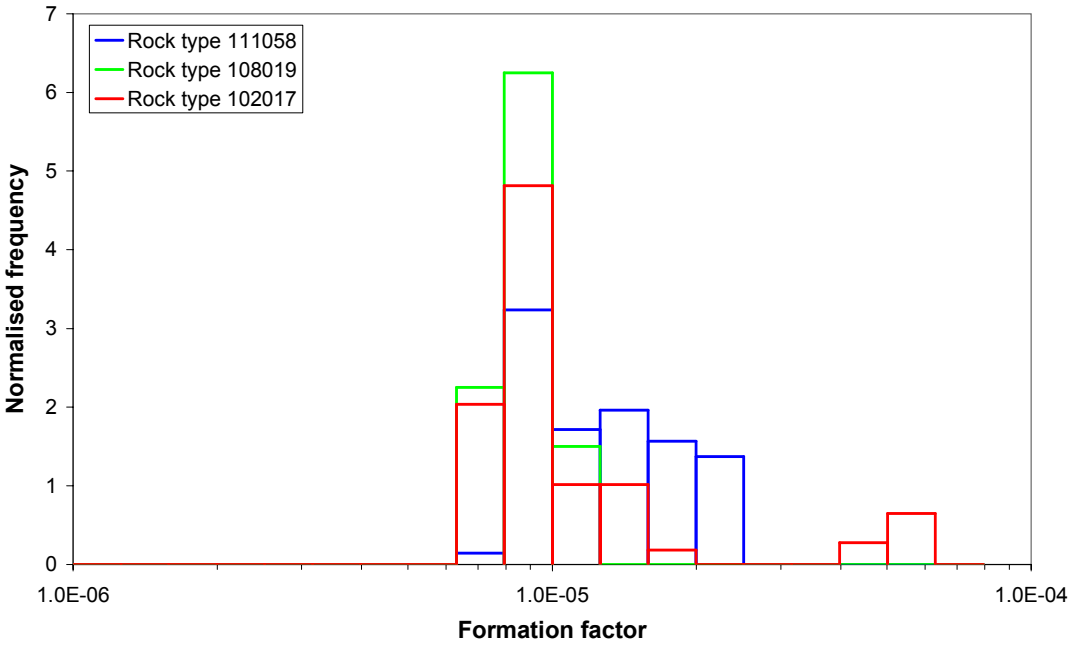

Number of data points: 111058: **204**, 108019: **40**, 102017: **108**

Rock types:
111058 = Granite, fine- to medium-grained
108019 = Calc-silicate rock (skarn)
102017 = Amphibolite

Appendix D2: Histograms of fractured rock formation factor KFM01A

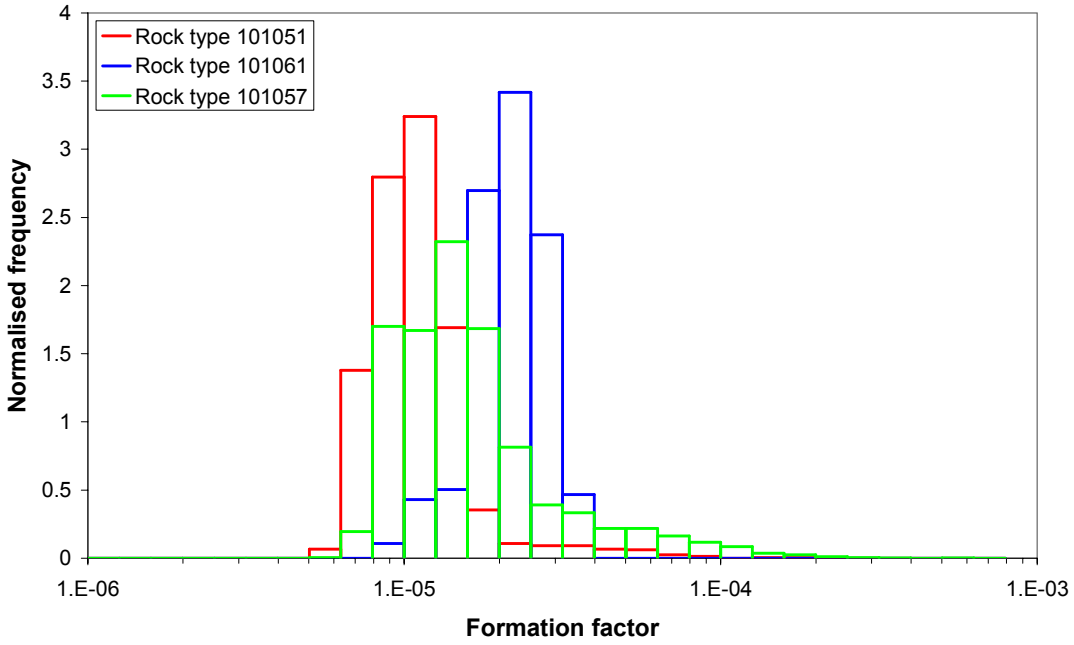

Number of data points: 101051: **1945**, 101061: **278**, 101057: **14203**

Rock types:
101051 = Granite, granodiorite and tonalite, metamorphic, fine- to medium-grained
101061 = Pegmatite, pegmatitic granite
101057 = Granite to granodiorite, metamorphic, medium-grained

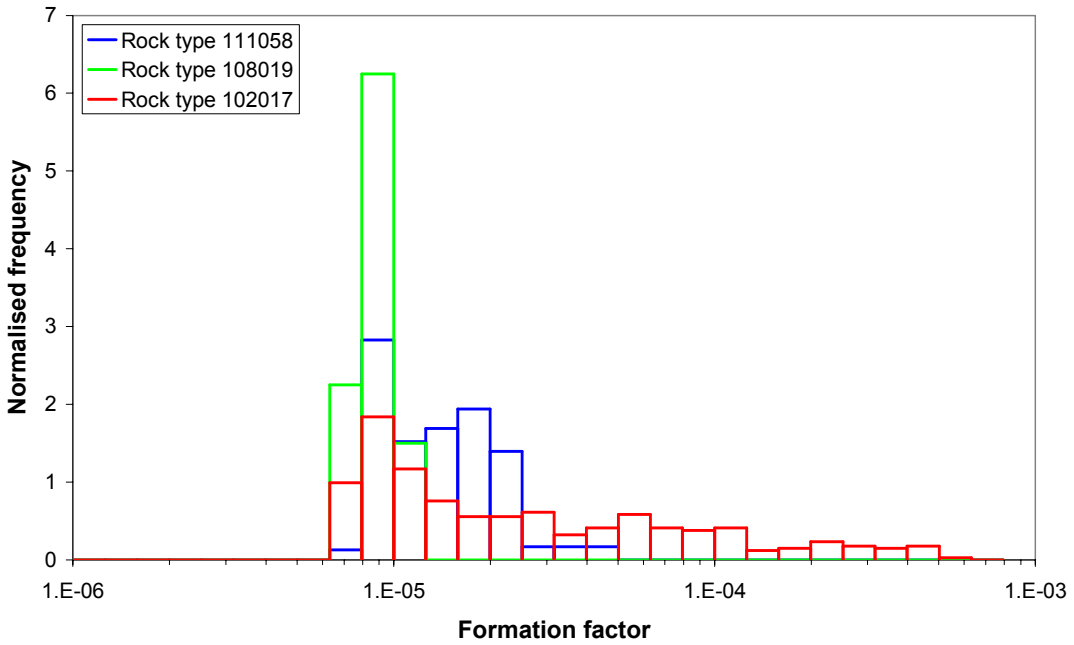

Number of data points: 111058: **237**, 108019: **40**, 102017: **343**

Rock types:
111058 = Granite, fine- to medium-grained
108019 = Calc-silicate rock (skarn)
102017 = Amphibolite

Appendix D3: Histograms of rock matrix formation factor KFM02A

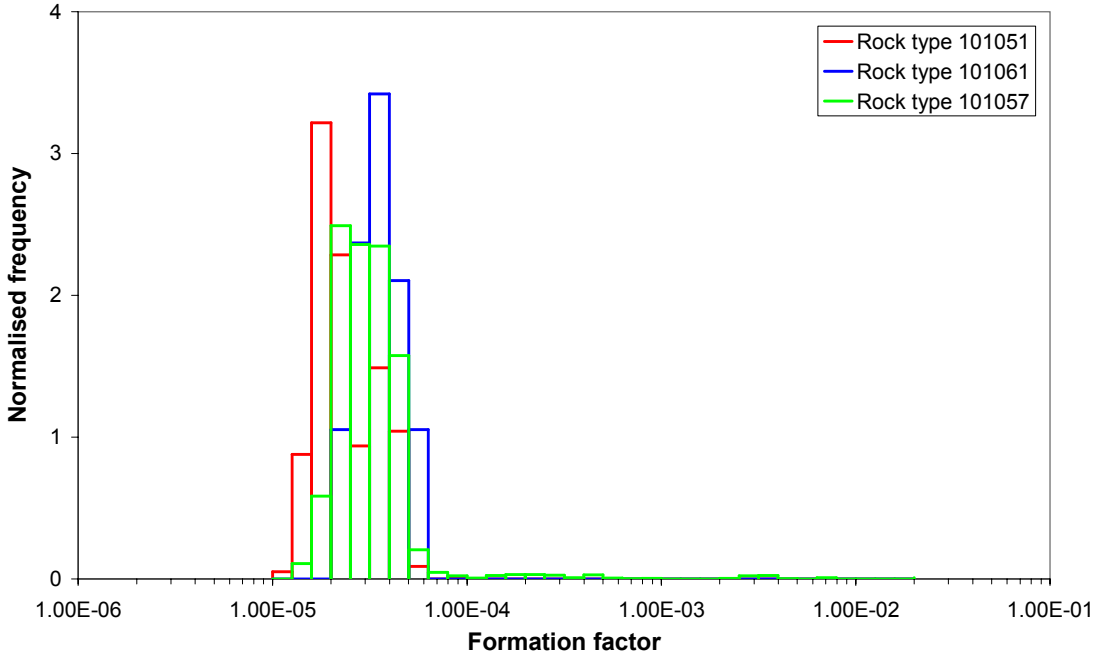

Number of data points: 101051: **1343**, 101061: **38**, 101057: **5882**

Rock types:
101051 = Granite, granodiorite and tonalite, metamorphic, fine- to medium-grained
101061 = Pegmatite, pegmatitic granite
101057 = Granite to granodiorite, metamorphic, medium-grained

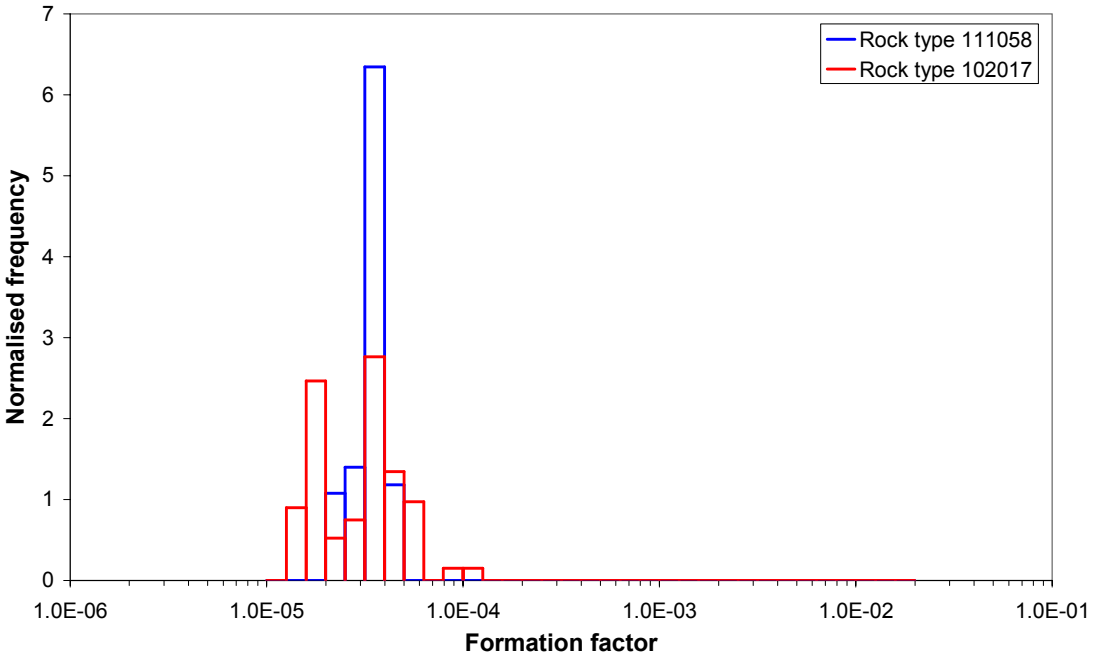

Number of data points: 111058: **93**, 102017: **134**

Rock types:
111058 = Granite, fine- to medium-grained
102017 = Amphibolite

Appendix D4: Histograms of fractured rock formation factor KFM02A

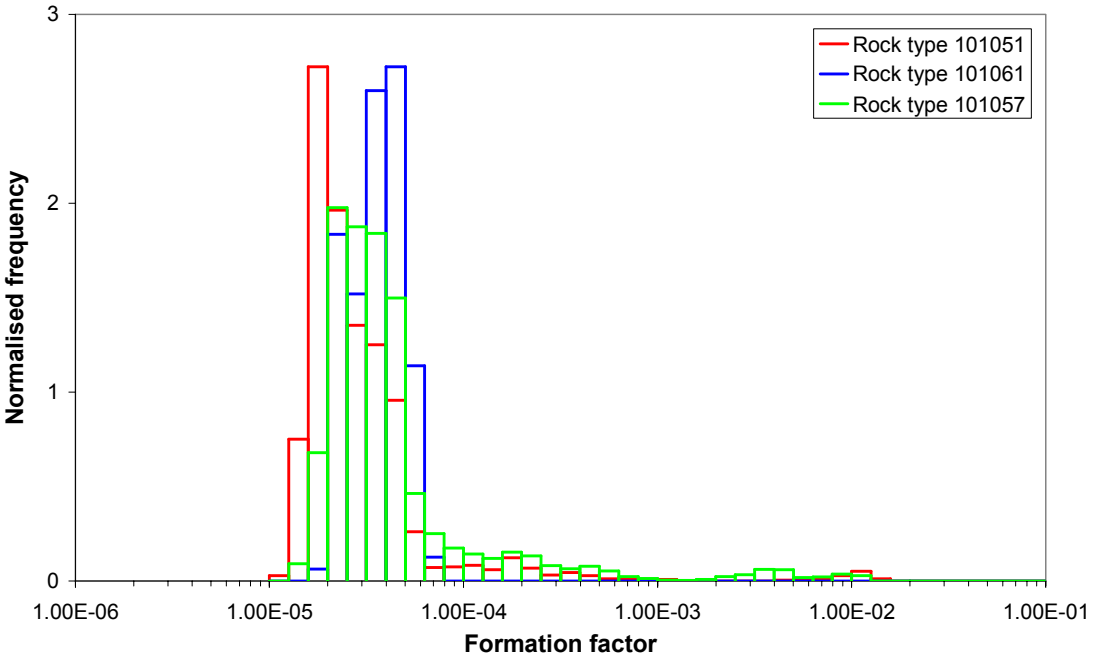

Number of data points: 101051: **2542**, 101061: **158**, 101057: **12234**

Rock types:
101051 = Granite, granodiorite and tonalite, metamorphic, fine- to medium-grained
101061 = Pegmatite, pegmatitic granite
101057 = Granite to granodiorite, metamorphic, medium-grained

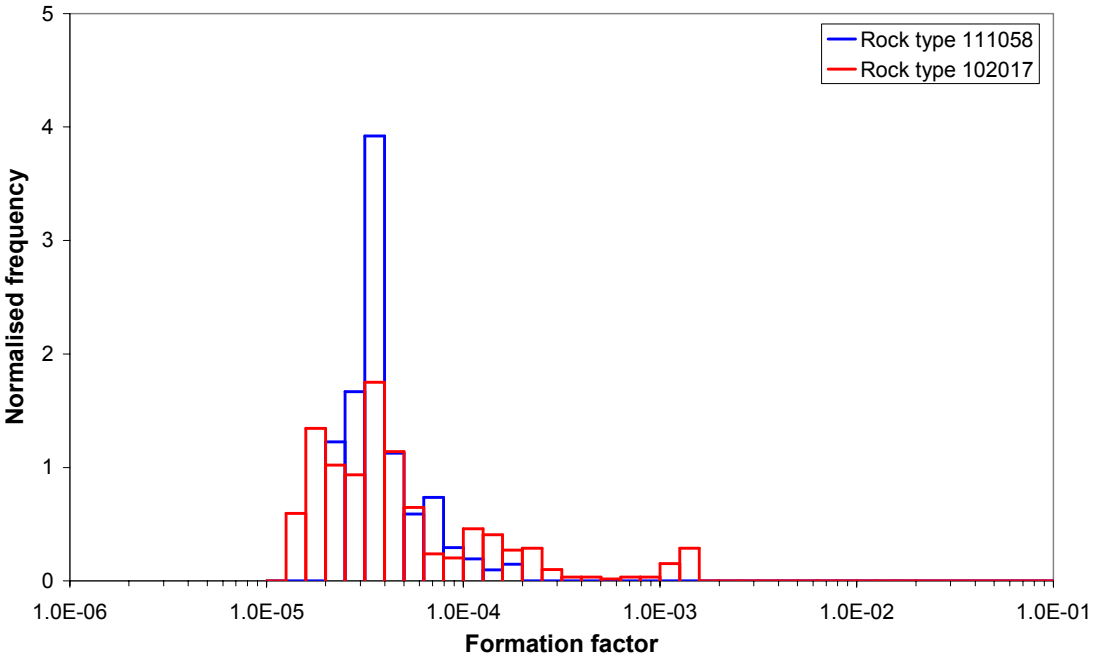

Number of data points: 111058: **204**, 102017: **558**

Rock types:
111058 = Granite, fine- to medium-grained
102017 = Amphibolite